EFFECTS OF STRUCTURAL SPIN-ORBIT COUPLING IN TWO DIMENSIONAL ELECTRON AND HOLE LIQUIDS

A Dissertation

Submitted to the Faculty

of

Purdue University

by

Stefano Chesi

In Partial Fulfillment of the

Requirements for the Degree

of

Doctor of Philosophy

May 2007

Purdue University

West Lafayette, Indiana

ACKNOWLEDGMENTS

This work would have been impossible without the assistance and guidance of my advisor, prof. Gabriele F. Giuliani, and his invaluable support, not only in the academic activity.

Stimulating and useful discussions with other faculties and students at Purdue also largely contributed to parts of this thesis. In particular with prof. Leonid Rokhinson, prof. Yuli Lyanda-Geller and Zoltan Gecse. Practical and financial support from the Department of Physics and Purdue University is also acknowledged, in particular the award of an Andrews Fellowship in the 2002-2004 period and a Grodzins Summer Research Award in 2006.

I will always remember with pleasure the company of many friends who helped and were close to me during this period. Finally, I want to express the most sincere gratitude to my family: my parents Lina and Fabio and my brother Tiziano.

TABLE OF CONTENTS

LIST OF TABLES

LIST OF FIGURES

Figure Page

ABBREVIATIONS

2D	two-dimensional
FXY	in-plane ferromagnetic
FZ	transverse ferromagnetic
HF	Hartree-Fock
HH	heavy-hole
LH	light-hole
PM	paramagnetic
SO	spin-orbit

ABSTRACT

Chesi, Stefano Ph.D., Purdue University, May, 2007. Effects of structural spin-orbit coupling in two dimensional electron and hole liquids. Major Professor: Gabriele F. Giuliani.

The recent interest in spin-dependent phenomena in semiconductor heterostructures motivates our detailed study of the structural spin-orbit coupling present in clean two-dimensional electron and hole liquids. Interesting polarization effects are produced in a system out of equilibrium, as when a finite current flows in the sample. In particular, the consequences of a lateral confinement creating a quasi one-dimensional wire are studied in detail, partially motivated by a recent experimental investigation of the point-contact transmission for two-dimensional holes.

We also address the role of the electron-electron interaction in the presence of spin-orbit coupling, which has received little attention in the literature. We discuss the formulation of the Hartree-Fock approximation in the particular case of linear Rashba spin-orbit. We establish the form of the mean-field phase diagram in the homogeneous case, which shows a complex interplay between paramagnetic and ferromagnetic states. The latter can be polarized in the plane or in a transverse direction, and are characterized by a complex spin structure and nontrivial occupation. The generality of the Hartree-Fock method allows a simple treatment of the Pauli spin susceptibility, and the application to different forms of spin-orbit coupling.

Correlation corrections can be obtained in an analytic form for particular asymptotic regimes. For linear Rashba spin-orbit we identified the relevance of the large spin-orbit limit, dominated by many-body effects, and explicitly treated the high density limit, in which the system is asymptotically noninteracting. As a special case, we derive a new exact formula for the polarization dependence of the ring-diagram correlation energy.

1. Introduction

The physics of two-dimensional electronic systems is a traditional subject of research, which is still under active investigation [1, 2]. While a noninteracting description of semiconductor heterostructures is well understood in the framework of the envelope-function approximation [3], it is often useful to unitary transform the resulting complicated multiband hamiltonians to effective models in which the effects of the band-structure are included in the form of nonparbolic corrections and spin-orbit coupling perturbations to the simple effective-mass parabolic dispersion.

The role of the spin-orbit interaction is especially important, since it leads to qualitatively new polarization phenomena with possible technological implications. Several realizations have been studied in the literature [4, 5], of which the recently demonstrated spin-Hall effect is perhaps the best known example [6]. The promise of realizing new devices exploiting the spin degree of freedom [7] has already been realized in several applications and has given rise to the field denoted as Spintronics [8–10]. The spin-orbit coupling is expected to play a central role in this context, since it allows to control the spin via conventional electrical means. In fact, the spin-orbit coupling is produced in the presence of nonuniform external fields, and therefore can be practically modified with the use of external gates [11, 12].

It has also to be noted that the spin-orbit coupling produced in semiconductors by smooth potentials is orders of magnitudes larger than in vacuum. This is due to the fact that the coupling coefficient is determined by the band structure, and accounts for the much larger electric fields of the crystalline field.

We devote our attention in this Thesis to structural spin-orbit coupling. This is present in the ideally clean systems, and is distinct from the so-called extrinsic spin-orbit, due to the inhomogeneous potential introduced by disorder. In the bulk of standard III-V semiconductors the spin-orbit interaction is directly produced by

the crystalline potential: it determines the structure of the highest valence bands (light-holes, heavy-holes and split-off band) and it produces a finite Dresselhaus spin-orbit splitting in the conduction band [13]. These properties are also reflected in the two-dimensional system produced by an external confinement, on which we focus in this Thesis.

In the two-dimensional case, an additional source of spin-orbit coupling is provided by the gradient of the confining potential, which determines the so-called Rashba spin-orbit coupling in the case of conduction electrons [14, 15]. The detailed origin of this term and the single-particle properties of the two-dimensional hamiltonian are reviewed in Chapter 2. A parallel treatment for the case of holes has to account of the intricacies of the valence band and is presented in Chapter 3.

Chapters 4 and 5 are also devoted to the properties of the noninteracting system. Here the effect of a lateral confinement producing a quasi one-dimensional system is treated for the case of electrons and holes respectively. In particular, we determine the properties of the spectrum and of the eigenstates and we study the finite polarization produced by the spin-orbit coupling in the presence of a finite current flowing in the system. In Chapter 5 we discuss the experimentally relevant situation of holes transmitted through a point contact [4].

The remaining part of this Thesis is devoted to many-body effects of the Coulomb interactions, which are generally neglected in the literature. Some quasiparticle properties are discussed in the early and limited attempt of Ref. [16] and are also treated in the more recent Ref. [17], for the case of high densities. A sound set of general theoretical notions about the effects of the electron-electron interactions in the presence of spin-orbit coupling is not established and a systematic analysis of this problem would be of great usefulness. In fact, interaction effects are very relevant in a wide range of accessible densities of modern quasi two-dimensional electron liquid devices [18, 19]. The most interesting case is perhaps provided by two-dimensional holes, which display large spin-orbit effects. At the same time, it is easier for holes to attain a low density regime characterized by strong many-body effects. Recent experiments [20]

have shown the anomalous behavior of this particular system, with respect to the well understood case when the spin-orbit is negligible.

Patterning the general approach on that followed for the familiar case of the electron liquid in the absence of spin-orbit coupling [1], the first step in tackling the many-electron problem is to establish a meaningful mean-field theory. We present in the following the detailed treatment of the Hartree-Fock approximation in the presence of spin-orbit coupling, which we established in its general form for the homogeneous case [21].

As it turns out, the high density paramagnetic phase can be treated in this framework by simply including the effect of the exchange energy, which is done in Chapter 6 for a generic form of spin-orbit coupling. In the following Chapters 7-10 the particular case of Rashba spin-orbit is treated in detail. The general formulation is presented in Chapter 7, while Chapter 8 discusses explicit mean-field solutions in the simplifying assumption that the isotropy in the plane of motion is preserved. This includes the paramagnetic phase and a low-density ferromagnetic phase, with polarization perpendicular to the plane of motion. In Chapter 9 we calculate the many-body enhancement of the linear spin response of the paramagnetic phase to an external magnetic field. The analysis reveals the differential instability to in-plane polarized solutions. Finally, Chapter 10 is devoted to the study of these anisotropic states with in plane polarization, which have complex features that in general have to be computed numerically. This concludes our study of the homogeneous phases, and allows to complete the corresponding mean-field phase diagram. The treatment is easily extended to other types of spin-orbit coupling, as briefly discussed in Chapter 11.

In Chapter 12 we consider the high-density limit in the presence of Rashba spin-orbit, and correlation corrections to the exchange contribution are explicitly examined in this regime. As a byproduct of the treatment, an interesting new result for the the correlation energy of a traditional polarized liquid is obtained [22, 23]. The high density limit of a polarized two-dimensional liquid *without* spin-orbit coupling is described in Chapter 13.

2. Noninteracting electrons with Rashba spin-orbit coupling

We consider in this Chapter the particular type of spin-orbit interaction called Rashba spin-orbit [14,15], which is relevant for conduction electrons confined in two-dimensions:

$$\hat{R}_0 = \alpha(\hat{\sigma}_x\hat{p}_y - \hat{\sigma}_y\hat{p}_x) \ . \tag{2.1}$$

The origin of this term rests with the asymmetry of the confining potential, in the z direction. A detailed derivation of this term in typical III-V semiconductors heterostrucures is presented in the following pages, and its magnitude is estimated with reference to the experimental literature. Finally, the single-particle properties in the presence of this particular form of spin-orbit coupling are also discussed.

Eq. (2.1) represents a useful model of spin-orbit coupling. However, a detailed study of spin-orbit effects arising from the band structure is in general complicated, and we refer to the literature for an extensive treatment (in particular, to reference [3]). We will present more general expressions in the next Chapter, while discussing the case of holes in two-dimensional heterostructures.

A type of spin-orbit equivalent to Eq. (2.1) originates directly from the bulk conduction band spin-splitting in materials without inversion symmetry (the so-called Dresselhaus spin-orbit [13]). In fact, in the particular case of confinement in the [001] direction we obtain:

$$\hat{D}_0 = \beta(\hat{\sigma}_x\hat{p}_x - \hat{\sigma}_y\hat{p}_y) \ . \tag{2.2}$$

We note that if only $\hat{D}_0$ is present, it can be easily transformed into $\hat{R}_0$ by means of a unitary rotation in the spin space but we cannot transform $\hat{R}_0 + \hat{D}_0$ to $\hat{R}_0$ only. The case of $\hat{R}_0 + \hat{D}_0$ with $\alpha = \beta$ proves trivial.

2.1 Envelope functions approximation

We consider the motion of a single electron in a crystal, in the presence of an external potential:

$$\hat{H} = \hat{H}_{crystal} + V(\hat{\mathbf{r}}) \ , \tag{2.3}$$

where $\hat{H}_{crystal}$ is the periodic crystalline hamiltonian, and $V(\hat{\mathbf{r}})$ is an external potential which is not periodic (e.g. the confining potential of an heterostructure). Although $V(\hat{\mathbf{r}})$ breaks the translational symmetry, we require it to be slowly varying on the length scale of the lattice constant. More explicitly:

$$\hat{H} = \Big[\frac{\hat{\mathbf{p}}^2}{2m_0} + V_{crystal}(\hat{\mathbf{r}}) + \frac{\hbar}{4m_0^2c^2}\,\hat{\boldsymbol{\sigma}}\cdot\vec{\nabla}V_{crystal}(\hat{\mathbf{r}})\times\hat{\mathbf{p}}\Big] + V(\hat{\mathbf{r}}) \ , \tag{2.4}$$

where $V_{crystal}(\hat{\mathbf{r}})$ is the crystalline potential. We have included the spin-orbit interaction in $\hat{H}_{crystal}$ while we have neglected the term from $V(\hat{\mathbf{r}})$ which is slowly varying. If $V(\hat{\mathbf{r}}) = 0$ then we obtain the band structure of the crystal $E_n(\mathbf{k})$ with corresponding Bloch wave eigenfunctions $\psi_{n,\mathbf{k}}(\mathbf{r},\sigma) = e^{i\mathbf{k}\,\mathbf{r}}u_{n,\mathbf{k}}(\mathbf{r},\sigma)$ (where $(\mathbf{r},\sigma)$ refer to the orbital and spin coordinates respectively).

In the case of $V(\mathbf{r}) \neq 0$ we try to find solutions of the form:

$$\psi(\mathbf{r},\sigma) \ = \ \sum_n F_n(\mathbf{r})\psi_{n,\mathbf{k_0}}(\mathbf{r},\sigma) \ . \tag{2.5}$$

In the formula above $\mathbf{k_0}$ is a fixed wave vector inside the Brillouin zone. Usually $\mathbf{k_0}$ is chosen at an extremum and in most cases at the Γ point. We therefore assume $\mathbf{k_0} = 0$ in the following. The functions $F_n(\mathbf{r})$ are called *envelope functions*. Using the Fourier expansion $F_n(\mathbf{r}) = \sum_{\mathbf{k}} \tilde{F}_n(\mathbf{k})e^{i\mathbf{k}\,\mathbf{r}}$ we have:

$$\begin{aligned}\psi(\mathbf{r},\sigma) \ &= \ \sum_{n,\mathbf{k}} \tilde{F}_n(\mathbf{k})e^{i\mathbf{k}\,\mathbf{r}}u_{n,0}(\mathbf{r},\sigma) \\ &= \ \sum_{n,\mathbf{k}} \tilde{F}_n(\mathbf{k})\varphi_{n,\mathbf{k}}(\mathbf{r},\sigma) \ ,\end{aligned} \tag{2.6}$$

a result that shows that the expansion (2.5) defining the envelope functions is quite general. In fact, it is not difficult to prove that $\varphi_{n,\mathbf{k}}(\mathbf{r},\sigma) = e^{i\mathbf{k}\,\mathbf{r}}u_{n,0}(\mathbf{r},\sigma)$ constitutes a complete set.

In the approximation of very slowly varying external potential, the envelope functions are slowly varying as well and in particular we can neglect the Fourier components of $F_n(\mathbf{r})$ outside the Brillouin zone. Following [24], the Shrödinger equation $\hat{H}\psi = E\psi$ can be rewritten in the following approximate form, involving thr envelope functions only:

$$\sum_m \left[T_{n,m}(-i\vec{\nabla})\, F_m(\mathbf{r})\right] + V(\mathbf{r})\, F_n(\mathbf{r}) = E\, F_n(\mathbf{r}) \ . \tag{2.7}$$

The first term has to be intended as $\sum_{\mathbf{k}\,m} T_{n,m}(\mathbf{k})\, \tilde{F}_m(\mathbf{k}) e^{i\mathbf{k}\,\mathbf{r}}$ where

$$T_{n,m}(\mathbf{k}) = \langle \varphi_{n,\mathbf{k}} | H_{crystal} | \varphi_{m,\mathbf{k}} \rangle \ . \tag{2.8}$$

This is an infinite set of coupled differential equations to be solved. Here n and m run over all the bands of the crystal. The motion of the electrons is determined by the external potential $V(\mathbf{r})$. The crystalline potential does not appear explicitly, but its effect is reflected in the kinetic energy operator $T_{n,m}$.

The simplest case of the effective mass approximation is obtained when it is sufficient to consider one band only. In fact, near a band maximum or minimum, the kinetic energy operator takes the form:

$$T_{n,n}(\mathbf{k}) \simeq \langle \psi_{n,\mathbf{k}}(\mathbf{r}) | H_{crystal} | \psi_{n,\mathbf{k}}(\mathbf{r}) \rangle = E_n(\mathbf{k}) \simeq \pm \frac{\hbar^2 \mathbf{k}^2}{2m} \ , \tag{2.9}$$

while in general a more complicated expression has to be considered.

2.2 Kane model

The Kane model considers only the top valence band and the lowest conduction band of common direct gap semiconductors such as $GaAs$. If we neglect the spin-orbit coupling, the upper valence band is six times degenerate. The orbital part transforms as Γ_5 and can be denoted as X, Y, Z, the remaining twofold degeneracy stemming from the spin degeneracy. The lower conduction band has only the spin degeneracy. The orbital part transforms as Γ_1 and is denoted as S. It is also convenient to construct combinations of valence band functions that diagonalize the spin

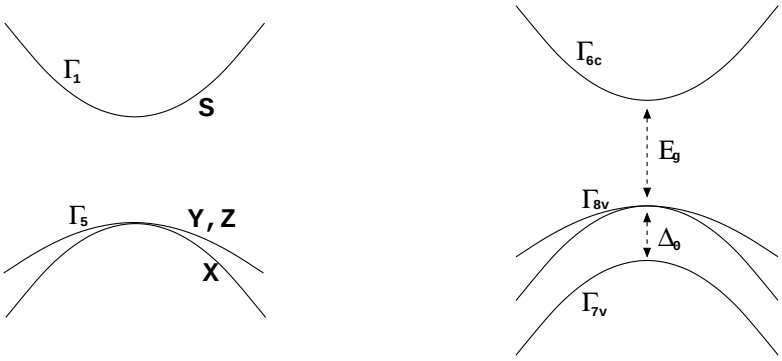

Figure 2.1. Bands considered in the Kane model, without and with spin-orbit.

orbit interaction. We have two irreducible representations: $\Gamma_5 \otimes \Gamma_6 = \Gamma_7 \oplus \Gamma_8$. The states are obtained as respectively $1/2$ and $3/2$ angular momentum combinations of the orbital functions with spin, i.e.

$$\begin{aligned} \psi^8_{\pm 1/2} &= \frac{2Z|\pm\rangle \mp (X \pm iY)|\mp\rangle}{\sqrt{6}} \\ \psi^8_{\pm 3/2} &= \frac{\mp(X \pm iY)|\pm\rangle}{\sqrt{2}} \\ \psi^7_{\pm 1/2} &= -\frac{(X \pm iY)|\mp\rangle \pm Z|\pm\rangle}{\sqrt{3}} \end{aligned} \tag{2.10}$$

The conduction band states transform as Γ_6 and the states are simply $\psi^6_{\pm 1/2} = S|\pm\rangle$.

The effective mass hamiltonian $(T_{n,m} + V\delta_{n,m})$ can be obtained using the formula:

$$T_{n,m}(\mathbf{k}) = \left(E_n(0) + \frac{\hbar^2\mathbf{k}^2}{2m_0}\right)\delta_{n,m} + \frac{\hbar}{m_0}\,\mathbf{k}\cdot\boldsymbol{\pi}_{n,m}\ , \tag{2.11}$$

where $\boldsymbol{\pi} = \mathbf{p} + \frac{\hbar}{4m_0c^2}\,\boldsymbol{\sigma}\times\vec{\nabla}V_{crystal}$. As a further simplifications we also take $\boldsymbol{\pi}_{n,m} \simeq \mathbf{p}_{n,m}$ and the matrix elements of $\mathbf{p}$ between X, Y, Z and S can be all expressed in terms of the single parameter $P = \frac{\hbar}{m_0}\langle S|p_z|Z\rangle$ (we use a phase choice such that S is purely imaginary and P real). We can also neglect the term $\frac{\hbar^2\mathbf{k}^2}{2m_0}$ because the bare electron mass is usually much larger compared to the effective mass in semiconductors. The final result is expressed in Table 2.1.

There E_g and Δ_0 are the fundamental energy gap and the spin-orbit splitting of the valence band. We note that the only place where we did not neglect the spin-orbit

Table 2.1
Explicit expression of $T(\mathbf{k})$ for the Kane model.

$$\begin{pmatrix}
0 & 0 & \frac{-1}{\sqrt{2}}Pk_+ & \sqrt{\frac{2}{3}}Pk_z & \frac{1}{\sqrt{6}}Pk_- & 0 & \frac{-1}{\sqrt{3}}Pk_z & \frac{-1}{\sqrt{3}}Pk_- \\
0 & 0 & 0 & \frac{-1}{\sqrt{6}}Pk_+ & \sqrt{\frac{2}{3}}Pk_z & \frac{1}{\sqrt{2}}Pk_- & \frac{-1}{\sqrt{3}}Pk_+ & \frac{1}{\sqrt{3}}Pk_z \\
\frac{-1}{\sqrt{2}}Pk_- & 0 & -E_g & 0 & 0 & 0 & 0 & 0 \\
\sqrt{\frac{2}{3}}Pk_z & \frac{-1}{\sqrt{6}}Pk_- & 0 & -E_g & 0 & 0 & 0 & 0 \\
\frac{1}{\sqrt{6}}Pk_+ & \sqrt{\frac{2}{3}}Pk_z & 0 & 0 & -E_g & 0 & 0 & 0 \\
0 & \frac{1}{\sqrt{2}}Pk_+ & 0 & 0 & 0 & -E_g & 0 & 0 \\
\frac{-1}{\sqrt{3}}Pk_z & \frac{-1}{\sqrt{3}}Pk_- & 0 & 0 & 0 & 0 & -E_g-\Delta_0 & 0 \\
\frac{-1}{\sqrt{3}}Pk_+ & \frac{1}{\sqrt{3}}Pk_z & 0 & 0 & 0 & 0 & 0 & -E_g-\Delta_0
\end{pmatrix}$$

interaction are the diagonal terms of the above hamiltonian, where the parameter Δ_0 appears. We used the notation $k_\pm = k_x \pm ik_y$, where $\mathbf{k} = -i\vec{\nabla}$. In the presence of a magnetic field we have $\mathbf{k} = (-i\vec{\nabla} + \frac{e}{\hbar}\mathbf{A})$ instead, from where the commutation relations $\mathbf{k} \times \mathbf{k} = -i\frac{e\mathbf{B}}{\hbar}$ follow.

The form of the matrix operator is simple enough that the valence band components can be eliminated by substitution. The following hamiltonian is obtained for conduction band electrons [3]:

$$\begin{aligned}\hat{H}_0 = &\left[\frac{1}{E_g + \Delta_0 + E - V} + \frac{2}{E_g + E - V}\right] \frac{P^2}{3}\, \mathbf{k}^2 + V(\mathbf{r}\,) + \\ &+ \left[\frac{1}{E_g + \Delta_0 + E - V} - \frac{1}{E_g + E - V}\right] \frac{P^2}{3}\frac{e}{\hbar}\, \boldsymbol{\sigma} \cdot \mathbf{B} + \\ &+ \left[\frac{1}{(E_g + \Delta_0 + E - V)^2} - \frac{1}{(E_g + E - V)^2}\right] \frac{P^2}{3}\, \boldsymbol{\sigma} \cdot \vec{\nabla} V(\mathbf{r}) \times \mathbf{k} + \\ &+ \left[\frac{1}{(E_g + \Delta_0 + E - V)^2} + \frac{2}{(E_g + E - V)^2}\right] \frac{P^2}{3}\, (-i\, \vec{\nabla} V(\mathbf{r}) \cdot \mathbf{k})\ ,\end{aligned} \tag{2.12}$$

which contains the Zeeman term, the spin-orbit interaction and the Darwin term. Using the fact that typically $(E - V) \ll E_g$ we obtain the following two important formulas, estimating the effective mass and the effective g-factor:

$$\frac{1}{2m} = \frac{1}{2m_0} + \left[\frac{1}{E_g + \Delta_0} + \frac{2}{E_g}\right] \frac{P^2}{3\hbar^2}\ , \tag{2.13}$$

$$g\ = 2 + \left[\frac{1}{E_g + \Delta_0} - \frac{1}{E_g}\right] \frac{P^2}{3\hbar}\frac{2e}{\mu_B}\ , \tag{2.14}$$

in which the bare values are taken in account. In a Quantum Well the term in the third line of Eq. (2.12) gives rise to the so called Rashba spin-orbit, which we discuss in more detail in the next section.

2.3 Rashba spin-orbit

We consider now electrons confined by an asymmetric potential $V(z)$, of which the gradient is in the $\hat{z}$ direction. The Darwin term does not introduce any kind of

spin-splitting and will be neglected in the following. In the absence of magnetic field the (2.12) simplifies to the following form:

$$\hat{H}_0 = \frac{\hat{\mathbf{p}}^2}{2m} + \alpha(\hat{\sigma}_x\hat{p}_y - \hat{\sigma}_y\hat{p}_x) \ , \tag{2.15}$$

where $\hat{\sigma}_i$ are Pauli matrices. We considered the external potential acting as an average electric field [1] $\langle\vec{\nabla}V/e\rangle \simeq \mathcal{E}_z\hat{z}$ and the coupling constant of the Rashba spin orbit term is approximately given by:

$$\hbar\alpha = \left[\frac{1}{E_g^2} - \frac{1}{(E_g+\Delta_0)^2}\right]\frac{P^2 e}{3}\,\mathcal{E}_z \ . \tag{2.16}$$

We notice that the strength of the spin-orbit coupling is proportional to $\mathcal{E}_z$ and therefore can in principle be controlled from an external gate.

We estimated the spin-orbit coupling strength for common III-V semiconductors using Eq. (2.16). The parameter P can be calculated using (2.13) from the directly accessible quantities m, E_g and Δ_0 and the results are collected in Table 2.2. The maximum electric field can be estimated as $\mathcal{E}_z = 2\pi ne/\epsilon$, where a typical value of the electron density is $n = 10^{12}\,\mathrm{cm}^{-2}$ is used to obtain the values of Table 2.2. A sense of the reliability of the results for $\hbar\alpha$ can be obtained by comparing the values for the effective g-factor to the experimental measurements: for large gap semiconductors the order of magnitude of the estimate is correct, but contributions from remote bands are important while for small gap semiconductors the g-factor is fairly large and the estimate is quite satisfactory. A similar situation is expected for $\hbar\alpha$.

In the last part of the table we list other quantities that will be of special relevance in the following Chapters. In particular, the density parameter is given by $r_s = 1/\sqrt{\pi n a_B^2})$, where a_B is the effective Bohr radius. We notice that, unfortunately, for small gap III-V semiconductors it is difficult to achieve large values of the density parameter r_s, due to the small effective mass, and large effects from electron-electron interactions are not expected.

[1] According to the Ando argument the electric field is vanishing small, due to the fact that $\langle\nabla V\rangle = 0$ for an eigenstate of $\hat{p}^2/2m + \hat{V}$. However, the potential entering the spin-orbit term is the one relative to the valence band. Due to different band offsets in an heterostructure, this is in general different from the confining potential for the electrons and a non-vanishing spin-orbit is obtained. We refer to [3] for a more detailed discussion of this rather subtle point.

Table 2.2
Estimates for several quantities of common III-V semiconductors.

		GaAs	AlAs	InSb	InAs	AlSb
m/m_0		0.0665	0.150	0.0139	0.0229	0.120
E_g	(eV)	1.519	3.13	0.237	0.418	2.384
Δ_0	(eV)	0.341	0.300	0.810	0.380	0.673
ϵ	(eV)	12.4	10.06	17.9	14.6	12.04
P	(eV Å)	9.30	8.34	9.29	8.99	8.48
$\mathcal{E}_z$	(MV/m)	7.30	8.99	5.05	6.20	7.51
g		0.17	1.65	-47.3	-14.1	0.838
g_{exp}		-0.44	1.52	-51.56	-14.9	0.843
$\hbar\alpha$	(meV Å)	3.04	0.36	245.7	69.3	1.24
r_s		0.57	1.59	0.083	0.167	1.06
$\bar{\alpha}$		0.0026	0.0002	0.31	0.07	0.001
χ		0.0021	0.0006	0.036	0.017	0.0016

A way to measure the spin orbit coupling is offered by the study of the Shubnkov-de Haas oscillations [25–28]. A simple semiclassical argument gives that the frequency of such magneto-oscillations due to electrons in a subband is proportional to its population. If the spin up/down subbands have the same population, only one frequency is observed but the Rashba spin-orbit lifts the spin degeneracy, and a beating pattern in the oscillations is observed due to the slightly different populations of the two subbands. The control of α from an external gate was also experimentally demonstrated [11, 12]. The measured values of $\hbar\alpha$ are consistent with Table 2.2.

2.4 Noninteracting ground state

We first discuss the eigenstates and eigenvalues of $\hat{H}_0$. These are easily obtained by noticing that the eigenfunctions are plane waves with wave-vector $\mathbf{k}$. Therefore the Rashba term becomes of the form $-\hbar\alpha\, k\, \hat{\phi}_{\mathbf{k}} \cdot \boldsymbol{\sigma}$, where $\hat{\phi}_{\mathbf{k}} = \frac{(-k_y, k_x)}{k}$ is an azimuthal unit vector perpendicular to $\mathbf{k}$ (in the counterclockwise direction). In the following we will use $\hat{s}_{\mathbf{k}}$ to denote the spin quantization axis of plane wave states with wavevector $\mathbf{k}$. For the noninteracting case we simply have $\hat{s}_{\mathbf{k}} = \hat{\phi}_{\mathbf{k}}$. In particular:

$$\varphi_{\mathbf{k},\pm}(\mathbf{r}) = \frac{e^{i\mathbf{k}\cdot\mathbf{r}}}{\sqrt{2L^2}} \begin{pmatrix} \pm 1 \\ i e^{i\phi_{\mathbf{k}}} \end{pmatrix} , \tag{2.17}$$

where L is the linear size of the system and $\phi_{\mathbf{k}}$ is the polar angle between $\mathbf{k}$ and the x-axis. The corresponding eigenvalues are:

$$\epsilon_{\mathbf{k}\pm} = \frac{\hbar^2\mathbf{k}^2}{2m} \mp \hbar\alpha\, k \ . \tag{2.18}$$

The energy surfaces and the spin quantization of these single particle eigenstates are shown in Figure 2.2. We notice that there are two energy subbands with opposite chirality: by definition, a state with positive chirality has the spin oriented counterclockwise. Without loss of generality we assume from now on $\alpha > 0$, so that states with positive chirality have lower energy.

We consider now many-body noninteracting states, which are Slater determinants constructed with the single particle-states (2.17). The ground state is obtained by

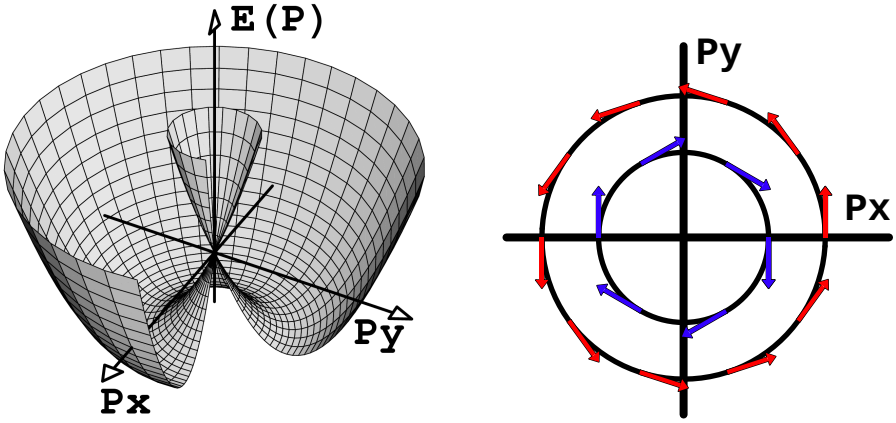

Figure 2.2. Noninteracting energies and states.

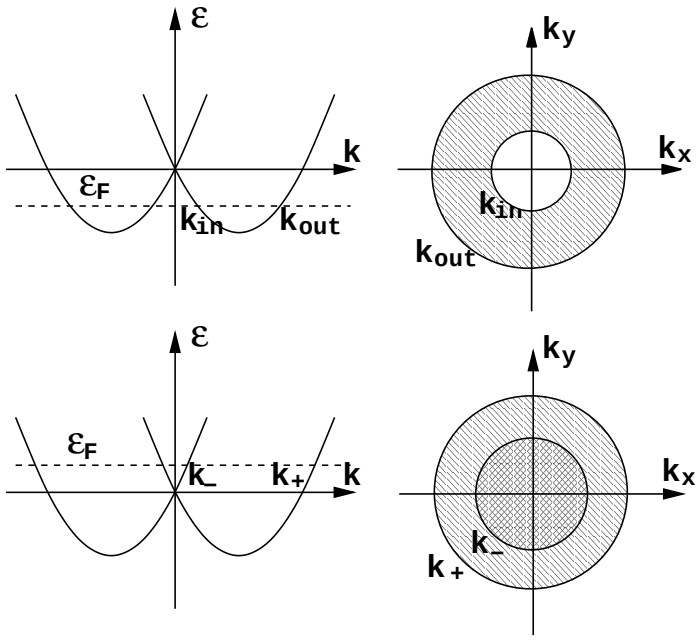

Figure 2.3. Two different ways to occupy states in momentum space.

occupying the lowest N states up to the Fermi energy ϵ_F, and two different cases can occur, as depicted in Figure 2.3. When the electron density is small we have that $\epsilon_F < 0$. Only the lower branch is occupied and the occupied states form a ring in the momentum space, where k_{in} and k_{out} are the inner and outer radii. Above a certain density value we have that $\epsilon_F > 0$ and the occupation of each of the two branches is a circle with radius $k_{\pm}$. The difference of the two radii is the constant $k_+ - k_- = 2m\alpha/\hbar$.

2.5 The generalized chirality

It is natural to define the chiral polarization (or *chirality*) in terms of the occupations $N_{\pm}$ of each band:

$$\chi_0 = \frac{N_+ - N_-}{N_+ + N-} \ . \tag{2.19}$$

This definition is useful for high density states, when two bands are occupied and $\chi_0 \leq 1$. On the other end, when $\epsilon_F < 0$ only the lowest branch is occupied, and $\chi_0 = 1$ irrespective of the density. Therefore it is useful to define the following quantity, which we will refer to as the *generalized chirality*:

$$\chi = \begin{cases} \chi_0 & \text{for } 0 \leq \chi_0 < 1 \\ \frac{k_{out}^2 + k_{in}^2}{k_{out}^2 - k_{in}^2} & \text{for } \chi_0 = 1 \end{cases} \ , \tag{2.20}$$

which together with the electron density n completely specifies the geometrical parameters that characterize the occupation in momentum space:

$$k_{\pm} = \sqrt{2\pi n(1 \pm \chi)} \qquad \text{for } 0 \leq \chi < 1 \ , \tag{2.21}$$

$$k_{out/in} = \sqrt{2\pi n(\chi \pm 1)} \qquad \text{for } \chi \geq 1 \ . \tag{2.22}$$

The usefulness of the generalized chirality lies in the fact that, once the density n is fixed, χ parameterizes a large class of Slater determinants with isotropic, compact occupation of the type depicted in Figure 2.3. These isotropic, compact occupations correspond in general to excited states, the ground state being determined by the particular value of χ that minimizes the energy.

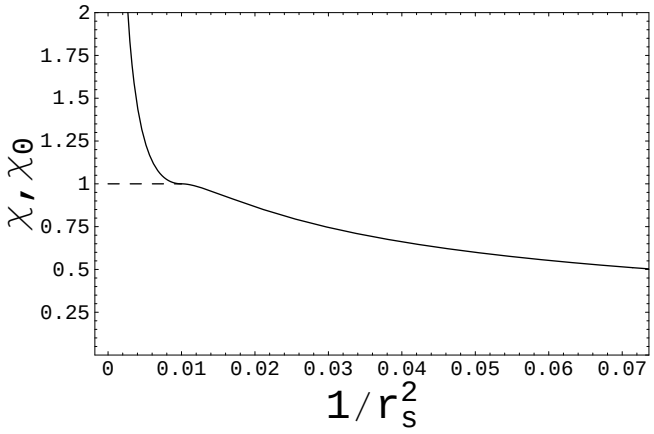

Figure 2.4. Plot of χ (solid) and χ_0 (dashed) as function of the density for the noninteracting ground state at $\bar{\alpha} = 0.1$

When $0 \leq \chi < 1$ total energy per particle in Ry units can be expressed as:

$$\mathcal{E}_0(\bar{\alpha}, r_s, \chi) = \frac{(1+\chi^2) - (\chi-1)^2\theta(\chi-1)}{r_s^2} + \bar{\alpha}\,\frac{2\sqrt{2}}{r_s}\,\frac{\sqrt{|1-\chi|^3} - \sqrt{|1+\chi|^3}}{3}\ , \quad (2.23)$$

where r_s is the density parameter $r_s = 1/\sqrt{\pi n a_B^2}$ and we introduced the dimensionless spin-orbit coupling $\bar{\alpha} = \frac{\hbar\alpha}{e^2}$. The first term is the kinetic energy and the second the Rashba contribution.

By imposing the minimum condition $\partial\mathcal{E}_0/\partial\chi = 0$, we obtain the desired value of the generalized chirality for the noninteracting ground state:

$$\chi^{(0)}_{min}(\bar{\alpha}, r_s) = \begin{cases} \bar{\alpha} r_s \sqrt{2 - (\bar{\alpha} r_s)^2} & \text{for } 0 \leq \bar{\alpha} r_s < 1 \\ \frac{1}{2}\left[(\bar{\alpha} r_s)^2 + \frac{1}{(\bar{\alpha} r_s)^2}\right] & \text{for } \bar{\alpha} r_s \geq 1 \end{cases}\ , \quad (2.24)$$

We show in Figure 2.4 the plot of $\chi^{(0)}_{min}(\bar{\alpha}, r_s)$ as function of the density, for a particular value of the spin-orbit coupling $\bar{\alpha}$.

2.6 Effect of a Zeeman term

We consider now the effect of an external magnetic field. This is treated by adding to the hamiltonian (2.15) a perturbing Zeeman term

$$\hat{H}_Z = \frac{g\mu_B}{2}\,\mathbf{B}\cdot\hat{\boldsymbol{\sigma}}\ , \quad (2.25)$$

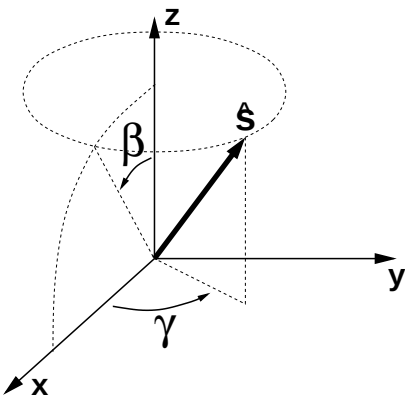

Figure 2.5. Orientation of the spin quantization axis $\hat{s}_{\mathbf{k}}$.

while smaller orbital magnetic effects are neglected. The eigenfunctions of the perturbed hamiltonian are plane waves, while the spin has to be quantized along a direction $\hat{s}_{\mathbf{k}}$ which results from the combined effect of the Rashba spin-orbit and the Zeeman term. The orientation of $\hat{s}_{\mathbf{k}}$ is determined by the polar and azimuthal angles $\beta_{\mathbf{k}}$ and $\gamma_{\mathbf{k}}$, which are defined in Figure 2.5. Notice that the choice $\gamma_{\mathbf{k}} = \phi_{\mathbf{k}} + \frac{\pi}{2}$ and $\beta_{\mathbf{k}} = \frac{\pi}{2}$ leads to the eigenstates of $\hat{H}_0$ of Eq. (2.17).

More explicitly, if we consider a magnetic field $\mathbf{B} = B\hat{z}$ perpendicular to the plane of motion we obtain $\gamma_{\mathbf{k}} = \frac{\pi}{2}$ and $\beta_{\mathbf{k}}$ is determined by $\tan\beta_{\mathbf{k}} = -\frac{2\hbar\alpha\, k}{g\mu_B B}$. The corresponding eigenenergies are also easily obtained:

$$\epsilon^{\perp}_{\mathbf{k}\pm} = \frac{\hbar^2\mathbf{k}^2}{2m} \mp \sqrt{(\hbar\alpha\, k)^2 + \left(\frac{g\mu_B B}{2}\right)^2}\,. \tag{2.26}$$

For a magnetic field $\mathbf{B} = B\hat{y}$ in the plane of motion we obtain $\beta_{\mathbf{k}} = \frac{\pi}{2}$ and $\gamma_{\mathbf{k}}$ is determined by $\tan(\gamma_{\mathbf{k}} - \phi_{\mathbf{k}}) = \frac{g\mu_B B\cos\phi_{\mathbf{k}} - 2\hbar\alpha\, k}{g\mu_B B\sin\phi_{\mathbf{k}}}$, while the eigenenergies are given by:

$$\epsilon^{\parallel}_{\mathbf{k}\pm} = \frac{\hbar^2\mathbf{k}^2}{2m} \mp \sqrt{\left(\hbar\alpha\, k - \frac{g\mu_B B}{2}\cos\phi_{\mathbf{k}}\right)^2 + \left(\frac{g\mu_B B}{2}\sin\phi_{\mathbf{k}}\right)^2}\,. \tag{2.27}$$

An important difference between the two cases is that for a transverse magnetic field the degeneracy at $\mathbf{k} = 0$ is removed and the two bands are separated by a finite gap. Instead, in the in plane case the degeneracy point is displaced from the origin in

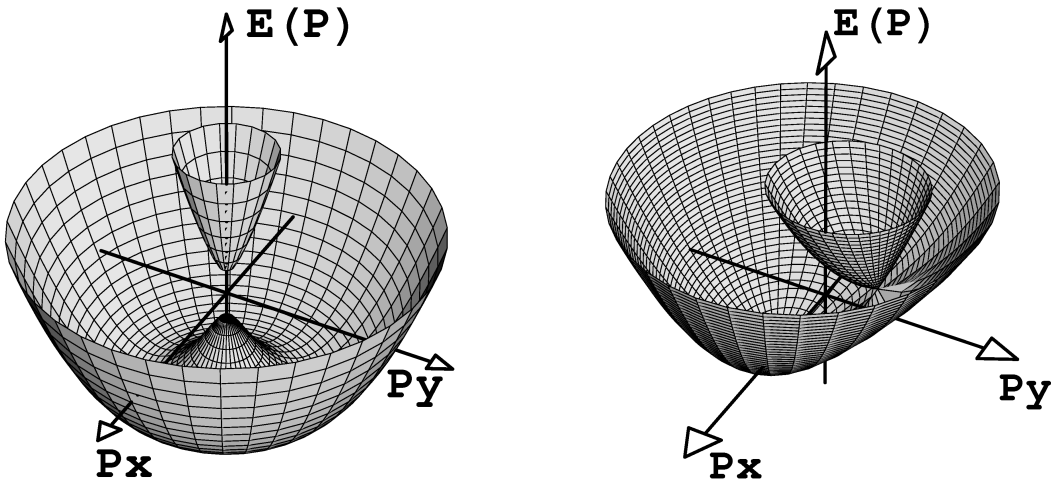

Figure 2.6. Noninteracting single particle bands in the presence of an external magnetic field. Left: transverse magnetic field. Right: in plane magnetic field along the x-axis.

a direction perpendicular to the magnetic field, and in particular at the wavevector such that $k_x = \frac{g\mu_B B}{2\hbar\alpha}$. Furthermore, because of the in plane anisotropy introduced by the magnetic field, the circular symmetry of the bands is lost. We show in Figure 2.6 two examples illustrating these two different situations.

The spin susceptibility is obtained with a straightforward calculation from the perturbed eigenfunctions, with spin oriented as discussed above, and the new occupation numbers, as determined by (2.26) and (2.27) and the Fermi energy ϵ_F. The final result is:

$$\chi_{S0}^{\parallel(\perp)}(\bar{\alpha}, r_s) = \begin{cases} \chi_P & \text{for } 0 \leq \bar{\alpha} r_s < 1 \\ \frac{\chi_P}{(r_s\bar{\alpha})^2} & \text{for } \bar{\alpha} r_s \geq 1 \end{cases} , \tag{2.28}$$

where $\chi_P = \frac{m}{\pi\hbar^2}\left(\frac{g\mu_B}{2}\right)^2$ is the usual Pauli susceptibility.

Another quantity of some interest is the adiabatic spin susceptibility $\tilde{\chi}_S$, which is obtained by calculating the magnetization due to the perturbation of the wavefunctions only, while using the unperturbed occupation numbers. In this case the result

is different for the two orientations of the magnetic field and to linear order in B we get:

$$\tilde{\chi}_{S0}^{\perp} = \chi_S \ , \tag{2.29}$$

$$\tilde{\chi}_{S0}^{\parallel} = \chi_S/2 \ . \tag{2.30}$$

3. Structural spin-orbit coupling for two-dimensional holes

We consider in this Chapter the form of the spin-orbit interaction for two-dimensional heavy holes in a typical III-V semiconductor, and in particular for the case of $GaAs$. The holes are described in the framework of the Luttinger hamiltonian [29], from which the form of the spin-orbit coupling produced by an asymmetric confinement can be derived. It is found that the spin-orbit coupling is approximately cubic in the holes wavevector, as opposed to the Rashba spin-orbit of Eq. (2.1).

We also examine the effect of an in-plane magnetic field which, besides contributions independent of the hole momentum (analogous to the familiar Zeeman term), introduces a peculiar form of quadratic spin-orbit. Finally, we discuss the noninteracting properties in the presence of a suitable generalized spin-orbit coupling, which covers all the relevant spin-orbit terms discussed in this and in the previous Chapter.

3.1 Luttinger hamiltonian

The topmost valence bands of bulk $GaAs$ are characterized by a fourfold degeneracy at the Γ point, due to the Γ_8 cubic symmetry (see Figure 2.1). The holes can be described as having an effective spin $J = \frac{3}{2}$ and the hamiltonian is given by [29]:

$$H_{\Gamma_8} = \frac{\hbar^2}{2m_0}\left\{\gamma_1 k^2 - 2\gamma_2[(J_x^2 - \frac{1}{3}J^2)k_x^2 + \text{c.p.}] - \gamma_3[\{J_x, J_y\}\{k_x, k_y\} + \text{c.p.}]\right\} \ , \quad (3.1)$$

where m_0 is the bare electron mass, $\{a,b\} = ab + ba$ and c.p. refers to additional terms obtained by cyclic permutations of (x,y,z). The explicit form of the spin-3/2 matrices is:

$$J_x = \begin{pmatrix} 0 & \frac{\sqrt{3}}{2} & 0 & 0 \\ \frac{\sqrt{3}}{2} & 0 & 1 & 0 \\ 0 & 1 & 0 & \frac{\sqrt{3}}{2} \\ 0 & 0 & \frac{\sqrt{3}}{2} & 0 \end{pmatrix} , \quad J_y = \begin{pmatrix} 0 & -\frac{\sqrt{3}}{2}i & 0 & 0 \\ \frac{\sqrt{3}}{2}i & 0 & -i & 0 \\ 0 & i & 0 & -\frac{\sqrt{3}}{2}i \\ 0 & 0 & \frac{\sqrt{3}}{2}i & 0 \end{pmatrix} , \quad J_z = \begin{pmatrix} \frac{3}{2} & 0 & 0 & 0 \\ 0 & \frac{1}{2} & 0 & 0 \\ 0 & 0 & -\frac{1}{2} & 0 \\ 0 & 0 & 0 & -\frac{3}{2} \end{pmatrix} , \tag{3.2}$$

and the Luttinger parameters for $GaAs$ have the following values [30]:

$$\gamma_1 = 6.85 \qquad \gamma_2 = 2.10 \qquad \gamma_3 = 2.90 \ . \tag{3.3}$$

Degenerate states at the Γ point with $J_z = \pm\frac{3}{2}$ or $J_z = \pm\frac{1}{2}$ are denoted as *heavy holes* (HH) and *light holes* (LH). At finite wavevector the degeneracy between HH and LH is removed and off-diagonal terms of (3.1) introduce HH-LH mixing. A common approximation is to consider $\gamma_2 \simeq \gamma_3 \simeq \tilde{\gamma}$, which leads to a spherically symmetric hamiltonian:

$$H'_{\Gamma_8} = \frac{\hbar^2}{2m_0}\left[(\gamma_1 + \frac{5}{2}\tilde{\gamma})\,k^2 - 2\tilde{\gamma}(\mathbf{J}\cdot\mathbf{k})^2\right] \ . \tag{3.4}$$

We will use $\tilde{\gamma} = (\gamma_2 + \gamma_3)/2 = 2.5$ in the case of $GaAs$.

3.2 Cubic spin-orbit coupling

We now consider a potential that confines the holes along a spatial direction. The external potential removes the fourfold degeneracy at the Γ point, and the two-dimensional subbands have a twofold degeneracy at $\mathbf{k} = 0$. In the same way as in the previous Chapter, the twofold degeneracy is removed at finite wavevectors if the confinement is asymmetric, and the spin splitting is approximately proportional to the external electric field[1].

[1]This is the case when the heavy hole-light hole subband splitting is independent of the field. See however the discussion in Ref. [31]

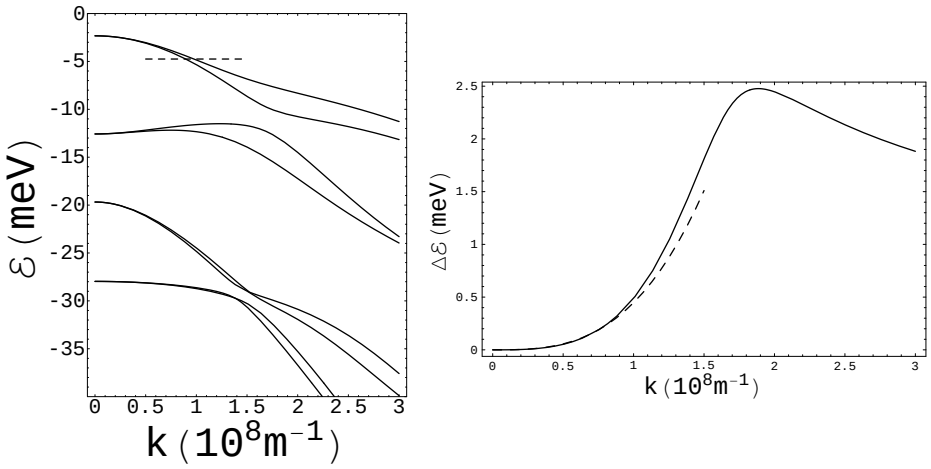

Figure 3.1. Left: Two dimensional energy subbands for holes in a $W = 150\,\text{Å}$ thick $GaAs$ quantum well, in the spherical approximation. The electric field is $\mathcal{E}_z = 1$ MV/m and the dashed line is a Fermi energy corresponding to a total density of holes $n = 1.4\ 10^{11}$ cm^{-1}, as in Ref. [4]. Right: spin splitting of the two highest subbands. The dashed line is the cubic approximation given by Eqs. (3.7) and (3.8).

To exemplify this point we consider a model calculation of holes confined by infinite barriers, while the electric field is uniform inside the quantum well:

$$V(\mathbf{r}) = \begin{cases} \mathcal{E}_z e z \,\text{if}\ \ 0 \le z \le W \\ +\infty \,\text{otherwise} \end{cases} , \tag{3.5}$$

where W is the thickness of the quantum well.

For simplicity, we restrict ourselves to the spherical approximation of the Luttinger hamiltonian, as given in (3.4). The spectrum can be obtained by straightforward numerical diagonalization of H'_{Γ_8} in the complete set:

$$\psi_{n\mathbf{k}}(\mathbf{r}, J_z) = \frac{e^{-i\mathbf{k}\cdot\mathbf{r}}}{\sqrt{L^2}} \sqrt{\frac{2}{W}} \sin\frac{n\pi z}{W} \left|J_z\right\rangle , \tag{3.6}$$

where $\mathbf{k}$ is in the x, y plane and L is the linear size of the two-dimensional system. The result is plotted in the first panel of Figure 3.1, for the case of $GaAs$ and a particular choice of the parameters $W = 150$ Å and $\mathcal{E}_z = 1$ MV/m.

As it is shown in the second panel of Figure 3.1, the spin splitting is not linear. The form of the spin-orbit coupling can be obtained approximately using the unperturbed solutions at zero in-plane wavevector [3]. In fact, Eq. (3.4) simplifies to $\frac{\hbar^2}{2m_0}\left[\gamma_1+\tilde{\gamma}(\frac{5}{2}-2\tilde{\gamma}J_z^2)\right]\hat{k}_z^2$, which is immediately diagonalized by the eigenfunctions $\psi_{n\mathbf{0}}(\mathbf{r},J_z)$ as in (3.6). Standard perturbative treatment at small in-plane wavevectors $\mathbf{k}$ and electric field $\mathcal{E}_z$ allows one to obtain the following spin-orbit contribution:

$$\hat{H}_0=\frac{\hat{\mathbf{p}}^2}{2m}+\frac{i\gamma}{2}\left(\hat{p}_-^3\hat{\sigma}_+-\hat{p}_+^3\hat{\sigma}_-\right)\,, \tag{3.7}$$

where $\hat{p}_\pm=\hat{p}_x\pm i\hat{p}_y$ and $\hat{\sigma}_\pm=\hat{\sigma}_x\pm i\hat{\sigma}_y$. As anticipated, the spin-orbit term has a cubic dependence in the hole momentum.

The explicit value of the spin-orbit coupling is

$$\gamma=\frac{512\,e\,\tilde{\gamma}^2\,W^4}{9\hbar^3\pi^6\,(\gamma_1-2\,\tilde{\gamma})(3\gamma_1+10\,\tilde{\gamma})}\,\mathcal{E}_z\,, \tag{3.8}$$

which gives $\hbar^3\gamma\simeq 200$ eVÅ^3 with the parameters of Figure 3.1. As it can be seen in the second panel, the perturbative formula is in good agreement with the exact result. Furthermore, the spin-orbit splitting in our crude model is comparable to the experimental findings. In fact, we find from Figure 3.1 that the difference of the Fermi wavevectors of the two branches is $\Delta p_F=5.4\times10^{-9}\,\mathrm{eV\,s/m}$, compared to the experimental value $\Delta p_F=14\times10^{-9}\,\mathrm{eV\,s/m}$ of Ref. [4].

3.3 Effect of an in-plane magnetic field

We obtain and discuss here spin dependent contributions to the effective hamiltonian appropriate to the highest two-dimensional heavy hole subband in the presence of an in-plane magnetic field $\mathbf{B}=B_x\hat{x}+B_y\hat{y}$. We show that the magnetic field introduces a spin-orbit coupling quadratic in the hole momentum.

As in the previous section, we begin by approximately describing the motion of the holes in the bulk through the spherical approximation of the Luttinger hamiltonian [29], given in Eq. (3.4). Within this context the effect of the magnetic field can be described by introducing the Zeeman hamiltonian $\hat{H}_Z=-2\kappa\,\mu_B\,\mathbf{B}\cdot\hat{\mathbf{J}}$, where for $GaAs$

$\kappa = 1.2$. Orbital effects are treated by including the vector potential in the following convenient form: $\mathbf{A} = zB_y\hat{x} - zB_x\hat{y}$.

For simplicity we consider again the confinement associated with an infinite rectangular well of width W. The corresponding effective hamiltonian for holes in the highest two-dimensional subband can be written as:

$$\hat{H}_0 + \delta\hat{H}_{21} + \delta\hat{H}_{03} \ , \tag{3.9}$$

where $\hat{H}_0$ is the unperturbed effective hamiltonian (at $\mathbf{B} = 0$), which is approximately expressed by Eq. (3.7). $\delta\hat{H}_{21}$, $\delta\hat{H}_{03}$ are spin dependent terms associated with the external magnetic field. The sub-indices indicate respectively the power of the dependence on the hole momentum and the magnetic field. Their explicit form can be found by making use of perturbation theory in $\mathbf{B}$ and in the wave vector $\mathbf{k}$, in a way similar to the derivation of the cubic spin-orbit appearing in Eq. (3.7) [3]. For the first term we obtain:

$$\delta\hat{H}_{21} = \frac{a\mu_B W^2}{\pi^2\hbar^2}\,\frac{B_+p_+^2\hat{\sigma}_- + B_-p_-^2\hat{\sigma}_+}{2} \ , \tag{3.10}$$

where $B_\pm = B_x \pm iB_y$ and the explicit form of the numerical coefficient is given by $a = \frac{1024\tilde{\gamma}^2}{9\pi^2(3\gamma_1+10\tilde{\gamma})} - \frac{3\kappa}{2}$. For the second term we find:

$$\delta\hat{H}_{03} = b\mu_B^3\left(\frac{m_0W^2}{\pi^2\hbar^2}\right)^2\,\frac{B_+^3\hat{\sigma}_- + B_-^3\hat{\sigma}_+}{2} \ , \tag{3.11}$$

where $b = \frac{\kappa(\pi^2-6)}{2} - \frac{27\tilde{\gamma}^2}{8(2\gamma_1+5\tilde{\gamma})}$. We should remark that the present results do differ from the ones one would infer from the corresponding formulas appearing in Ref. [3]. For $GaAs$ we have $a \simeq -0.2$ and $b \simeq 1.5$.

For a given growth direction, these results can be extended beyond the spherical approximation to include the appropriate cubic anisotropy as for instance done in Ref. [3]. Following this procedure one then obtains in (3.9) an additional anisotropic linear Zeeman term. By choosing coordinates along the principal axes, this can be generally expressed as:

$$\delta\hat{H}_{01} = \frac{\mu_B}{2}(g_xB_x\hat{\sigma}_x + g_yB_y\hat{\sigma}_y) \ . \tag{3.12}$$

As it turns out, this term vanishes (even beyond the spherical approximation) for the high symmetry growth directions [100] and [111]. However, in the case of the experimentally relevant [113] growth direction, (3.12) is non vanishing and the principal axes x and y are along the $[1\bar{1}0]$ and $[33\bar{2}]$ respectively. A perturbative estimate of the suitable Landé g-factors for the case of an infinite rectangular well gives $g_x \simeq -0.17$ and $g_y \simeq 0.41$ [3].

3.4 Generalized spin-orbit coupling

We consider here a formulation that elegantly includes all the possible forms of spin-orbit coupling discussed so far. We introduce the following single-particle hamiltonian:

$$\hat{H}_{0,n} = \frac{\hat{\mathbf{p}}^2}{2m} + i\gamma \frac{(\hat{p}_-)^n \hat{\sigma}_+ - (\hat{p}_+)^n \hat{\sigma}_-}{2} \ , \tag{3.13}$$

the motion taking place in the x, y plane. In Eq. (3.13) we have $\hat{p}_\pm = \hat{p}_x \pm i\hat{p}_y$ and $\hat{\sigma}_\pm = \hat{\sigma}_x \pm i\hat{\sigma}_y$, while n is an integer number assuming values from 0 to 3. In view of its structure we will refer to the second term in (3.13) as a generalized spin-orbit coupling.

In the simplest case, $n = 0$ corresponds to the familiar Zeeman coupling with $\gamma = \frac{g\mu_B B}{2}$ while, for $n > 0$, Eq. (3.13) describes different types of bona fide spin-orbit interactions. For $n = 1$ we obtain a form equivalent to the Rashba [14, 15] or Dresselhaus [13] spin-orbit hamiltonians discussed in the previous Chapter while $\delta\hat{H}_{21}$ and $\delta\hat{H}_{03}$ are of the type $n = 2$ and $n = 0$ respectively.

Because of the isotropy implied by the spherical approximation, the value of the corresponding coupling strength γ extracted by comparison to (3.13) only depends on the magnitude of the magnetic field B and is immediately found to be:

$$\gamma_{21} = \frac{a\mu_B W^2 B}{\pi^2\hbar^2} \ , \tag{3.14}$$

and

$$\gamma_{03} = b\mu_B^3 \left(\frac{W^2 m_0}{\pi^2\hbar^2}\right)^2 B^3 \ , \tag{3.15}$$

for $\delta\hat{H}_{21}$ and $\delta\hat{H}_{03}$ respectively.

The coupling strength γ of the $n = 0$ term $\hat{H}_{01}$ of Eq. (3.12) depends on the direction of the magnetic field, and is given by:

$$\gamma_{01}^{i} = \frac{g_i \, \mu_B}{2} B \ , \tag{3.16}$$

for the particular case of an external field of magnitude B along one of the two principal axes ($i \equiv x$ or y).

Finally, the $n = 3$ term of (3.13) corresponds to the cubic Rashba spin-orbit coupling of Eq. (3.7) and the value of γ is given in (3.8).

3.5 Non interacting ground state

We now discuss the non interacting problem in the presence of generalized spin-orbit and introduce the important concept of generalized polarization. The eigenstates of (3.13) are plane waves, a fact that allows one to write the spin-orbit term in the form $-\gamma \, (\hbar k)^n \, \boldsymbol{\sigma} \cdot \hat{s}_{\mathbf{k}}$, where $\hat{s}_{\mathbf{k}}$ is defined as follows:

$$\hat{s}_{\mathbf{k}} = -\sin(n\phi_{\mathbf{k}})\hat{x} + \cos(n\phi_{\mathbf{k}})\hat{y} \ . \tag{3.17}$$

Here $\phi_{\mathbf{k}} = \arctan(k_y/k_x)$ is the polar angle spanned by $\mathbf{k}$. The unit vector $\hat{s}_{\mathbf{k}}$ determines the direction of the quantization axis for the particular value of the wave vector $\mathbf{k}$. The two possible spin orientations immediately give the eigenstates:

$$\varphi_{\mathbf{k},\pm}(\mathbf{r}) \ = \ \frac{e^{i\mathbf{k}\cdot\mathbf{r}}}{\sqrt{2L^2}} \begin{pmatrix} \pm 1 \\ i e^{in\phi_{\mathbf{k}}} \end{pmatrix} \ , \tag{3.18}$$

with energies[2]:

$$\epsilon_{\mathbf{k},\pm} = \frac{\hbar^2 k^2}{2m} \mp \gamma (\hbar k)^n \ , \tag{3.19}$$

which generalize the results discussed in the previous Chapter for the $n = 1$ case of Rashba spin-orbit.

[2]The form of the spin-orbit coupling we consider is obviously not valid at large k.

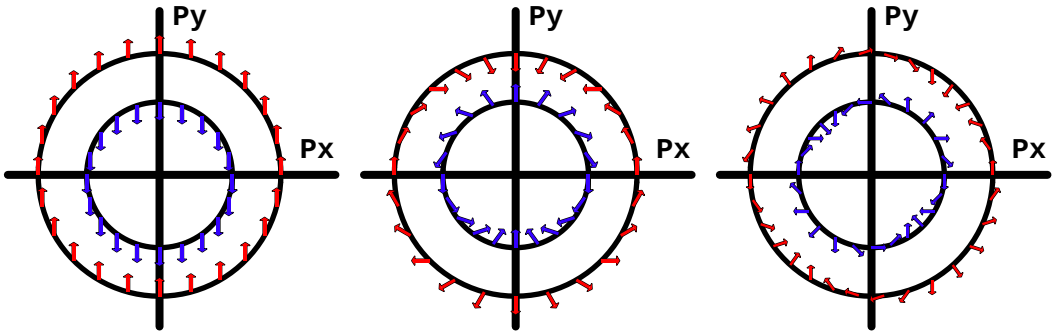

Figure 3.2. Orientation of the spin for noninteracting eigenstates in the presence of generalized spin-orbit. The cases $n = 0$, 2 and 3 are displayed from left to right. The case $n = 1$ is displayed in Figure 2.2.

We notice that in view of the structure of the spinors the integer n can be seen as a spin direction winding number. A schematic representation of the eigenstates for the cases of $n = 0, 2, 3$ is shown in Figure 3.2. The case $n = 1$ is displayed in Figure 2.2.

As in the previous Chapter, an important class of determinantal many-body states with compact momentum space occupation which are homogeneous and isotropic in the plane of motion [21] are uniquely determined by the number density n and the *generalized polarization* defined by:

$$p = \frac{n_+ - n_-}{n} \ , \tag{3.20}$$

where $n_\pm$ refers to the particle density corresponding to the two spin subbands. It must be immediately noted here that in the general case p should not be interpreted as a spin polarization for this is in general vanishing in these states. p does merely determines the two Fermi vectors $k_\pm$ of the so called spin-split subbands via the relations:

$$k_\pm = \sqrt{2\pi n(1 \pm p)} \ , \tag{3.21}$$

which uniquely determine the occupation numbers $n_{\mathbf{k}\pm}$ of the subbands.

In the particular case $n = 1$ it is obvious that the generalized polarization p is equivalent to the chirality χ_0, defined in Eq. (2.19). For simplicity, we will restrict

ourselves to the regime when both spin-split subbands are occupied, so that $p < 1$. For $n = 1$ the more general treatment in terms of the generalized chirality is discussed in the previous Chapter.

It is readily found that the non interacting energy per particle (in Rydbergs) is given by:

$$\mathcal{E}_{0,n}(\bar{\gamma}, r_s, p) = \frac{1+p^2}{r_s^2} - \bar{\gamma}\,\frac{2^{\frac{n}{2}}}{r_s^n}\,\frac{(1+p)^{1+\frac{n}{2}} - (1-p)^{1+\frac{n}{2}}}{1+\frac{n}{2}}\ , \tag{3.22}$$

which is a generalization of Eq. (2.23) (for $p < 1$). The dimensionless coupling is defined by:

$$\bar{\gamma} = \frac{m^{n-1}e^{2(n-2)}}{\hbar^{n-2}}\,\gamma\ , \tag{3.23}$$

The first term in (3.22) is the contribution of the kinetic energy while the second corresponds to the spin-orbit interaction.

In this case, minimization of the total energy with respect to the value of p, $\frac{\partial \mathcal{E}_{0,n}}{\partial p} = 0$, leads to the ground state value of the equilibrium generalized polarization $p^{(0)}_{min}$. Interestingly the result only depends on the dimensionless quantity

$$g \ = \ 2^{\frac{n}{2}}\bar{\gamma} r_s^{2-n}\ , \tag{3.24}$$

so that it can be compactly expressed as follows:

$$p^{(0)}_{min} = \begin{cases} g & \text{for } n = 0\ , \\ g\sqrt{1-\frac{g^2}{4}} & \text{for } n = 1\ , \\ g & \text{for } n = 2\ , \\ g\sqrt{\frac{-3g^4+6g^2-2+2(1-2g^2)^{3/2}}{g^6}} & \text{for } n = 3\ . \end{cases} \tag{3.25}$$

For small coupling this quantity behaves as

$$p^{(0)}_{min} \ \simeq \ g + \frac{n(n-2)}{8}g^3 + O(g^5)\ . \tag{3.26}$$

One can then immediately notice that since for $n = 1$ we have $g = \sqrt{2}\bar{\gamma} r_s$, in this case the high-density regime is equivalent to a vanishing spin-orbit. The opposite obtains for $n = 3$, since $g = 2\sqrt{2}\bar{\gamma}/r_s$. For quadratic spin-orbit $g = 2\bar{\gamma}$, and the fractional generalized polarization p is independent of the density.

It is also useful to define here the depopulation coupling strength $\bar{\gamma}_d^{(0)}$ as the particular value of $\bar{\gamma}$ for which, at a given density, the upper band empties and $p_{min}^{(0)} = 1$. This is readily obtained from (3.25):

$$\bar{\gamma}_d^{(0)} = \begin{cases} \frac{1}{r_s^2} & \text{for } n = 0 \ , \\ \frac{r_s^{n-2}}{2^{n-1}} & \text{for } n = 1, 2, 3 \ . \end{cases} \tag{3.27}$$

4. Effects of the lateral confinement with Rashba spin-orbit coupling

We consider in this and in the next Chapter the properties of a noninteracting two-dimensional liquid, in the presence of spin-orbit coupling and lateral confinement. We assume that the lateral confinement is realized with hard boundaries, which has little consequence on the nature of the spin-polarization effects displayed by the system, but allows a simple treatment of the problem.

We first examine the case of linear Rashba spin-orbit, by studying in detail the spectrum and the inhomogeneous spin-polarization of the eigenstates, resulting from the presence of the external potential. Special emphasis is given to the out-of-plane component that is produced from coherent superposition of in-plane polarized two-dimensional eigenstates.

While the total equilibrium polarization is vanishing, a finite result is obtained in the presence of a nonequilibrium population, as in the particular case of a finite current flowing through the system. This fact is well known in bulk two-dimensional electronic system where a current forced along the x direction will be accompanied by an in plane polarization along y [32–36]. By a perturbative analysis we show that in the strong confined regime this component is quenched and the polarization is mostly out-of plane. The crossover between the two regimes is discussed.

4.1 Formulation of the problem and boundary conditions

The model Hamiltonian we consider is the following:

$$\hat{H} = \frac{\hat{\mathbf{p}}^2}{2m} + \alpha(\hat{\sigma}_x \hat{p}_y - \hat{\sigma}_y \hat{p}_x) + V(\hat{y}) \ , \tag{4.1}$$

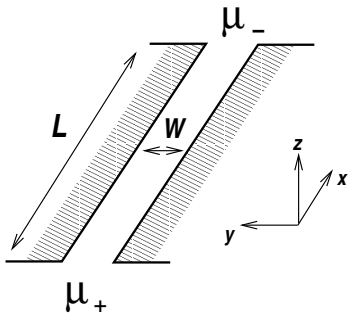

Figure 4.1. Schematic of our model quantum wire obtained by pinching along the y direction a quantum well of side L by means of a hard-wall lateral confining potential.

where the motion is restricted to the x, y plane and the lateral confining potential is given by:

$$V(y) = \begin{cases} 0 & \text{for } |y| < W/2 \ , \\ \infty & \text{for } |y| \geq W/2 \ . \end{cases} \tag{4.2}$$

The setup is schematically depicted in Figure 4.1.

Since the system is translationally invariant along the x direction, the eigenfunctions of the problem can be constructed by linear superposition of free space ($V(y) = 0$) eigenstates with definite values of k_x, which are given in (2.17). The corresponding eigenenergies are in (2.18). Because of time reversal, states within the same band with opposite wave vectors have opposite spins, which allows to assume $k_x > 0$ without loss of generality.

The surfaces (lines) at constant energy ϵ are concentric circles with radii $K_\pm$. These are given as the positive solutions of the equation

$$\epsilon = \frac{\hbar^2 K_\pm^2}{2m} \mp \hbar\, \alpha\, K_\pm \ . \tag{4.3}$$

Constant energy lines are schematically displayed in Figure 4.2.

At a given energy ϵ, there are only four free space eigenstates that can be combined to form solutions satisfying the zero boundary condition of the inhomogeneous

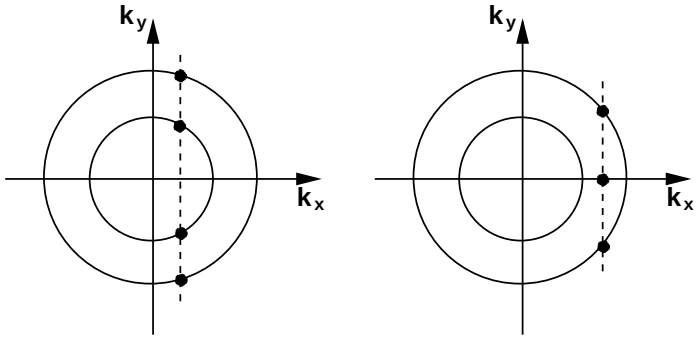

Figure 4.2. Possible free space states that can be superimposed to obtain confined eigenstates. On right we show a situation for which the two states of the upper branch have $\mathrm{Re}[k_y] = 0$.

problem. This is depicted in Figure 4.2: for each spin subband $\pm$ we have two states with opposite value of k_y. The four possible values of k_y are $\pm k_y^{\pm}$, with

$$k_y^{\pm} = \sqrt{K_{\pm}^2 - k_x^2}\ , \tag{4.4}$$

where $K_{\pm}$ are given in Eq. (4.3) above.

Since we are interested in spatially undamped solutions, we always take $k_x < K_+$. However, it will necessary to include the case $K_- < k_x < K_+$, where $k_y^- = i|k_y^-|$ is purely imaginary. We also define the angles $\phi_{\pm}$ by means of:

$$\phi_{\pm} = \arctan \frac{k_y^{\pm}}{k_x}\ . \tag{4.5}$$

If $k_y^- = i|k_y^-|$ we have that also ϕ_- is purely imaginary and from the above formula we get $\phi_- = i\mathrm{arctanh}\frac{|k_y^-|}{k_x}$.

It is convenient to consider the following two couples of (unnormalized) states, which are also eigenstates of the reflection symmetry $y \to -y$:

$$\psi_{\pm\pm}(\epsilon, k_x, y) = \begin{pmatrix} \cos\left(k_y^{\pm} y - \frac{\phi_{\pm}}{2}\right) \\ \pm i \cos\left(k_y^{\pm} y + \frac{\phi_{\pm}}{2}\right) \end{pmatrix} e^{ik_x x}\ , \tag{4.6}$$

$$\psi_{\pm\mp}(\epsilon, k_x, y) = \begin{pmatrix} \sin\left(k_y^{\pm} y - \frac{\phi_{\pm}}{2}\right) \\ \pm i \sin\left(k_y^{\pm} y + \frac{\phi_{\pm}}{2}\right) \end{pmatrix} e^{ik_x x}\ . \tag{4.7}$$

The first $\pm$ subscript refers to the chirality of the spin subband while the second $\pm$ subscript refers to the reflection operation $y \to -y$. The eigenstates in the confined system are then expressed in the following way:

$$\varphi_n^+(k_x, y) = c_n^{++}\psi_{++} + c_n^{-+}\psi_{-+} \ , \tag{4.8}$$

$$\varphi_n^-(k_x, y) = c_n^{+-}\psi_{+-} + c_n^{--}\psi_{--} \ , \tag{4.9}$$

where the superscript in $\varphi_n^\pm$ refers to the reflection parity, and not to the chirality. As one would expect, the solutions of the confined system are an admixture of states with different chirality. A spin subband index will be introduced as an approximate quantum number in the case of small spin orbit in a following Section where we present a perturbative treatment of the problem.

Imposing the boundary condition at $y = W/2$ for the $\varphi_n^\pm$ leads to the following conditions:

$$\begin{pmatrix} \cos\left(\frac{k_y^+ W - \phi_+}{2}\right) & \sin\left(\frac{k_y^- W - \phi_-}{2}\right) \\ i\cos\left(\frac{k_y^+ W + \phi_+}{2}\right) & -i\sin\left(\frac{k_y^- W + \phi_-}{2}\right) \end{pmatrix} \begin{pmatrix} c_n^{++} \\ c_n^{-+} \end{pmatrix} = 0 \ , \tag{4.10}$$

$$\begin{pmatrix} \sin\left(\frac{k_y^+ W - \phi_+}{2}\right) & \cos\left(\frac{k_y^- W - \phi_-}{2}\right) \\ i\sin\left(\frac{k_y^+ W + \phi_+}{2}\right) & -i\cos\left(\frac{k_y^- W + \phi_-}{2}\right) \end{pmatrix} \begin{pmatrix} c_n^{+-} \\ c_n^{--} \end{pmatrix} = 0 \ . \tag{4.11}$$

At fixed k_x, the determinants of (4.10) and (4.11) are functions of ϵ, through the implicit dependence of $k_y^\pm$ and $\phi_\pm$. The zeros of these determinants provide two sets of discrete energies $\epsilon_n^\pm(k_x)$, corresponding to states of opposite parity.

If one is not interested in separating states with different reflection parity, one can combine the conditions ensuing from (4.10) and (4.11) into the compact equation:

$$\begin{aligned} &(1 - \cos k_y^+ W \cos k_y^- W)\sin\phi_+ \sin\phi_- \\ &+(1 - \cos\phi_+ \cos\phi_-)\sin k_y^+ W \sin k_y^- W = 0 \ , \end{aligned} \tag{4.12}$$

which gives the whole spectrum for a given k_x. The eigenfunctions, dropping the reflection parity index, are henceforth quite generally denoted as $\varphi_\nu(k_x, y)$.

We finally notice that for values of ϵ and k_x such that k_y^- is purely imaginary, the structure of the above formulas still holds, and one need only substitute hyperbolic for trigonometric functions.

4.2 Solution of the problem

4.2.1 Exact solution at $k_x = 0$

A case in which the solutions can be expressed in simple closed form is that of $k_x = 0$. For this particular value of k_x it is immediate to see that Eq. (4.1) admits solutions which are eigenstates of $\hat{\sigma}_x$. Assuming the following form for the wavefunctions

$$e^{\mp i \frac{m\alpha}{\hbar} y} \Phi(y) |\pm\rangle_x \ , \tag{4.13}$$

$\Phi(y)$ is found to satisfy:

$$\left[-\frac{\hbar^2}{2m} \frac{\partial^2}{\partial y^2} + V(y) - \frac{1}{2} m\alpha^2 \right] \Phi(y) = \epsilon \, \Phi(y) \ . \tag{4.14}$$

This result is quite general holding for an arbitrary form of the confining potential $V(y)$. For the case of an infinite well we obtain:

$$\epsilon_n = \frac{\hbar^2}{2m} \left(\frac{\pi n}{W} \right)^2 - \frac{1}{2} m\alpha^2 \ , \tag{4.15}$$

where n is a positive integer. For every eigenvalue there is an additional twofold spin degeneracy.

4.2.2 Numerical results

We reproduce in Figures 4.3-4.7 numerical results, calculated with the methods of the previous Section. In Figure 4.3 and 4.4 we present two examples of the energy spectrum as function of k_x for different values of the spin-orbit coupling α.

The properties of the eigenfunctions are perhaps more interesting and can be best exemplified by the corresponding number and spin polarization densities. Figures 4.5, 4.6 and 4.7 refer to these properties of the eigenfunctions, and have been obtained with the same parameters of Figure 4.3 and an occupation characterized by a Fermi energy $\epsilon_F = 6$ meV. In particular, we show there for each state the relative number

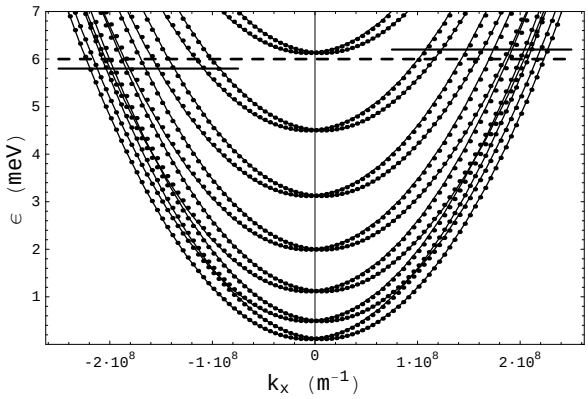

Figure 4.3. Energy spectrum of a $W = 0.1$ μm wide quantum wire. For clarity the exact energy bands are only shown (dots) for discrete values of k_x, while the perturbative results from Eq. (4.21) are also plotted (solid lines) for comparison. The parameters values are as follows: $\hbar\alpha = 2\ 10^{-9}$meV m and $m = 0.3m_0$. The horizontal dashed line marks a Fermi level of 6 meV and is significant in relation to Figures 4.5, 4.6 and 4.7. The corresponding electron density is 0.67 10^{12} cm^{-2}.

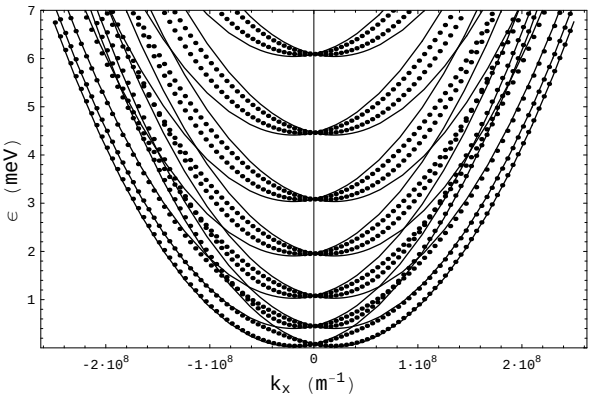

Figure 4.4. Same as in Figure 4.3 but with a larger value of the spin orbit coupling: $\hbar\alpha = 5\ 10^{-9}$ meV m. Strong deviations from perturbation theory are due to anti-crossing of bands.

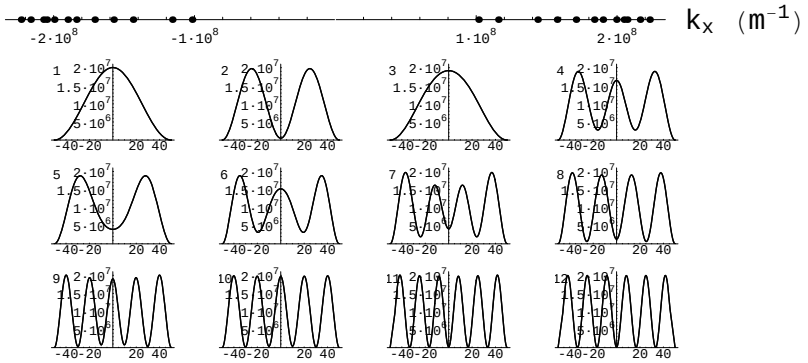

Figure 4.5. Number density $\mathcal{N}_\nu(y)$ (in m^{-1} units) of individual eigenstates at the Fermi level of a quantum wire. The parameters are the same as in Figure 4.3. The wave vector values are determined by the crossings of the bands with the horizontal dashed line at 6 meV in Figure 4.3 and are given at the top (dots on the k_x line). The corresponding $\mathcal{N}_\nu(y)$ functions are shown in the panels, where the numbers label the first twelve wave vectors, counted from left to right on the top k_x line. States with opposite wave vectors have the same density.

density $\mathcal{N}_\nu(k_x, y)$ and spin polarization density $\vec{\mathcal{P}}_\nu(k_x, y)$. These quantities are defined as follows:

$$\mathcal{N}_\nu(k_x, y) \;=\; \langle \varphi_\nu(k_x, y')|\delta(y - \hat{y}')|\varphi_\nu(k_x, y')\rangle \;, \tag{4.16}$$

$$\vec{\mathcal{P}}_\nu(k_x, y) \;=\; \langle \varphi_\nu(k_x, y')|\hat{\vec{\sigma}}\delta(y - \hat{y}')|\varphi_\nu(k_x, y')\rangle \;. \tag{4.17}$$

From simple symmetry considerations, it follows that the polarization is vanishing in the x direction, along the wire, and states with the same energy and opposite values of k_x have the same density but opposite spin polarization. As it will be discussed in a following Section, this fact allows in principle to produce a net spin polarization along the y and z direction, by driving an electrical current along the wire.

4.2.3 Perturbation theory

Although the numerical analysis provides the complete answer to the problem, useful insight can be gained from an examination of the perturbative approach. We

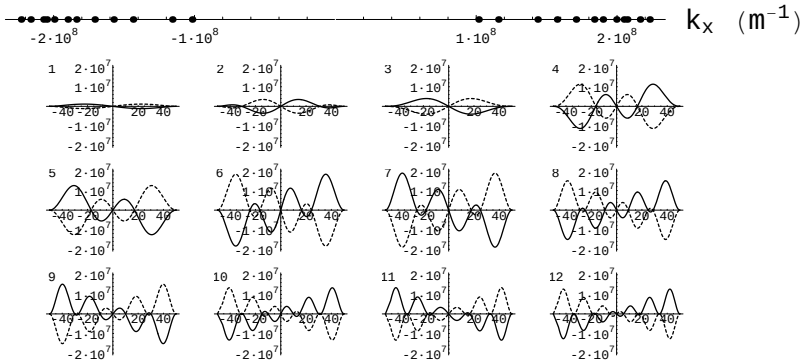

Figure 4.6. Spin polarization density $\mathcal{P}^z_\nu(y)$ along the z direction (in m^{-1} units) of the same eigenstates of Figure 4.5. States with opposite wave vectors have polarization of opposite sign. Solid lines correspond to the first twelve k_x values, counted from left to right on the top k_x line, while dashed lines refer to $-k_x$.

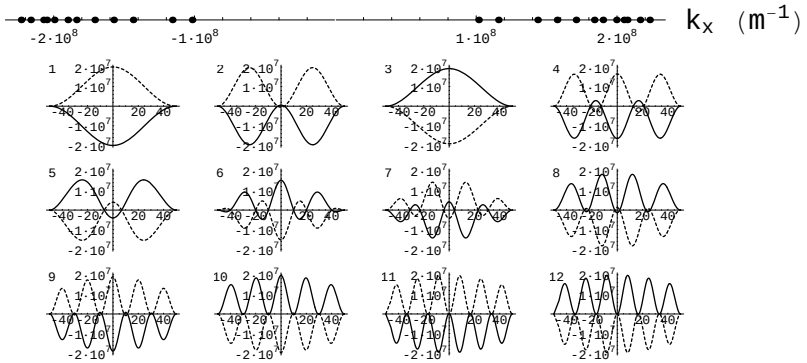

Figure 4.7. Spin polarization density $\mathcal{P}^y_\nu(y)$ along the y direction (in m^{-1} units) of the same eigenstates of Figure 4.5. States with opposite wave vectors have polarization of opposite sign. Solid lines correspond to the first twelve k_x values, counted from left to right on the top k_x line, while dashed lines refer to $-k_x$.

therefore consider next the case of small spin orbit coupling and will assume that the Rashba term can indeed be treated as a perturbation. In order to simplify the notation, in this Section we consider a potential that confines the electrons in $0 < y < W$ rather than $-W/2 < y < W/2$. For simplicity we will label the perturbed eigenstates via the (approximate) quantum numbers of the unperturbed solutions. Accordingly we write

$$\varphi_{n\pm}(k_x, y) = \varphi^0_{n\pm}(k_x, y) + O(\alpha) \ , \tag{4.18}$$

where

$$\varphi^0_{n\pm}(k_x, y) = \sqrt{\frac{2}{LW}}\, e^{ik_x x} \sin\frac{n\pi y}{W}\, |\pm\rangle_y \ , \tag{4.19}$$

with n a positive integer. We also find convenient to choose the spinors along y, in such a way that the states are eigenstates of the y reflection symmetry. The relevant matrix elements of the spin orbit interaction are:

$$\begin{aligned} \langle\varphi^0_{n'\pm}|\hat{R}_0|\varphi^0_{n\pm}\rangle &= \mp\hbar\alpha k_x \delta_{nn'}\delta_{k_x k'_x} \ , \\ \langle\varphi^0_{n'\mp}|\hat{R}_0|\varphi^0_{n\pm}\rangle &= \mp\frac{2\hbar\alpha}{W}\frac{nn'(1-(-1)^{n+n'})}{(n^2-n'^2)}\,\delta_{k_x k'_x} \ . \end{aligned} \tag{4.20}$$

We can easily obtain the form of the perturbation expansion, up to second order:

$$\begin{aligned} \epsilon_{n\pm}(k_x) = &\frac{\hbar^2}{2m}\left(\frac{\pi n}{W^2}\right)^2 + \frac{\hbar^2 k_x^2}{2m} \\ &\mp\hbar\alpha k_x - \frac{1}{2}m\,\alpha^2 + O(\alpha^3) \ . \end{aligned} \tag{4.21}$$

Higher order terms are also readily obtained.

The necessary condition for the validity of the perturbative expansion is that the matrix elements (4.20) be smaller than the unperturbed energy differences. The latter are of order $\frac{\hbar^2}{mW^2}$. This gives:

$$\alpha \ll \frac{\hbar}{mk_x W^2} \quad \text{and} \quad \alpha \ll \frac{\hbar}{mW} \ . \tag{4.22}$$

Clearly the perturbative expansion fails for large values of k_x, or for a channel with large W.

The perturbation theory allows us to explicitly calculate a number of interesting quantities. In particular the z-component of the spin polarization density of the confined states (see Eq. (4.17)) is given by:

$$\begin{aligned}\mathcal{P}^z_{n\pm}(k_x,y) &= \langle\varphi_{n\pm}(k_x,y')|\hat{\sigma}_z\delta(y-\hat{y}')|\varphi_{n\pm}(k_x,y')\rangle \\ &= \mp\frac{\alpha m}{\hbar}F_n(y/W) - \left(\frac{\alpha m W}{\hbar}\right)^2 k_x G_n(y/W) + O(\alpha^3)\ ,\end{aligned} \tag{4.23}$$

where the functions F_n and G_n are given by:

$$\begin{aligned}F_n(y/W) &= \frac{64}{\pi^2}{\sum_m}' \frac{nm}{(n^2-m^2)^2}\sin\frac{\pi n y}{W}\sin\frac{\pi m y}{W}\ , \\ G_n(y/W) &= \frac{256}{\pi^4}{\sum_m}' \frac{nm}{(n^2-m^2)^3}\sin\frac{\pi n y}{W}\sin\frac{\pi m y}{W}\ ,\end{aligned} \tag{4.24}$$

where the sum extends over positive even (odd) integers m for odd (even) n.

In the same way, while $\mathcal{P}^x_{n\pm}(k_x,y)$ vanishes, the corresponding perturbative result for the polarization along y of the $n\pm$ states can be expressed as:

$$\begin{aligned}\mathcal{P}^y_{n\pm}(k_x,y) &= \langle\varphi_{n\pm}(k_x,y')|\hat{\sigma}_y\delta(y-\hat{y}')|\varphi_{n\pm}(k_x,y')\rangle \\ &= \pm\frac{2}{W}\sin^2\frac{\pi n y}{W} \mp \left(\frac{\alpha m}{\hbar}\right)^2 W H_n(y/W) + O(\alpha^3)\ ,\end{aligned} \tag{4.25}$$

where the function H_n is defined as follows:

$$\begin{aligned}H_n(y/W) = \frac{128}{\pi^4}\Bigg[&{\sum_m}' \frac{m^2n^2}{(n^2-m^2)^4}\sin^2\frac{\pi n y}{W} \\ &+2{\sum_{m,n'}}' \frac{m^2 nn'}{(n^2-m^2)^2(n^2-n'^2)(m^2-n'^2)}\sin\frac{\pi n y}{W}\sin\frac{\pi n' y}{W} \\ &+{\sum_{m,m'}}' \frac{mm'n^2}{(n^2-m^2)^2(n^2-m'^2)^2}\sin\frac{\pi m y}{W}\sin\frac{\pi m' y}{W}\Bigg]\ ,\end{aligned} \tag{4.26}$$

where the sums extend over the positive integers. In particular while n' is of the same parity as n, both m and m' are of opposite parity. Moreover $n' \neq n$.

Notice that as expected, in all these formulas the substitution $k_x \to -k_x$ and $\pm \to \mp$ gives a state with the same energy and opposite spin polarization.

4.3 Edge spin polarization

We consider here the spin accumulation at the boundaries of the wire in the presence of an electric current in the x direction.

Although the response of a system of electrons subject to Rashba spin orbit and an applied electric field is quite complicated and requires a careful analysis [32, 33], for simplicity sake we will model here a current carrying steady state by assuming a modified electron occupation distribution. In particular we will assume that a finite chemical potential difference $\delta\mu = \mu_+ - \mu_-$ is established between the right moving and left moving states. This is depicted in Figure 4.3 by the two short horizontal solid lines (whose separation from the equilibrium Fermi level - dashed - is not in scale). The present model is meant to describe ballistic transport with all the chemical potential drop occurring at the contacts at $x = \pm\infty$.

Within this framework, the total spin polarization density due to the current flux can be obtained in the linear regime from the relation:

$$\vec{\mathcal{M}}(y) \;=\; \pm\frac{g\mu_B}{2}\tilde{\sum_{\nu}}\frac{\delta\mu}{2\pi\hbar\, v_{F\nu}}\vec{\mathcal{P}}_\nu(k_{F\nu},y)\;, \tag{4.27}$$

where the sum is restricted to the occupied one-dimensional subbands with $k_{F\nu}$ and $v_{F\nu}$ being the (positive) Fermi wave vector and Fermi velocity relative to the occupied band as labeled by the index ν. In this formula the positive sign refers to the case of hole transport. As a consequence the direction of the magnetization only depends on the current direction and not on the type of carrier involved.

The perturbative result for the z component $\mathcal{M}_z$ is readily obtained from Eqs. (4.24):

$$\mathcal{M}_z(y) \;\simeq\; \mp\,\delta\mu\frac{mg\mu_B}{2\pi\hbar^2}\left(\frac{m\alpha W}{\hbar}\right)^2\tilde{\sum_{n}}G_n(y/W)\;, \tag{4.28}$$

where the sum is limited to the positive integers corresponding to the occupied bands. The results of the (exact) numerical calculations of $\mathcal{M}_z(y)$ are shown in Figure 4.8.

Interestingly the expression given in (4.25) is not sufficient to obtain the leading corresponding perturbative expression for $\mathcal{M}_y(y)$. The reason is simply that in the confined geometry the first finite contribution to this quantity is clearly of order α^3

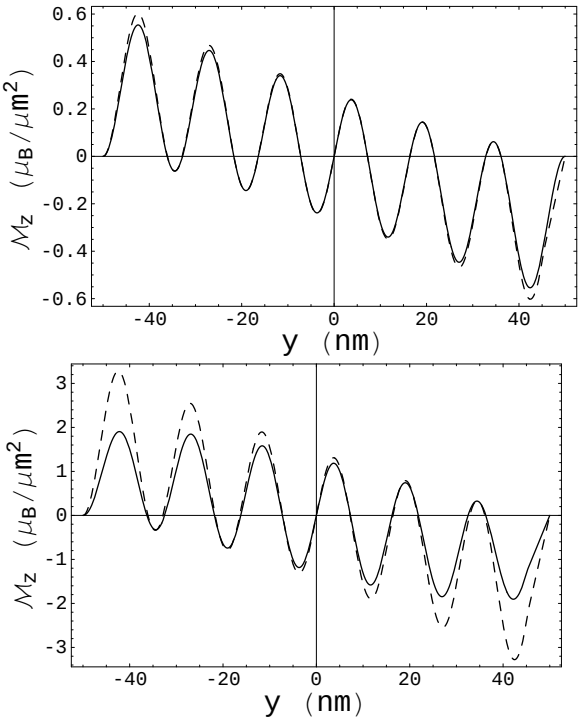

Figure 4.8. Spin polarization density in the z direction of a $W = 0.1$ μm wide quantum wire, for carriers with effective mass $m = 0.3m_0$ and $g = 2$. The Fermi energy is $\epsilon_F = 6$ meV, which corresponds to an electron density of $0.67\ 10^{12}$ cm^{-2}. We used $\delta\mu = 0.1$ meV which gives a current in the wire of 23 nA. In the top panel $\hbar\alpha = 1.5\ 10^{-9}$ meV m while in the bottom one $\hbar\alpha = 3.5\ 10^{-9}$ meV m. The perturbative result is also plotted (dashed). As a comparison of the magnitude of the effect, the Pauli susceptibility is $\chi_P = 72.5\ \mu_B/(\mu\text{m}^2\,\text{T})$.

(see also below). This term can be of course readily calculated. The results for the exact calculation of $\mathcal{M}_y(y)$ are plotted in Figure 4.9 alongside the perturbative expression.

It is remarkable that the z component of the magnetization is larger for small values of the spin-orbit coupling constant while the two components become comparable for larger values. Furthermore, while $\mathcal{M}_z(y)$ changes sign and displays an asymmetric behavior across the wire, $\mathcal{M}_y(y)$ remains of the same sign and is instead symmetric.

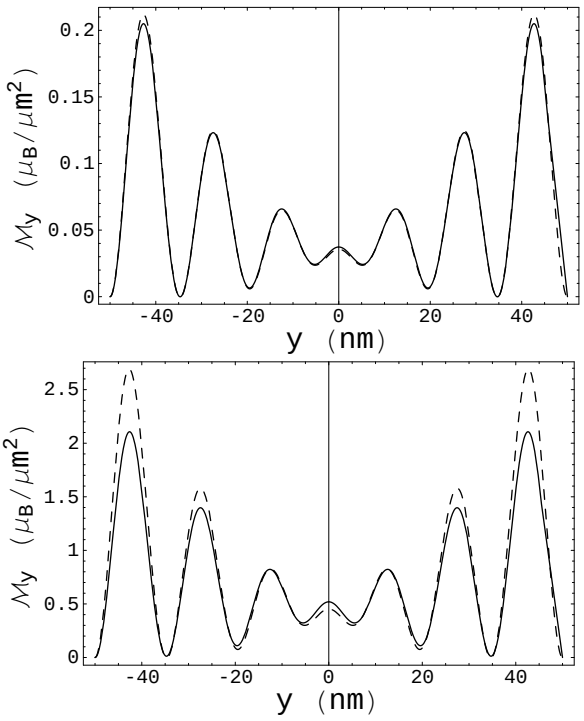

Figure 4.9. Spin polarization in the y direction corresponding to the same parameters of the previous Figure 4.8. In the top panel $\hbar\alpha = 1.5\ 10^{-9}$ meV m while in the bottom one $\hbar\alpha = 3.5\ 10^{-9}$ meV m. The leading perturbative contribution (cubic in α) is also plotted (dashed).

As expected, in all cases, there is good agreement with the approximate analytical formula (4.28) for small values of α. In this respect, we notice that the choice of the parameters of Figs. 4.8 and 4.9 refers to typical values reported in the experimental literature for holes [4]. The choice is motivated from the fact that, due to the value of the effective mass, larger values of the polarization are attained. For the case of electrons, the effect would be suppressed by a factor $(m_e/m_h)^3$ in the transverse case, as apparent from (4.28), and by a factor $(m_e/m_h)^4$ for the in-plane polarization, as it is clear from the previous discussion. Therefore the effect would be accurately described by the perturbative expressions, and the discussed quenching of the y polarization compared to the z component would be more evident.

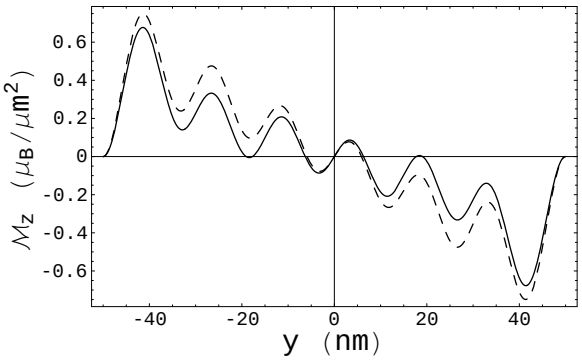

Figure 4.10. Magnetization density of a $W = 0.1$ μm wide quantum wire, for carriers with same parameters as the first panel of Figure 4.8. We used $E = 1$ kV/m and a constant value for $\tau = 7.3\ 10^{-13}$ s, which gives the same current in the wire of Figure 4.8. The perturbative result is also plotted (dashed). The magnetization is somewhat different from the previous case, where the oscillations of the magnetization are more pronounced. The overall sign of the effect is the same.

Our theory can be extended to the case of non ballistic transport. A simple treatment of such a situation can be obtained by setting $\delta\mu \to eEv_{F\nu}\tau_\nu$ in Eq. (4.27). Here E is the magnitude of the driving electric field and $v_{F\nu}\tau_\nu$ is the elastic mean free path appropriate for the states of the one dimensional subband ν, a length scale that we assume much larger than the width W of the wire. By taking for simplicity the same scattering time for all subbands $\tau_\nu = \tau$ the ensuing magnetization can be obtained. The results for $\mathcal{M}_z(y)$ are plotted in Figure 4.10. We notice that the oscillations of the magnetization are somewhat damped as compared to the ballistic case. On the other hand, the overall sign of the effect is unchanged, the behavior being in disagreement with the experimental results of Ref. [37]. We haste to state however that our model is rather different from the situation of a dirty three-dimensional sample dealt with in the experiment.

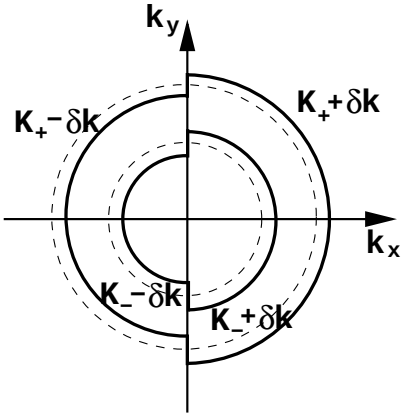

Figure 4.11. Distorted momentum space occupation distribution used to calculate the bulk value of the magnetization. $K_{\pm}$ are defined in Eq. (4.3).

4.4 Discussion

As we have noted, while for small spin orbit the out of plane (z-axis) polarization $\mathcal{M}_z(y)$ induced by an x-axis current is quadratic in the coupling constant, the in plane (y-axis) polarization $\mathcal{M}_y(y)$ is much smaller, first appearing in third order. This result is only in apparent contradiction with the well known corresponding bulk result in two dimensions which entails a linear dependence of $\mathcal{M}_y(y)$ on the coupling constant. Within the simplified model used in Section 4.3 such a behavior can be readily derived by assuming the distorted momentum space electron distribution function of Figure 4.11. The final expression is given by

$$\frac{1}{L^2}\langle\hat{\sigma}_y\rangle \;=\; \frac{\alpha\, m^{\frac{3}{2}}\,\delta\mu}{\pi^2\hbar^2\sqrt{2\epsilon_F + m\alpha^2}}\;, \tag{4.29}$$

where $\delta\mu = 2\hbar v_F \delta k$. As expected for small α $\mathcal{M}_y(y)$ is linear in the coupling constant[1].

The difference lies with a quenching of the y-axis polarization due to the confining potential. As it can be surmised by inspecting Eq. (4.25), this effect can be

[1]It must be noted for completeness that within the more rigorous microscopic approach in which the effect of impurities is accounted for (see for instance Ref. [32] and [33]) the coefficient of the linear contribution to $\mathcal{M}_y(y)$ depends on the specific electron impurity potential assumed.

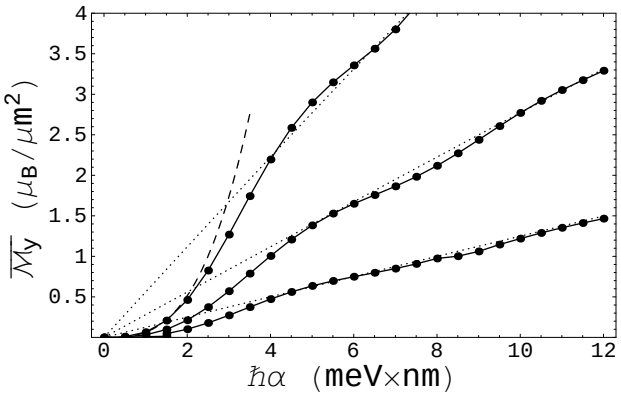

Figure 4.12. Average spin polarization density in the y direction as a function of α. The parameters used are: $W = 0.15$ μm, $\epsilon_F = 2.5, 10, 40$ meV, $\delta\mu = 0.05$ meV, and $m = 0.3m_0$ (mass as in previous Figures). Here the dots represent the (exact) numerical result, while the dotted curves are obtained from Eq. (4.29) in the text. The dashed line is a guide to the eye representing a pure cubic behavior.

readily seen to originate from the lowest order cancellation of the contributions to $\mathcal{M}_y(y)$ stemming from states within the same spin-split one dimensional band. The cancellation only occurs when the spin-splitting is smaller than the energy quantization associated with the one-dimensional confining potential. This is of course not operational in the bulk since in such a situation the energy spectrum is continuum.

The crossover between these two regimes approximately occurs when the spin-splitting equals the energy spacing between the eigenvalues of the confining potential along the y direction, i.e. for $\frac{m\alpha W}{\hbar} \simeq 1$. In order to exemplify this phenomenon we have plotted in Figure 4.12 the spatially averaged magnetization density

$$\overline{\mathcal{M}_y} \;=\; \frac{1}{W}\int_{-W/2}^{W/2} \mathcal{M}_y(y)\mathrm{d}y \;, \tag{4.30}$$

as a function of the value $\hbar\alpha$ of the spin orbit coupling constant. With the parameters chosen in Figure 4.12 the crossover occurs approximately for $\hbar\alpha = 1.7\,10^{-9}\,\mathrm{meV\,m}$. The dashed curve superimposed to the $\epsilon_F = 2.5$ meV dotted line is purely cubic and provides a useful guide to the eye for that case.

Exactly the opposite mechanism is responsible for the case of $\mathcal{M}_z(y)$, which, as we have seen, is instead vanishing in the bulk. Interestingly, as one can infer from Figure 4.12, the expression of Eq. (4.29), formally valid in the bulk for finite values of α when in principle the perturbative condition is inapplicable, still gives good results for the case of a rather narrow channel with $W = 0.15$ μm.

We discuss next how the different behaviors of the two components of the spin polarization we have just discussed are compatible with a quite general and rigorous argument regarding the parity of $\mathcal{M}_z(y)$ and $\mathcal{M}_y(y)$ with respect to the sign of the spin orbit coupling constant. Consider the effect on the hamiltonian (including contributions from the electron electron interaction and non magnetic impurities) of the application of the operator $\hat{\sigma}_z$. Clearly $\hat{\sigma}_z \hat{H}(\alpha)\hat{\sigma}_z = \hat{H}(-\alpha)$. Then it immediately follows that given an eigenstate of the problem for a given value of α, the corresponding solution for $-\alpha$ can be obtained simply by application of $\hat{\sigma}_z$. This in turn implies that, quite generally, while $\mathcal{M}_z(y)$ is even with respect to α, $\mathcal{M}_y(y)$ is odd.

In concluding, we notice that the effect we described is phenomenologically analogous to, yet distinct, from the spin-Hall effect that has recently been the subject of intense discussion (for a useful review, see Ref. [6]) and was demonstrated experimentally [37–40]. The mechanism relevant to the present discussion simply stems from the structure of the electronic wavefunctions in a confined geometry. Accordingly, there is no need to make appeal to spin currents or impurity scattering. Moreover its geometric nature should leave the phenomenon mostly unchanged in the presence of a moderate amount of impurities in the wire.

Interestingly we believe that some of the features observed in model calculations specifically designed to study the spin-Hall effect (see for instance reference [41]) must in fact be ascribed to the simple phenomenon described here. A similar effect should also be relevant in the case of electronic states localized by an impurity potential as well as in the transition to a low density Wigner crystal in the presence of Rashba spin orbit.

5. Effects of the lateral confinement for holes in $GaAs$

In this last Chapter devoted to properties of the noninteracting system we consider the effect of the lateral confinement on two-dimensional holes. This problem has great interest, since it is the object of recent experimental activity which has shown the relevance of the spin-orbit coupling in the point-contact transmission of holes in $GaAs$ [4, 42].

Due to the peculiar form of the spin-orbit coupling, the one-dimensional spectrum resulting from the lateral confinement substantially differs from the case of linear Rashba spin-orbit discussed in the previous Chapter. The most relevant feature is the crossing of the two lowest lying spin-split subbands at a finite value of the momentum along the wire. The presence of the crossing can be controlled by an external magnetic field or electric gating. Interesting polarization properties of the point-contact transmission are well understood on a qualitative level from the form of the one-dimensional spectrum and are confirmed by the explicit solution of a simple model for the point-contact.

5.1 Qualitative introduction

We discussed at length in the previous Chapter the effect of the lateral confinement in the presence of a linear Rashba spin-orbit term:

$$\hat{H}_{0,1} = \frac{\hat{\mathbf{p}}^2}{2m} + \alpha \left(\hat{\sigma}_x \hat{p}_y - \hat{p}_x \hat{\sigma}_y \right) , \tag{5.1}$$

which is appropriate for particles with spin $|\pm 1/2\rangle$. In the case of holes of typical III-V semiconductors (as in particular $GaAs$), the highest two-dimensional subband of a quantum well is approximately formed by heavy-holes with spin $|\pm 3/2\rangle$. For this

reason one obtains that the cubic term discussed in Chapter 3 is the main contribution to the spin-orbit coupling:

$$\hat{H}_{0,3} = \frac{\hat{\mathbf{p}}^2}{2m} + \frac{i\gamma}{2}\left(\hat{p}_-^3\hat{\sigma}_+ - \hat{p}_+^3\hat{\sigma}_-\right) , \tag{5.2}$$

where $\hat{p}_\pm = \hat{p}_x \pm i\hat{p}_y$ and $\hat{\sigma}_\pm = \hat{\sigma}_x \pm i\hat{\sigma}_y$.

While the form of $\hat{H}_{0,3}$ is well established in the theoretical literature (for reviews, see Refs. [3, 6]), a clear experimental demonstration that distinguishes between the two types of spin-orbit might be difficult to obtain. We suggest that clear evidence of the different form of the spin-orbit mechanism is obtained in the presence of a lateral confinement. In fact, the hamiltonians (5.1) and (5.2) lead to a very different form of the energy dispersion of the one-dimensional subbands, as it is obtained next with a "back of the envelope" calculation.

5.1.1 The one-dimensional spectrum

In the limit of strong lateral confinement (when the one-dimensional quantization energy is much larger than the spin-orbit splitting) one can substitute for the lowest one dimensional subband $p_y^2 \sim \left(\frac{\hbar\pi}{W}\right)^2$, where W is the extent in the y direction of the laterally confining potential. Furthermore, in the case of for a symmetric potential, one can also substitute $p_y \sim 0$. This gives:

$$\hat{H}_{1D,1} = \frac{\hat{p_x}^2}{2m} - \alpha\,\hat{p}_x\hat{\sigma}_y + \frac{\hbar^2\pi^2}{2mW^2} , \tag{5.3}$$

for the linear case and:

$$\hat{H}_{1D,3} = \frac{\hat{p_x}^2}{2m} + \gamma\left(\frac{3\hbar^2\pi^2}{W^2}\hat{p}_x - \hat{p}_x^3\right)\hat{\sigma}_y + \frac{\hbar^2\pi^2}{2mW^2} , \tag{5.4}$$

for the cubic case.

The (5.3) and (5.4) are readily diagonalized, and the main difference between them is that in the first case the spin orbit splitting is $2\alpha\hbar k_x$, which is linearly increasing with the wavevector k_x, and vanishes only at $k_x = 0$. On the other side, the spin splitting in (5.4) is zero also at the finite wavevectors $k_x = \pm\sqrt{3}\frac{\pi}{W}$.

This degeneracy at $k_x = \pm\sqrt{3}\frac{\pi}{W}$ can be lifted by applying an external potential which violates the particular symmetry corresponding to the crossing behavior of the one-dimensional subbands. In fact $\hat{\sigma}_y$ is conserved in (5.4) and the two subbands are relative to different values of the spin projection. More generally, we can observe that the physical system is invariant upon reflection in a transverse plane parallel to the longitudinal direction of the wire. Therefore, every perturbation that violates this symmetry will produce an anticrossing behavior which results in the removal of the degeneracy. Examples are a longitudinal magnetic field and an asymmetry in the lateral confinement along y, which both introduce in (5.4) terms proportional to $\hat{\sigma}_x$.

5.1.2 The point contact problem

For a point contact, the lateral confinement of the external potential slowly changes along the x propagation direction of the holes, forming a narrow constriction at $x = 0$.

In the simplest case, for a sufficiently smooth potential, the holes transmitted through the constriction follow adiabatically the one-dimensional spectrum instantaneously determined by the lateral confinement, with a constant energy determined by the chemical potential of the injecting reservoir. A quantized step in the conductance of e^2/h is observed every time the gating potential allows the transmission of an additional non-degenerate one-dimensional channel through the constriction.

This picture of adiabatic transmission is experimentally violated in the spin focusing experiment of Ref. [4], when a magnetic field is applied that removes the spin degeneracy. It is observed here that the holes transmitted at the onset of the conducting regime are not those with largest wavevector, as one would expect if they were to adiabatically follow the *first* one-dimensional subband (with lowest energy).

This anomaly is explained accounting the crossing behavior of the one-dimensional subbands discussed in the previous paragraph. In fact the condition for adiabatic transmission is violated at the (quasi)degenerate points, at small magnetic fields.

To obtain an explicit condition, one can consider the spin precession in the total magnetic field $\vec{B}_{tot}$, which is the sum of the fixed external field and the field produced by the spin-orbit coupling. The latter is determined by the instantaneous velocity of the hole. The condition for adiabaticity is $\omega_Z \gg \frac{\mathrm{d}B_{tot}/\mathrm{d}t}{B_{tot}}$, where $\hbar\omega_Z$ is the gap between the two spin states. At the (quasi)degenerate points the spin-orbit field is zero so that we have $B_{tot} = B$ and $\hbar\omega_Z = g\mu_B B$, where B is the value of the external field. To estimate the rate we have that the change in B_{tot} is only determined by the spin-orbit field, and therefore $\frac{g\mu_B}{2}\frac{\mathrm{d}B_{tot}}{\mathrm{d}t} \simeq \frac{\gamma\hbar^3 k_F^3}{\mathcal{L}/v}$, where v is the instantaneous velocity and $\mathcal{L}$ is a typical length of the point contact. Finally:

$$B \gg \frac{\hbar^2(2\gamma k_F^3 v/\mathcal{L})^{1/2}}{g\mu_B} \ . \tag{5.5}$$

This condition is easier to satisfy at $k_x \simeq 0$, since v is small. At $k_x = \pm\sqrt{3}\frac{\pi}{W}$ the velocity is larger (in fact, is of the order of the Fermi velocity v_F) and (5.5) is violated up to sizable values of the magnetic field. In this conditions, the holes cannot adiabatically follow the lower/higher one-dimensional band at the (quasi)degenerate point, but cross to the higher/lower one. Therefore the transmission of holes at the onset of the conducting regime is preferentially in the *second* subband, as observed in Ref. [4].

The adiabatic condition for the transmission is of course recovered if a large enough magnetic field is applied, such that a large gap is always present between spin-split subbands.

5.2 Spectrum of two-dimensional holes with lateral confinement

While the previous introductory discussion provides the main qualitative features of the one-dimensional spectrum, the calculation can be extended to more accurately compute the eigenvalues of the hamiltonian (5.2) in the presence of a laterally confining potential. However, some mathematical difficulties are encountered. These ultimately originate from the perturbative character of (5.2), which is valid in the

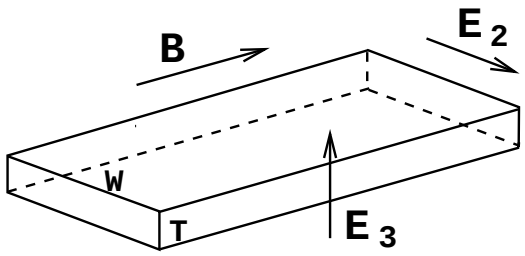

Figure 5.1. Schematic setup of a one-dimensional channel with transverse dimensions W and T, obtained from the bulk by means of hard-boundary barriers along [113] and $[1\bar{1}0]$ or [113] and $[22\bar{3}]$. A transverse electric field E_3 is always present in the [113] growth direction and the effect of a lateral electric field E_2 and a longitudinal magnetic field B are also considered.

limit of small wavevectors, while the presence of the lateral potential requires in general this requirement to be violated.

Results of numerical calculations using (5.2) and hard-wall lateral confinement can be found in the literature related to the spin-Hall effect [6, 43, 44]. Therefore we find useful to discuss in more detail this particular example in Appendix A.

In the present Section we prefer to treat the problem directly using the Luttinger hamiltonian given in Eq. (3.1), from which (5.2) can be derived [3]. This also allows to discuss effects due to the cubic crystalline potential.

The confinement potential is chosen to be:

$$V(x_2, x_3) = \begin{cases} 0 & \text{for } |x_2| \leq W/2 \text{ and } |x_3| \leq T/2 \ , \\ +\infty & \text{otherwise} \ , \end{cases} \tag{5.6}$$

where x_3 is along the growth direction of the quantum well, and x_2 is an in-plane direction of lateral confinement. The complete hamiltonian is:

$$\hat{H}_{3D,V} = \hat{H}_{3D} + V(\hat{x}_2, \hat{x}_3) + E_3 e\, \hat{x}_3 \ , \tag{5.7}$$

where the transverse electric field (perpendicular to the plane of the quantum well) is responsible to produce the inversion-asymmetry spin-orbit splitting. The setup considered here is schematically depicted in Figure 5.1.

We will consider in the following the experimentally relevant case [4, 42] of the [113] growth direction, while x_2 is chosen to be along either $[1\bar{1}0]$ or $[33\bar{2}]$. In the first case, the one-dimensional subbands resulting from the numerical diagonalization of (5.7) are plotted in the first panel of Figure 5.2. For the two highest subbands, the similarity to the simplified model (5.4) is apparent, since the two highest subbands cross at a finite value of the longitudinal wavevector k.

In the second panel of of Figure 5.2 we plotted the spectrum for the second lateral confinement direction, along $[33\bar{2}]$. Here the one dimensional subbands display an anticrossing behavior, due to the absence of the reflection symmetry operation $x_2 \rightarrow -x_2$. This is broken by the crystalline potential, which is asymmetric along $[33\bar{2}]$. The situation has to be contrasted to the previous case, where the lateral confinement is along the highly symmetric crystallographic axis $[1\bar{1}0]$.

The subbands splitting can be introduced or modified by making use of external perturbations. We present in the first panel of Figure 5.3 the case of an external magnetic field, which is treated introducing a Zeeman coupling term in (5.7):

$$\hat{H}_Z = -2\kappa\mu_B \vec{B} \cdot \hat{\mathbf{J}} \ , \tag{5.8}$$

where $\vec{B}$ is taken along the wire and $\kappa = 1.2$ for $GaAs$. Orbital effects are neglected for simplicity.

A similar effect is produced by an externally induced asymmetry in the confinement potential. This is exemplified in the second panel of Figure 5.3, which shows the spin splitting between the two highest subbands, including a lateral electric field term $E_2 e\, \hat{x}_2$ in the hamiltonian (5.7). At variance with the longitudinal magnetic field, only the degeneracy at finite wavevector is removed, while at $k = 0$ the degeneracy due to the time-inversion symmetry is preserved.

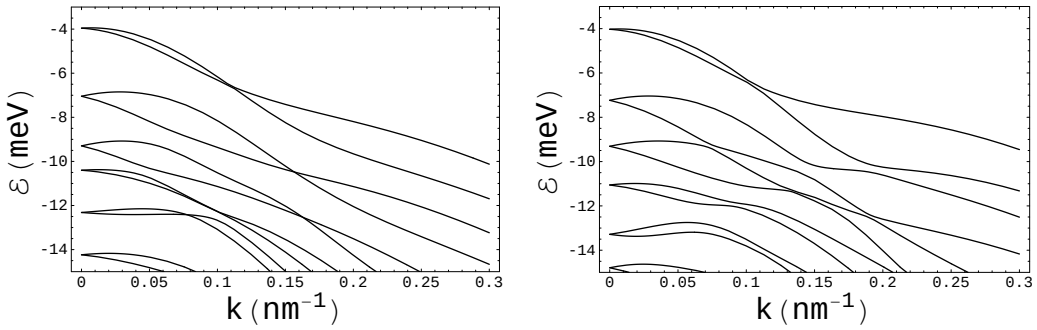

Figure 5.2. One-dimensional subbands for wires obtained from a quantum well with growth direction along [113] and lateral confinement along $[1\bar{1}0]$ (left) and $[33\bar{2}]$ (right) directions. We used parameters $T = 15$ nm and $W = 40$ nm and transverse electric field $E_3 = 1$ MV/m.

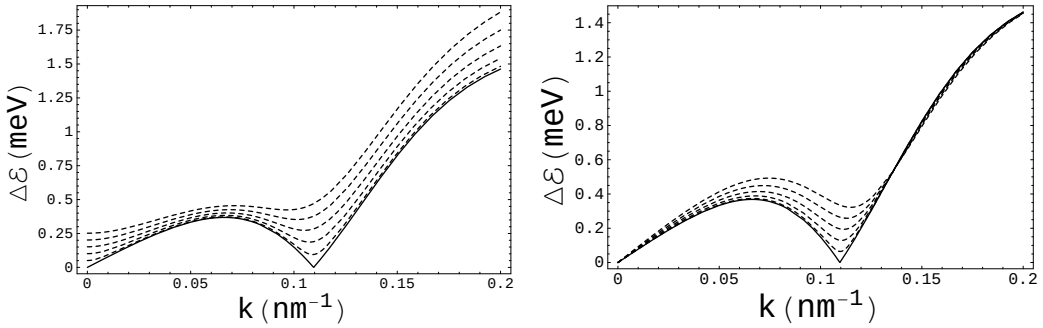

Figure 5.3. Left panel: effect of a finite longitudinal magnetic field (in the same direction of the wire). The splitting between the two higher subbands is plotted at $B = 0, 1, \ldots 5$ T. Right panel: effect of a finite lateral electric field. The splitting between the two highest subbands is plotted at increasing values of $E_2 = 0, 25, \ldots 125$ kV/m. In both figures the solid line represents the unperturbed case ($B = 0$ or $E_2 = 0$). The lateral confinement is along $[1\bar{1}0]$ in both cases and we used $T = 15$ nm and $W = 40$ nm.

5.3 Spin-resolved point contact transmission

We consider in this section the transmission of holes trough a point contact which (we neglect henceforth the cubic anisotropy) we suppose to be formed in the (x, y) plane of the quantum well, with holes propagating in the x direction.

As a simple model of a point contact, we make use of the hamiltonian (5.4), which includes the two lowest spin-split subbands and allows to describe the onset of the conducting regime. In (5.4) we assume that the hard-wall lateral confinement has a varying width [45] $W(x)$ such that:

$$V(x) = \frac{\hbar^2\pi^2}{2mW(x)^2} = \frac{\hbar^2\pi^2}{2mW_0^2}\, e^{-x^2/\mathcal{L}^2} \ , \tag{5.9}$$

where W_0 is the (minimum) width of the constriction at $x = 0$ and $\mathcal{L}$ is a typical length of the point-contact.

The complete hamiltonian, including a longitudinal magnetic field (along the point contact direction) reads:

$$\hat{H}_{PC} = \frac{\hat{p_x}^2}{2m} + V(\hat{x}) + \frac{g\mu_B}{2}B\hat{\sigma}_x + \gamma\, \left[3m\{V(\hat{x}), \hat{p}_x\} - \hat{p}_x^3\right] \hat{\sigma}_y \ , \tag{5.10}$$

where we introduced the anticommutator $\{a, b\} = ab + ba$ in the spin-orbit term to obtain an hermitian hamiltonian. This modification has little effect in the limit of a smooth contact, when $\partial V/\partial x \to 0$.

Distant from the $x = 0$ constriction we have that the potential $V(x)$ is vanishing, and the (5.10) has eigenstates which are plane waves with wavevector k_x and a specific orientation of the spin, quantized in the same direction of total magnetic field $\vec{B}_{tot} = B\hat{x} - \frac{2\gamma\hbar^3k_x^3}{g\mu_B}\hat{y}$. The eigenstates of the free case, corresponding to the two spin branches, are denoted as $\psi_\pm(k_x)$ and have energies:

$$\epsilon_\pm(k_x) = \frac{\hbar^2k_x^2}{2m} \mp \sqrt{\gamma^2(\hbar k_x)^6 + (g\mu_B B/2)^2} \ . \tag{5.11}$$

The corresponding velocities are $v_\pm = \frac{\partial\epsilon_\pm}{\hbar\partial k_x}$. We will also assume that the asymptotic wavefunctions have amplitudes such that $|\langle\psi_\pm(k_x)|\psi_\pm(k_x)\rangle|^2 = 1$.

If we now solve the scattering problem for an incident hole injected in the state $\psi_\mu(k_\mu)$ of a definite spin branch μ, the transmitted wavefunction is $\psi^T_\mu(k_\mu)$ (at $x \to +\infty$). This is a superposition of the two possible states $\psi_\nu(k_\nu)$ ($\nu = \pm$) that have the same energy of the incident state, according to expression (5.11). In particular, $k_\nu = k_\mu$ if $\nu = \mu$ and k_+ is the largest of the two wavevectors, since it corresponds to the lower energy branch.

Therefore, we can define appropriate transmission coefficients given by the expression $T^{\mu\nu}_{12} = \frac{v_\nu}{v_\mu}|\langle\psi_\nu(k_\nu)|\psi^T_\mu(k_\mu)\rangle|^2$, which is a function of the energy of the incident (or transmitted) holes only. The label indicates that the hole is injected in the first contact (at $x \to -\infty$) and transmitted in the second contact (at $x \to +\infty$). The other case of $T^{\mu\nu}_{21}$ refers to the scattering problem in the opposite direction.

The total and spin-resolved conductances are given in the Landauer-Büttiker formalism respectively by [46]:

$$G = \frac{e^2}{h}\sum_{\mu,\nu=\pm} T^{\mu\nu}_{12} \ , \qquad G_\nu = \frac{e^2}{h}\sum_{\mu=\pm} T^{\mu\nu}_{12} \ , \tag{5.12}$$

where the $T^{\mu\nu}_{12}$ are evaluated at the fixed energy ϵ_F equal to the Fermi energy of the two-dimensional contacts.

These quantities are plotted for increasing values of B in Figures 5.4 and 5.5, which displays different clearly distinct regimes. These are discussed in more detail in the following and are consistent with the qualitative arguments presented in the Subsection 5.1.2.

The particular choice of parameters is: $m = 0.3m_0$, $g = 0.2$, $\gamma\hbar^3 = 0.15\,\mathrm{eV\,nm^3}$, $\mathcal{L} = 0.5\,\mu\mathrm{m}$ and $\epsilon_F = 1$ meV. A small value of g is chosen, appropriate for a magnetic field directed along $[1\bar{1}0]$. For the $[33\bar{2}]$ direction the value of g would be larger. We also add that the value of the g-factor is modified by the lateral confinement [47] and a possible dependence of g from the wavevector k_x is also neglected. However, in the simple model of Eq. (5.10), the specific value of g has the only consequence of a rescaling of B.

Vanishing magnetic field. The transmission is in this case exactly unpolarized. This is a consequence of the simple form of our model and, in particular, of the neglect of higher one-dimensional bands together with the conservation of the y component of the spin. These two facts reduce the problem to a two-terminal device for each spin orientation, for which $T_{12}^{\pm\pm} = T_{21}^{\pm\pm}$, that follows from the unitary of the 2×2 scattering matrices relative to each spin orientation $\pm$. By time inversion we also have $T_{12}^{\pm\pm} = T_{21}^{\mp\mp}$ which leads to $T_{12}^{++} = T_{12}^{--}$.

This property however is lost in more realistic models including scattering between the one-dimensional subbands (see for example Ref. [48]) and a finite polarization is present also at zero field.

Small magnetic field. In this case the current is polarized at the onset of the conducting regime, due to the removal of the spin degeneracy at $k_x = 0$. As anticipated, the violation of the adiabatic condition at the $k_x \neq 0$ degeneracy points leads to the fact that the transmitted holes are those injected originally in the second spin-split subband, i.e. those with smaller wavevector. In fact, at the degeneracy point occurring at finite wavevector the spin is approximately conserved at low magnetic field, and the holes are scattered from one band to the other.

The spin-resolved conductance of this band G_- is plotted in Figure 5.4 as a dotted line, while G_+ is the dashed curve. The opposite behavior for the relative magnitude of G_+ and G_- would be observed in the case of linear Rashba spin-orbit.

A second noticeable fact is that the first quantization plateau in the total conductance does not appear at e^2/h, but at somehow higher values. This is due to the fact that at small fields the adiabatic condition is only partially satisfied at $k_x = 0$ for the lowest values of the magnetic field, and the point contact is incapable to completely filter the holes of the suppressed spin subband. In fact, the plateau evolves to lower conductance values and eventually approaches the value e^2/h at higher magnetic fields, as it can be seen in the second and third panels of Figure 5.4. In the case of linear spin-orbit coupling a similar behavior would be observed.

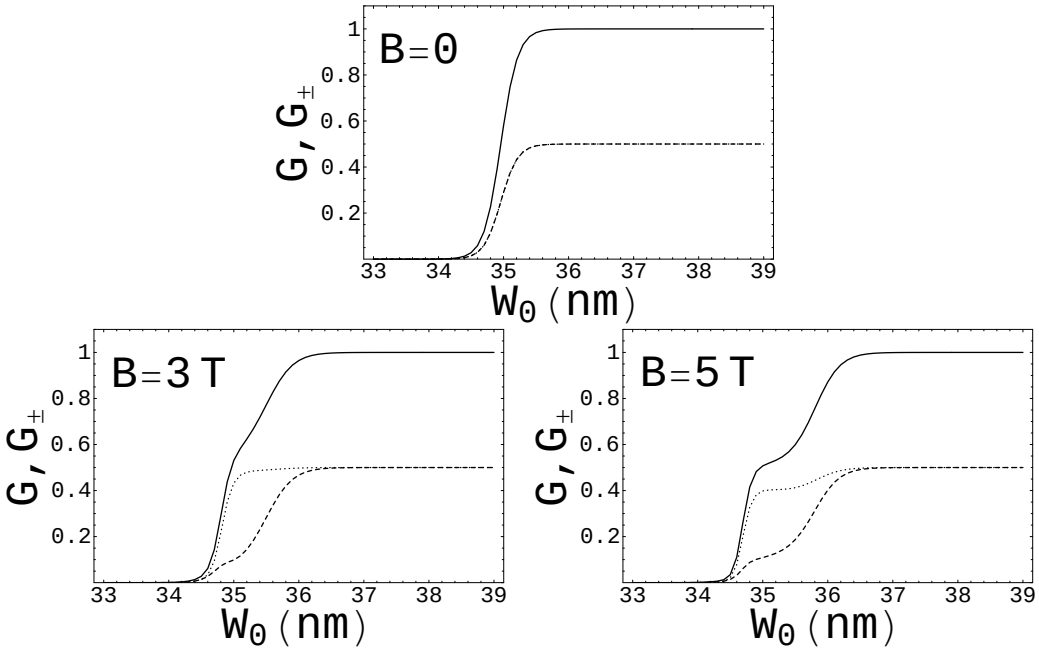

Figure 5.4. Total (solid) and spin-resolved (dashed and dotted lines) conductance as a function of the minimum width W_0 of the point contact. The dashed line refers to the + band, which is the lowest energy band at $x \to +\infty$, where it corresponds to holes transmitted with largest wavevector. We exemplify here the range of small values of B, such that the transmission is either unpolarized or polarized in the $-$ band. The conductances are expressed in units of $2e^2/h$ and the parameters used are listed in the text. The first plateau is seen to gradually evolve to the e^2/h value.

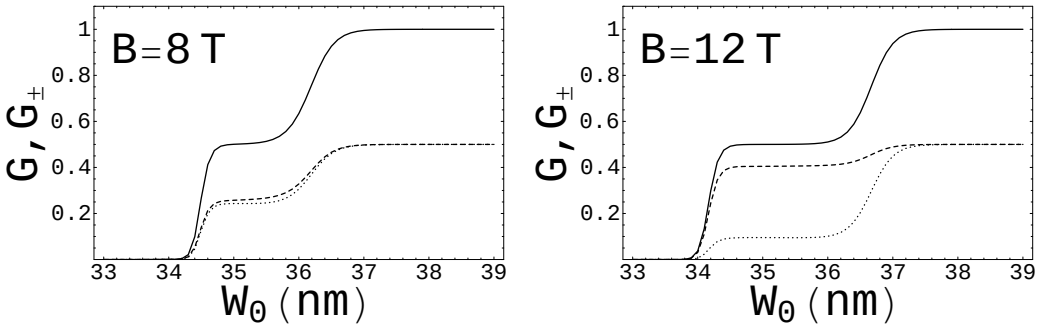

Figure 5.5. Same of Figure 5.4 at larger values of the magnetic field. The crossover to the adiabatic case of holes polarized in the + band is shown.

We also notice that the evolution of the first plateau has some resemblance to the phenomenon of the "0.7" anomaly, which it was proposed to occur in the presence of a finite polarization in the point-contact (see Ref. [42]). However, the "0.7" anomaly is observed at zero magnetic field and is possibly a many-body effect due to the Coulomb interaction, which is neglected here.

The condition following from (5.5) gives:

$$B \gg \frac{\hbar^3 \gamma (6k_F^5/\mathcal{L})^{1/2}}{g\mu_B} \ , \tag{5.13}$$

where we estimated $v = \frac{3\gamma\hbar^2\pi^2}{W_0^2} \simeq 3\gamma\hbar^2 k_F^2$ as obtained from Eq. (5.4) at $k_x = 0$ and $x = 0$. Using the parameters of Figure 5.4 and $W_0 = 35$ nm as appropriate at the onset of the conducting regime, we obtain that the e^2/h plateau is established at $B \gg 3.5$ T, which is in good agreement with Figure 5.4.

Intermediate magnetic field. At higher fields the crossover from the previous regime to the high-field adiabatic transmission is realized. The first panel of Figure 5.5 represents the situation in which the transmission is almost completely unpolarized.

Large magnetic field. At very large fields, the onset of the conduction occurs in the lowest energy band, as displayed in the second panel of Figure 5.5. In fact, the conductance at the e^2/h plateau is almost completely contributed by G_+.

This regime is established on a scale of larger values of B, as it can be estimated by (5.5). Neglecting the small spin-orbit and Zeeman energies, the onset of the conduction occurs at $\epsilon_F \simeq \frac{\hbar^2}{2mW_0^2}$ and $k_x^2 + \frac{\pi^2}{W^2} = \frac{\pi^2}{W_0^2}$ so that the condition $k_x = \frac{\sqrt{3}\pi}{W}$ is realized at $k_x \simeq \frac{\sqrt{3}\pi}{2W_0} \simeq \frac{\sqrt{3}}{2}k_F$. Therefore the velocity is of the order of v_F, larger than in the previous case around $k_x \simeq 0$. We obtain:

$$B \gg \frac{\hbar^2 (\sqrt{3}\gamma k_F^3 v_F/\mathcal{L})^{1/2}}{g\mu_B} \ , \tag{5.14}$$

and $B \gg 8$ T with the parameters of Figure 5.5, in good agreement with Figure 5.5[1].

[1] Accidentally the agreement is surprisingly accurate.

5.4 Discussion

The above discussion and numerical results show that the particular nature of the spin-orbit coupling for two-dimensional heavy holes has clear qualitative consequences on the polarization properties of the holes transmitted in the point contact. Our results are in agreement with the experimental evidence available so far from spin-focusing experiments [4]. We predict that a change in sign in the polarization of the transmitted holes can be observed in a regime of rather high magnetic fields.

Another interesting problem would be the effect of a magnetic field transverse to the channel, which was not considered here or in the experiment [4].

We also notice that a detailed theoretical treatment would require a more sophisticated approach that the one considered here to take in account the geometry of the smooth gating potentials producing the point-contact and the intricacies of the band-structure cubic symmetry. Regarding this last point, we notice that a different behavior is expected between wires oriented in the two different crystallographic directions, $[1\bar{1}0]$ or $[33\bar{2}]$, due to the fact that in the $[1\bar{1}0]$ case anticrossing gaps are opened in the spectrum at zero magnetic field, due to the broken reflection symmetry. In the same way, it is also interesting that the polarization of the carriers could be in principle influenced by purely electrical means, by tuning the symmetry of the lateral confinement by external gates.

Hints of the discussed new experimental features at larger magnetic fields and different crystal orientations are already observed [49]. However, no systematic study of all aspects of the polarized transmission is available to date, which is expected to reveal a rather reach phenomenology.

6. Exchange energy and generalized spin-orbit coupling

In this Chapter we start the study of the interacting problem. In particular, we consider the model two-dimensional electronic system described by the following hamiltonian[1]:

$$\hat{H}_n \;=\; \sum_i \hat{H}^{(i)}_{0,n} + \frac{1}{2}\sum_{i\neq j} \frac{e^2}{\epsilon|\hat{\mathbf{r}}_i - \hat{\mathbf{r}}_j|} \;, \tag{6.1}$$

where the single-particle terms are given in Eq. (3.13), which includes a generalized spin-orbit coupling. For easier notation we use in the following and $\epsilon = 1$.

As a preliminary analysis, we consider in this Chapter the effect of the exchange energy on the paramagnetic phase, for which a mean-field description in terms of noninteracting single-particle states is appropriate. The general description of the Hartree-Fock theory and the construction of low-density self-consistent polarized solutions is presented in the following Chapters, where the most interesting case of the linear Rashba spin-orbit is examined in great detail.

We will show here that the effect of the exchange energy is in most cases to suppress, rather to enhance, the generalized polarization of the system. This fact allows to qualitatively understand recent experimental results for polarized states of two-dimensional holes in a $GaAs$ heterostructures [20].

6.1 Exchange energy

For the standard $n = 0$ case of Eq. (6.1), the expression for the exchange energy per particle in a homogeneous electron liquid is well known [1]. In particular, for the

[1]In this expression standard terms associated with the neutralizing background have been omitted for simplicity [1].

two dimensional case, which is of relevance in the present discussion, the formula is given by (in Rydbergs):

$$\mathcal{E}_{x,0}(r_s,p) = -\frac{4\sqrt{2}}{3\pi}\frac{(1+p)^{\frac{3}{2}}+(1-p)^{\frac{3}{2}}}{r_s} \ , \tag{6.2}$$

where p is defined in Eq. (3.20).

It is important to notice that Eq. (6.2) is obtained under the assumption that the spins are quantized along a common arbitrary quantization axis $\hat{y}$. Therefore, when, as in this particular case, the label $\pm$ refers to the orientation $\uparrow\downarrow$ of the spin, p assumes the meaning of a fractional spin polarization. It is easy to see that the exchange energy (6.2) monotonically attains its maximum magnitude for $p = 1$, and therefore favors the polarization of the system. In fact, within the Hartree-Fock approximation, a transition to a fully spin polarized state occurs for $r_s = \frac{3\pi}{8(2-\sqrt{2})} \simeq 2.01$ [1].

As we will presently show, this scenario changes in interesting ways in the presence of the spin-orbit interaction. If translational invariance is not broken [21], a single Slater determinant can be constructed with plane waves states characterized by generic orientation of the spin quantization axis $\hat{s}_{\mathbf{k}}$ and occupation numbers $n_{\mathbf{k}\pm}$. The total exchange energy can be written in the following elegant general form [50]:

$$E_x = -\frac{1}{2L^2}\sum_{\mathbf{k},\mathbf{k}';\mu,\mu'=\pm} v_{\mathbf{k}-\mathbf{k}'}\,\frac{1+\mu\mu'\ \hat{s}_{\mathbf{k}}\cdot\hat{s}_{\mathbf{k}'}}{2}\,n_{\mathbf{k}\,\mu}n_{\mathbf{k}'\mu'} \ , \tag{6.3}$$

which represents a functional of $n_{\mathbf{k}\,\pm}$ and $\hat{s}_{\mathbf{k}}$. Eq. (6.3) immediately reduces to the familiar textbook result when $\hat{s}_{\mathbf{k}} = \hat{y}$. In this case only states with parallel spin contribute.

Making use of Eq. (3.17) in (6.3) leads to the following result for the exchange energy per particle (in Rydbergs):

$$\mathcal{E}_{x,n}(r_s,p) = \mathcal{E}_{x,0}(r_s,p) + \delta\mathcal{E}_{x,n}(r_s,p) \ , \tag{6.4}$$

where the correction to Eq. (6.2) can be obtained from the following quadrature:

$$\delta\mathcal{E}_{x,n}(r_s,p) = \frac{\sqrt{2}}{4\pi r_s}\int_{\sqrt{1-p}}^{\sqrt{1+p}}\kappa\,\mathrm{d}\kappa\int_{\sqrt{1-p}}^{\sqrt{1+p}}\kappa'\,\mathrm{d}\kappa'\int_0^{2\pi}\frac{1-\cos n\theta}{\sqrt{\kappa^2+\kappa'^2-2\kappa\kappa'\cos\theta}}\,\mathrm{d}\theta \ . \tag{6.5}$$

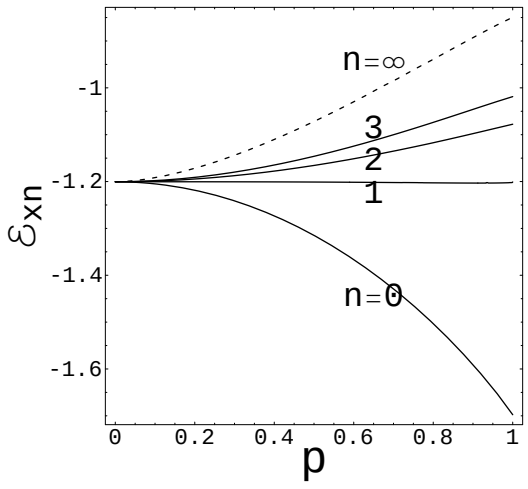

Figure 6.1. Plot of the exchange energy per particle $\mathcal{E}_{x,n}(r_s, p)$ (in Ry units) as a function of p. Here $r_s = 1$. The different values of n are noted, and the limiting curve $n = \infty$ is also displayed (dashed line).

The resulting exchange energy is plotted in Figure 6.1 as a function of p. We notice that for $p = 0$, the exchange energy is independent of the spin quantization axis orientations $\hat{s}_{\mathbf{k}}$. This can be understood by realizing that the corresponding many-body state can be constructed by repeated application of $b^{\dagger}_{\mathbf{k}+} b^{\dagger}_{\mathbf{k}-}$, an operator that creates a spin singlet and is therefore independent of the spin quantization direction. As a consequence the $\hat{s}_{\mathbf{k}}$ dependence of all the physical quantities (e.g. the exchange and the spin orbit energies) stems only from the existence of regions of momentum space where $n_{\mathbf{k}+} \neq n_{\mathbf{k}-}$. It is also important to remark that only for $n = 0$ is the magnitude of the exchange energy maximum for $p = 1$. For the other cases the minimum occurs at $p = p_1^* \simeq 0.915$ for $n = 1$ (see also the first panel of Figure 8.2) and at $p = 0$ for $n \geq 2$.

For completeness we remark that in the limiting case of very large winding number n the result can be obtained simply neglecting the $\cos n\theta$ contribution in Eq. (6.5). For comparison the corresponding curve is shown as a dashed line in Figure 6.1.

Notice that in this case the magnitude of the exchange energy is minimum for $p = 1$, the value being given by:

$$\lim_{n\to\infty} \mathcal{E}_{x,n}(r_s, 1) = -\frac{8}{3\pi r_s} \ . \tag{6.6}$$

6.2 Interacting generalized polarization

The value p_{min} of the ground state generalized polarization can be found by minimizing the total energy:

$$\mathcal{E}_n(r_s, p) = \mathcal{E}_n^{(0)}(r_s, p) + \mathcal{E}_{x,n}(r_s, p) \ , \tag{6.7}$$

where the noninteracting energy $\mathcal{E}_n^{(0)}(r_s, p)$ is given in (3.22) and the exchange contribution is described in the previous section.

The different behavior of the exchange energy in the various cases leads to dissimilar results. For $n = 0$, the fact that the minimum of $\mathcal{E}_{x,0}$ occurs at $p = 1$ leads to an enhancement of p_{min} i.e. to the familiar enhancement of the spin polarization. The opposite is true for $n \geq 2$ since in these cases the minimum of $\mathcal{E}_{x,0}$ occurs at $p = 0$. The $n = 1$ case is slightly more complex and is treated in detail in Chapter 8. A similar argument leads one to conclude that the critical value $\bar{\gamma}_d$ for which the upper spin band empties (at fixed r_s) decreases from its non interacting value for $n = 0$ ($g = 1$) while it does increase in the other cases.

Studying the limit of small p is of particular interest since it corresponds to a determination of the generalized susceptibility. In this case a direct inspection of the integral of Eq. (6.5) leads to the asymptotic formula:

$$\mathcal{E}_{x,n}(r_s, p) \simeq -\frac{8\sqrt{2}}{3\pi r_s} - \frac{C_n}{r_s} p^2 \ , \tag{6.8}$$

where we have defined the quantity

$$C_n \ = \ \frac{\sqrt{2}}{\pi} \sum_{m=0}^{n} \frac{1}{1-2m} \ . \tag{6.9}$$

The resulting value for p_{min} is then given by:

$$p_{min} \simeq \frac{g}{1 - C_n r_s} \ . \tag{6.10}$$

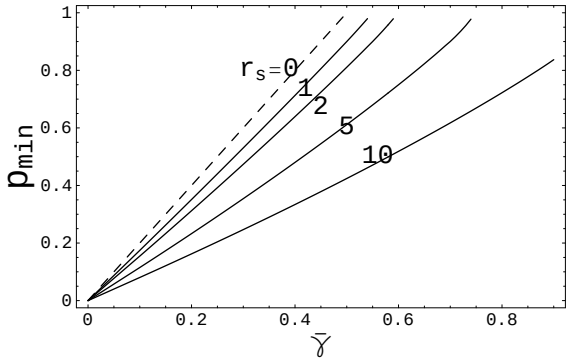

Figure 6.2. Plot of the fractional generalized polarization p_{min} as function of the parameter $\bar{\gamma}$ for different values of r_s. Here $n = 2$. The increase of the depopulation value $\bar{\gamma}_d$ with r_s is manifest.

Eq. (6.10) simply expresses the fact that in this limit the effect of the interactions is to renormalize the non interacting result $p_{min}^{(0)} \simeq g$ via the denominator $(1-C_n r_s)^{-1}$. Interestingly the latter corresponds to an enhancement only for $n = 0$.

In particular for $n = 0$ we recover the well known Hartree-Fock differential instability occurring at $r_s = \frac{\pi}{\sqrt{2}}$ [1]. On the other hand, for $n = 1$ we have $C_1 = 0$. In this case the whole renormalization effect is associated with higher order terms and it will be obtained explicitly in a later Chapter. Finally for $n \geq 2$, C_n is (ever increasingly) negative leading to a perhaps iconoclastic exchange driven quenching of the generalized polarization.

Expression (6.10) is valid in the limit of $\bar{\gamma} \to 0$ or, for $n > 1$, when r_s is large. The generic case when p_{min} is not small must be obtained numerically. As an example we show in Figure 6.2 the value of p_{min} as function of the dimensionless coupling strength $\bar{\gamma}$ for different values of the density parameter r_s in the case of $n = 2$. We notice that for low densities the depopulation value $\bar{\gamma}_d$, for which $p_{min} = 1$, is considerably increased by exchange. This is in stark contrast with the familiar $n = 0$ case. In particular, for the $n = 2$ case of Figure 6.2 we have:

$$\bar{\gamma}_d = \frac{1}{2} + \left(\frac{1}{12} - \frac{1}{9\pi}\right) r_s \ , \tag{6.11}$$

where the second term represents the increase of the depopulation field due to exchange effects. In this particular case the correction is linear in the density parameter r_s.

6.3 Application to spin polarized hole systems

Spin polarization experiments have recently been performed on $GaAs$ two dimensional hole systems with growth direction along [113] and [100] [20]. In these studies, the magnitude of the in-plane depopulation field B_d, when only one band is occupied, is surmised from the measured longitudinal magneto-resistance. While a small suppression of B_d with respect to its non interacting value B_d^0 is observed in the [113] case, basically no suppression is observed for the [100] growth direction. This must be contrasted with the fact that, as discussed in Ref. [20], in the absence of spin-orbit interaction and at the densities under consideration, the expected ratio for electrons is of order $B_d^0/B_d \sim 10$.

The experiments of Ref. [20] are carried out at somewhat low densities ($r_s \simeq 10 - 15$) a regime in which a simple Hartree-Fock treatment, as well as somewhat more sophisticated analytical treatments designed to approximately include correlation effects, generally fail to provide reliable quantitative results. On the other hand, Monte Carlo analysis of the system being to date non existent, it is reasonable to expect that many of the qualitative features established by a study of the exchange energy will prove sufficiently robust to justify such a preliminary discussion.

In these quantum wells the introduction of a magnetic field induces in the effective hamiltonian of two-dimensional holes the spin dependent terms given in Eqs. (3.10), (3.11), and (3.12) of Section 3.3. All these terms can be reduced to some of the generic forms contemplated by our model hamiltonian (3.13). The corresponding coupling strength γ for each of these terms can then be extracted, as for instance explicitly done in (3.14), (3.15), and (3.16). One can then make use of the definitions

(3.23) and (3.24), alongside suitable numerical parameters, to determine the relevant dimensionless coupling strength.

For our numerical estimates we use values appropriate for the case of Ref. [20]. In particular: $W = 200$ Å for the width of the quantum well, $m \simeq 0.2\, m_0$ for the effective mass, $\epsilon = 12.4$ for the background dielectric constant, and $n = 3\ 10^{10}$ cm^{-2} for the hole density (corresponding to $r_s \simeq 10$).

We first consider the [113] growth direction. In this case the various physical properties are anisotropic in the plane, the principal directions being given by $x \equiv [1\bar{1}0]$ and $y \equiv [33\bar{2}]$. For the density under consideration the depopulation field is approximately given by $B_d \simeq 10$ T along x and $B_d \simeq 5$ T along y. This gives the following results for various dimensionless couplings:
For Eq. (3.10) we have

$$|g^x_{21}| = 0.19 \quad \text{and} \quad |g^y_{21}| = 0.09 \ ; \tag{6.12}$$

For Eq. (3.11):

$$|g^x_{03}| = 0.23 \quad \text{and} \quad |g^y_{03}| = 0.03 \ ; \tag{6.13}$$

Finally for Eq. (3.12):

$$|g^x_{01}| = 0.14 \quad \text{and} \quad |g^y_{01}| = 0.16 \ . \tag{6.14}$$

We recall here that (3.10) is a term of type $n = 2$, while (3.11) and (3.12) are both of type $n = 0$. We notice that the quadratic spin-orbit, although in general smaller, has a strength which is comparable to that of the terms of the Zeeman type.

For the [100] growth direction, the Zeeman term (3.12) is vanishing, and the depopulation magnetic field is approximately $B_d \simeq 10$ T. In this case, we obtain that the quadratic spin orbit and the Zeeman term cubic in B have comparable strength: $|g_{03}| \simeq |g_{21}| \simeq 0.2$.

These estimates suggest that the apparent quenching of the many-body enhancement of the spin susceptibility is due to the presence of a large $n = 2$ spin-orbit coupling. Moreover the presence of a sizable $n = 3$ Rashba spin-orbit term would

also result in a reduction of the generalized polarization. This is consistent with the experimental finding that the suppression is most noticeable for [100] quantum wells, for which the quadratic spin-orbit is comparatively stronger.

From our theory one can moreover surmise that a larger many-body enhancement of the susceptibility is expected in the limit of very low densities when, due to the $\propto k^2$ and $\propto k^3$ dependence, the $n = 2$ and $n = 3$ terms become less relevant. The enhancement should be also more noticeable in the limit of a very narrow well. In the particular case of the [113] growth direction, this happens because the linear Zeeman term (3.12) can in principle become dominant. For the [100] growth direction on the other hand, the term (3.12) vanishes while the cubic Zeeman term (3.11) is largest. This in spite of the $\sim W^4$ proportionality of the coupling strength. The reason is that the depopulation field is large in a very narrow well. This obtains since $B_d \sim 1/W^{\frac{4}{3}}$ while the magnitude of the quadratic spin-orbit (3.10) behaves like $\sim W^{\frac{2}{3}}$ thereby losing its relevance. It should be kept in mind that, being based on a perturbative treatment and not taking in account orbital effects, these conclusions should be taken at best as qualitative[2].

6.4 Discussion

The main conclusion of our analysis is that in the presence of quadratic and cubic spin-orbit interactions the magnitude of the exchange energy decreases with increasing generalized polarization. This results in a quenched value of p and in a corresponding increase of the value of the depopulation coupling $\bar{\gamma}_d$.

Being based on a study of the exchange energy only, our theory can be expected to be strictly valid in the high density limit. The reason is that it is in this regime that the exchange energy represents the first interaction correction to the non interacting result, correlation effects becoming comparatively smaller as r_s decreases. On the other hand, at not too low densities, the physics of the exchange is still expected to

[2]A potentially relevant phenomenon we have neglected is that of the effective mass enhancement associated with the magnetic field [20].

give qualitatively reasonable results. This conclusion appears to be corroborated by the apparent observed reduction of the many-body enhancement of the spin susceptibility in dilute hole systems in which, beside the familiar Zeeman term, the magnetic field also induces large quadratic spin-orbit interactions.

It will be also clear from the discussion in the following Chapters that, when the spin-orbit coupling terms described by Eq. (3.13) are present in isolation, the many-body states, as parameterized by r_s and p, are also self-consistent solutions of the Hartree-Fock equations. On the other hand this is not the case when multiple concomitant terms are present. In such situations the circular symmetry is broken, and the interacting problem is considerably more complicated. Such situations must be treated case by case. In particular the spin quantization directions $\hat{s}_{\mathbf{k}}$ must be determined self-consistently[3]. As we will see, this problem has nontrivial solutions in the case of broken symmetry states, like for instance in the case of ferromagnetic phases [50].

As a final remark we stress that since the generalized fractional polarization does not correspond directly to an actual magnetization, strictly speaking, one cannot draw direct conclusions about the enhancement of the spin-spin response from measurements of the depopulation field B_d. We will show that the spin susceptibility is enhanced by the exchange, in a way similar to the usual case without spin-orbit. The bare spin-spin susceptibility involves the response to a pure $n = 0$ perturbation which, from an experimental point of view, is not straightforward to realize for the case of hole systems of Ref. [20]. In fact, as we have argued, the external magnetic field induces also a change of the $n = 2$ spin-orbit coupling.

In the same way, the quenching of the generalized polarization do not correspond to a lower critical density for the transition to a ferromagnetic state. Interestingly, we will obtain that the Bloch transition occurs at densities that are in general *larger* than in the absence of spin-orbit interaction.

[3]This also happens in the presence of terms equivalent to the same n by different spin rotations, as for example in the simultaneous presence of Rashba and Dresselhaus spin-orbit.

7. Hartree-Fock theory with Rashba spin-orbit coupling

We start discussing in this Chapter the Hartree-Fock approximation in the presence of spin-orbit coupling. For definiteness, we consider the particular case of the linear Rashba spin-orbit, which turns out to be the case with most interesting features. The particular interacting hamiltonian $\hat{H}$ under consideration is given by Eq. (6.1), in the particular case $n = 1$.

We devote this Chapter to a general discussion of the HF approximation in presence of Rashba spin-orbit, and present explicit results in the following Chapters. The treatment can be easily generalized to other types of spin-orbit, and correlation effects that go beyond the mean field treatment can be approximately included in the high-density limit.

7.1 Hartree-Fock energy

We start from the second quantization form of the hamiltonian $\hat{H}$ expressed in the standard plane waves basis. The spin quantization axis is chosen along the z-axis, which by definition is perpendicular to the plane of the motion:

$$\begin{aligned}\hat{H} \ = & \sum_{\mathbf{k},\sigma} \frac{\hbar^2 \mathbf{k}^2}{2m} \, \hat{a}^\dagger_{\mathbf{k}\sigma} \hat{a}_{\mathbf{k}\sigma} + \sum_{\mathbf{k}} \alpha \hbar k \left(i e^{-i\phi_{\mathbf{k}}} \, \hat{a}^\dagger_{\mathbf{k}\uparrow} \hat{a}_{\mathbf{k}\downarrow} + h.c. \right) + \\ & + \frac{1}{2L^2} \sum_{\mathbf{k},\mathbf{k}',\mathbf{q}\neq 0,\sigma,\sigma'} v_{\mathbf{q}} \, \hat{a}^\dagger_{\mathbf{k}+\mathbf{q}\,\sigma} \hat{a}^\dagger_{\mathbf{k}'-\mathbf{q}\,\sigma'} \hat{a}_{\mathbf{k}'\,\sigma'} \hat{a}_{\mathbf{k}\,\sigma} \ ,\end{aligned} \tag{7.1}$$

where $v_{\mathbf{q}} = \frac{2\pi e^2}{|\mathbf{q}|}$.

Limiting our study to the case of homogeneous solutions, an interesting class of mean field states is represented by the Slater determinants formed occupying the single particle states obtained as the result of the following Bogolubov transformation:

$$\begin{pmatrix} \hat{b}^{\dagger}_{\mathbf{k}+} \\ \hat{b}^{\dagger}_{\mathbf{k}-} \end{pmatrix} = \begin{pmatrix} \cos\frac{\beta_{\mathbf{k}}}{2} & e^{i\gamma_{\mathbf{k}}}\sin\frac{\beta_{\mathbf{k}}}{2} \\ e^{-i\gamma_{\mathbf{k}}}\sin\frac{\beta_{\mathbf{k}}}{2} & -\cos\frac{\beta_{\mathbf{k}}}{2} \end{pmatrix} \begin{pmatrix} \hat{a}^{\dagger}_{\mathbf{k}\uparrow} \\ \hat{a}^{\dagger}_{\mathbf{k}\downarrow} \end{pmatrix} \ . \tag{7.2}$$

For a given $\mathbf{k}$, this transformation simply affects a rotation of the spin quantization axis from $\hat{z}$ to an arbitrary orientation $\hat{s}_{\mathbf{k}}$, as discussed in the previous Chapters. The geometry of this rotation as well as the definition of the corresponding polar and azimuthal angles $\beta_{\mathbf{k}}$ and $\gamma_{\mathbf{k}}$ are still provided in Figure 2.5. This choice of the single particle states is the most general if one assumes that translational invariance is preserved, while the instability to charge- and spin-density-wave type distortions has in general to be considered [21].

At this point we evaluate the expectation value of the exact hamiltonian $\hat{\mathcal{H}}$ over any determinantal state obtained filling states of the type (7.2). The total energy is given by the following expression:

$$\begin{aligned} E_{HF}[n_{\mathbf{k}\,\pm}, \hat{s}_{\mathbf{k}}] = & \sum_{\mathbf{k},\,\mu} \frac{\hbar^2\mathbf{k}^2}{2m}\, n_{\mathbf{k}\,\mu} - \hbar\alpha \sum_{\mathbf{k},\,\mu} \mu\, k\, \hat{\phi}_{\mathbf{k}} \cdot \hat{s}_{\mathbf{k}}\, n_{\mathbf{k}\,\mu} \\ & - \frac{1}{2L^2} \sum_{\mathbf{k},\mathbf{k}',\,\mu,\mu'} v_{\mathbf{k}-\mathbf{k}'}\, \frac{1+\mu\mu'\ \hat{s}_{\mathbf{k}} \cdot \hat{s}_{\mathbf{k}'}}{2}\, n_{\mathbf{k}\,\mu} n_{\mathbf{k}'\mu'} \ , \end{aligned} \tag{7.3}$$

where the indices μ and μ' are summed over the values $\pm$. The corresponding particle energies can be calculated from the expression:

$$\epsilon_{\mu}(\mathbf{k}) = \frac{\hbar\mathbf{k}^2}{2m} - \mu\hbar\alpha k\, \hat{\phi}_{\mathbf{k}} \cdot \hat{s}_{\mathbf{k}} - \frac{1}{2L^2} \sum_{\mathbf{k}',\mu'} v_{\mathbf{k}-\mathbf{k}'} (1 + \mu\mu'\ \hat{s}_{\mathbf{k}} \cdot \hat{s}_{\mathbf{k}'}) n_{\mathbf{k}'\mu'} \ , \tag{7.4}$$

which it is immediate to obtain from (7.3).

Clearly E_{HF} represents the (total) Hartree-Fock energy of this particular class of states and is a functional of the occupation numbers $n_{\mathbf{k}\pm}$ and of the orientation of the (wave vector space) local spin quantization axis unit vector $\hat{s}_{\mathbf{k}}$. It is still to be assessed which of these states correspond to actual solutions of the HF problem [1], which we discuss next.

7.2 Mean field diagonalization

The HF equations are obtained by means of a standard Wick theorem based decoupling and diagonalization of the Hamiltonian $\hat{H}$, expressed in terms of the operators $\hat{b}_{\mathbf{k}\pm}$. The kinetic and Rashba terms retain their quadratic form and in particular the kinetic energy remains diagonal. The electron-electron interaction can be reduced to a quadratic form with the use of the following approximation of the quartic products of $\hat{b}_{\mathbf{k}\pm}$ operators:

$$\begin{aligned} b^\dagger_{\mathbf{k}+\mathbf{q}\,\nu}\, b^\dagger_{\mathbf{k}'-\mathbf{q}\,\nu'}\, b_{\mathbf{k}'\mu'}\, b_{\mathbf{k}\,d\mu} \simeq\ & \langle b^\dagger_{\mathbf{k}+\mathbf{q}\,\nu}\, b_{\mathbf{k}'\mu'}\rangle \langle b^\dagger_{\mathbf{k}'-\mathbf{q}\,\nu'}\, b_{\mathbf{k}\,\mu}\rangle + \\ & -\langle b^\dagger_{\mathbf{k}+\mathbf{q}\,\nu}\, b_{\mathbf{k}'\mu'}\rangle\, b^\dagger_{\mathbf{k}'-\mathbf{q}\,\nu}\, b_{\mathbf{k}\,\mu} - \langle b^\dagger_{\mathbf{k}'-\mathbf{q}\,\nu'}\, b_{\mathbf{k}\,\mu}\rangle\, b^\dagger_{\mathbf{k}+\mathbf{q}\,\nu}\, b_{\mathbf{k}'\mu'}\ , \end{aligned} \tag{7.5}$$

where the averages are taken over the trial Slater determinant constructed with the $\hat{b}^\dagger_{\mathbf{k}\pm}$ operators, and are directly expressed in terms of the occupation numbers of the new single particle states:

$$\langle b^\dagger_{\mathbf{k}\,\mu}\, b_{\mathbf{k}'\mu'}\rangle = n_{\mathbf{k}\mu}\delta_{\mathbf{k}\mathbf{k}'}\delta_{\mu\mu'}\ . \tag{7.6}$$

The final result is a quadratic hamiltonian that is in general non diagonal in the chirality indexes. The mean field solutions are obtained by requiring that the coefficient of the $b^\dagger_{\mathbf{k}+}\, b_{\mathbf{k}-}$ term is vanishing:

$$\begin{aligned} & -i\,\hbar\alpha\, k\, e^{-i\phi_{\mathbf{k}}}(\cos^2\frac{\beta_{\mathbf{k}}}{2} + e^{2i(\phi_{\mathbf{k}}-\gamma_{\mathbf{k}})}\sin^2\frac{\beta_{\mathbf{k}}}{2}) - \frac{e^{-i\gamma_{\mathbf{k}}}}{L^2}\sum_{\mathbf{k}'} v_{\mathbf{k}'-\mathbf{k}}\ \frac{(n_{\mathbf{k}'+} - n_{\mathbf{k}'-})}{2} \times \\ & \times \left[\cos\beta_{\mathbf{k}'}\sin\beta_{\mathbf{k}} - e^{i(\gamma_{\mathbf{k}}-\gamma_{\mathbf{k}'})}\sin\beta_{\mathbf{k}'}\cos^2\frac{\beta_{\mathbf{k}}}{2} + e^{-i(\gamma_{\mathbf{k}}-\gamma_{\mathbf{k}'})}\sin\beta_{\mathbf{k}'}\sin^2\frac{\beta_{\mathbf{k}}}{2}\right] = 0\ , \end{aligned} \tag{7.7}$$

where the first contribution is from the Rashba spin-orbit and the second from the electron-electron interaction. By separating the real and imaginary part of the above equation, we are lead to the following conditions:

$$\hbar\alpha\, k\, \cos(\phi_{\mathbf{k}} - \gamma_{\mathbf{k}}) = \frac{1}{2L^2}\sum_{\mathbf{k}'} v_{\mathbf{k}-\mathbf{k}'}(n_{\mathbf{k}'+} - n_{\mathbf{k}'-})\sin(\gamma_{\mathbf{k}} - \gamma_{\mathbf{k}'})\sin\beta_{\mathbf{k}'}\ , \tag{7.8}$$

$$\tan\beta_{\mathbf{k}} = \frac{\frac{1}{2L^2}\sum_{\mathbf{k}'} v_{\mathbf{k}-\mathbf{k}'}(n_{\mathbf{k}'+} - n_{\mathbf{k}'-})\cos(\gamma_{\mathbf{k}} - \gamma_{\mathbf{k}'})\sin\beta_{\mathbf{k}'} + \hbar\alpha\, k \sin(\gamma_{\mathbf{k}} - \phi_{\mathbf{k}})}{\frac{1}{2L^2}\sum_{\mathbf{k}'} v_{\mathbf{k}-\mathbf{k}'}(n_{\mathbf{k}'+} - n_{\mathbf{k}'-})\,\cos\beta_{\mathbf{k}'}} \;, \tag{7.9}$$

which have a simple geometrical interpretation. If we define the following effective magnetic field:

$$\frac{g\mu_B}{2}\mathbf{B}_{eff}(\mathbf{k}) = -\hbar\alpha\, k\,\hat{\phi}_{\mathbf{k}} - \frac{1}{4L^2}\sum_{\mathbf{k}'}(n_{\mathbf{k}'+} - n_{\mathbf{k}'-})\, v_{\mathbf{k}-\mathbf{k}'}\,\hat{s}_{\mathbf{k}'} \;, \tag{7.10}$$

Eq. (7.8) requires $\mathbf{B}_{eff}(\mathbf{k})$ to be in the plane of $\hat{s}_{\mathbf{k}}$ and $\hat{z}$ and, given this condition, (7.9) requires $\mathbf{B}_{eff}(\mathbf{k})$ and $\hat{s}_{\mathbf{k}}$ to be parallel.

This result was obtained with a formal procedure but could have been surmised directly from the form of the energy functional (7.3), which has to be minimum for the HF ground state. If we fix the occupation numbers $n_{\mathbf{k}\pm}$, (7.3) only depends on the orientations $\hat{s}_{\mathbf{k}}$ and can be interpreted as the energy of a system of magnetic dipoles, placed at fixed positions in $\mathbf{k}$ space and in presence of an external azimuthal magnetic field arising from the Rashba spin-orbit. The exchange energy provides a dipole-dipole interaction which has a $1/|\mathbf{k}|$ dependence. In equilibrium, the direction $\hat{s}_{\mathbf{k}}$ of each magnetic dipole is parallel to $\mathbf{B}_{eff}$, which is the sum of the external Rashba field and the exchange field produced by the self-consistent distribution of all the remaining dipoles.

7.3 Energy minimization for $\mathbf{B} \neq 0$

We derive here the HF equations by direct minimization of the energy (7.3). This is an equivalent procedure to the formal mean field method we discussed in the previous section, the only difference being that we consider here the slightly more general situation in which an external magnetic field is present. This is treated by adding a perturbing Zeeman term to the single-particle hamiltonian (2.15) while

smaller orbital effects are neglected. The Zeeman term can be immediately included in the energy functional (7.3) by adding the following contribution:

$$E_Z[n_{\mathbf{k}\pm}, \hat{s}_{\mathbf{k}}] = \frac{g\mu_B}{2}\mathbf{B}\cdot\sum_{\mathbf{k},\,\mu}\mu\,\hat{s}_{\mathbf{k}}n_{\mathbf{k}\pm}\ . \tag{7.11}$$

We use in this section dimensionless units, and in particular we rescale the wavevectors as $\boldsymbol{\kappa} = \mathbf{k}/k_F$ where $k_F = \sqrt{2\pi n}$. The azimuthal angle of $\boldsymbol{\kappa}$ is denoted by ϕ, and the spin quantization axis is expressed as a function of dimensionless momenta via $\hat{s}(y,\phi)$, determined by $\hat{s}(k/k_F,\phi) = \hat{s}_{\mathbf{k}}$. The magnetic field is also rescaled as follows:

$$\bar{\mathbf{B}} = \frac{g\mu_B}{e^2k_F}\,\mathbf{B}\ . \tag{7.12}$$

We consider explicitly the particular case in which two bands are occupied. We assume that the occupation of each band is a simply connected region around the origin, and can be specified by the radial distances $\rho_\pm(\phi)$ which define the two Fermi surfaces. If only one band is occupied, such that the occupied states have momenta between the two Fermi surfaces as determined by $\rho_{in}(\phi)$ and $\rho_{out}(\phi)$, the treatment is very similar. The expressions only differ for the substitution $\rho_\pm \to \rho_{out(in)}$ and for a few other modifications that we are going to discuss when needed.

The total energy per particle in Ry units is expressed as the following sum:

$$\mathcal{E}_{HF}[\rho_\pm, \hat{s}] = \frac{E_{HF}[n_{\mathbf{k}\pm}, \hat{s}_{\mathbf{k}}]}{N\,Ry} = \mathcal{E}_Z + \mathcal{E}_K + \mathcal{E}_{so} + \mathcal{E}_x\ , \tag{7.13}$$

where each of the four terms is a functional of $\rho_\pm(\phi)$ and $\hat{s}(\kappa,\phi)$.

The first term refers to the Zeeman energy:

$$\mathcal{E}_Z = \frac{\sqrt{2}}{r_s}\,\bar{\mathbf{B}}\cdot\int_0^{2\pi}\frac{\mathrm{d}\phi}{2\pi}\int_{\rho_-(\phi)}^{\rho_+(\phi)}\hat{s}(\kappa,\phi)\,\kappa\mathrm{d}\kappa\ , \tag{7.14}$$

and the second to the kinetic energy:

$$\mathcal{E}_K = \frac{2}{r_s^2}\int_0^{2\pi}\frac{\mathrm{d}\phi}{2\pi}\left(\int_0^{\rho_+(\phi)}\kappa^3\mathrm{d}\kappa + \int_0^{\rho_-(\phi)}\kappa^3\mathrm{d}\kappa\right)\ , \tag{7.15}$$

where in the case of a single band the second integral in parenthesis has to be multiplied by -1. The third contribution refers to the Rashba spin-orbit:

$$\mathcal{E}_{so} = -\frac{2\sqrt{2}\,\bar{\alpha}}{r_s}\int_0^{2\pi}\frac{\mathrm{d}\phi}{2\pi}\int_{\rho_-(\phi)}^{\rho_+(\phi)}\hat{\phi}\cdot\hat{s}(\kappa,\phi)\,\kappa^2\mathrm{d}\kappa\ , \tag{7.16}$$

and the last to the exchange energy:

$$\mathcal{E}_x = -\frac{\sqrt{2}}{2r_s}\left[\int_0^{2\pi}\frac{\mathrm{d}\phi}{2\pi}\int_{\rho_-(\phi)}^{\rho_+(\phi)}\kappa\mathrm{d}\kappa\int_0^{2\pi}\frac{\mathrm{d}\phi'}{2\pi}\int_{\rho_-(\phi')}^{\rho_+(\phi')}\frac{1+\hat{s}(\kappa,\phi)\cdot\hat{s}(\kappa',\phi')}{\sqrt{\kappa^2+\kappa'^2-2\kappa\kappa'\cos(\phi-\phi')}}\kappa'\mathrm{d}\kappa'\right.$$
$$\left.+\,4\int_0^{2\pi}\frac{\mathrm{d}\phi}{2\pi}\int_0^{\rho_+(\phi)}\kappa\mathrm{d}\kappa\int_0^{2\pi}\frac{\mathrm{d}\phi'}{2\pi}\int_0^{\rho_-(\phi')}\frac{\kappa'\mathrm{d}\kappa'}{\sqrt{\kappa^2+\kappa'^2-2\kappa\kappa'\cos(\phi-\phi')}}\right], \tag{7.17}$$

where in the case of a single band the contribution in the second line is omitted.

In the minimization of $\mathcal{E}_{HF}$ one has to enforce the constraints that the $\hat{s}(\kappa,\phi)$ unit vectors are normalized:

$$\hat{s}(\kappa,\phi)\cdot\hat{s}(\kappa,\phi) = 1\ , \tag{7.18}$$

and that the particle number is conserved:

$$\int_0^{2\pi}\frac{\rho_+^2(\phi)+\rho_-^2(\phi)}{2}\frac{\mathrm{d}\phi}{2\pi} = 1\ . \tag{7.19}$$

In the case of a single band this second constraint involves the difference $\rho_{out}^2(\phi) - \rho_{in}^2(\phi)$ instead.

Finally, the quantity that has to be minimized is the following functional, where the appropriate Lagrange multipliers λ_1 and $\lambda_2(\kappa,\phi)$ have been introduced:

$$\mathcal{F}_{HF}[\rho_\pm,\hat{s}] = \mathcal{E}_{HF}[\rho_\pm,\hat{s}] - \lambda_1\int_0^{2\pi}\frac{\rho_+^2(\phi)+\mathrm{s}_-\rho_-^2(\phi)}{2}\frac{\mathrm{d}\phi}{2\pi}$$
$$-\int_0^{2\pi}\frac{\mathrm{d}\phi}{2\pi}\int_0^{+\infty}\lambda_2(\kappa,\phi)\ \hat{s}(\kappa,\phi)\cdot\hat{s}(\kappa,\phi)\,\kappa\mathrm{d}\kappa\ . \tag{7.20}$$

The minimization can be achieved as follows. The first condition $\frac{\delta\mathcal{F}_{HF}}{\delta\hat{s}(\kappa,\phi)} = 0$ leads to the equation:

$$\hat{s}(\kappa,\phi) = \frac{1}{\sqrt{2}\,r_s\lambda_2(\kappa,\phi)}\left[\bar{\mathbf{B}} - 2\bar{\alpha}\,\kappa\,\hat{\phi}\right. \tag{7.21}$$
$$\left.-\int_0^{2\pi}\frac{\mathrm{d}\phi'}{2\pi}\int_{\rho_-(\phi')}^{\rho_+(\phi')}\frac{\hat{s}(\kappa',\phi')}{\sqrt{\kappa^2+\kappa'^2-2\kappa\kappa'\cos(\phi-\phi')}}\kappa'\mathrm{d}\kappa'\right],$$

which remains unchanged in the case of a singly occupied band. The second functional derivative, $\frac{\delta\mathcal{F}_{HF}}{\delta\rho_\pm(\phi)} = 0$, gives the following two equations:

$$\lambda_1 = \frac{2\rho_\pm^2(\phi)}{r_s^2} \pm \frac{\sqrt{2}}{r_s}\left[\bar{\mathbf{B}}\cdot\hat{s}(\rho_\pm(\phi),\phi) - 2\bar{\alpha}\,\hat{\phi}\cdot\hat{s}(\rho_\pm(\phi),\phi)\,\rho_\pm(\phi)\right. \tag{7.22}$$

$$-\int_0^{2\pi}\frac{\mathrm{d}\phi'}{2\pi}\int_{\rho_-(\phi')}^{\rho_+(\phi')}\frac{1+\hat{s}(\rho_\pm(\phi),\phi)\cdot\hat{s}(\kappa',\phi')}{\sqrt{\rho_\pm^2(\phi)+\kappa'^2-2\rho_\pm(\phi)\kappa'\cos(\phi-\phi')}}\,\kappa'\mathrm{d}\kappa'\Bigg]$$
$$-\frac{2\sqrt{2}}{r_s}\int_0^{2\pi}\frac{\mathrm{d}\phi'}{2\pi}\int_0^{\rho_\mp(\phi')}\frac{\kappa'\mathrm{d}\kappa'}{\sqrt{\rho_\pm^2(\phi)+\kappa'^2-2\rho_\pm(\phi)\kappa'\cos(\phi-\phi')}}\,.$$

In the case of a single band the latter has to be modified as follows: the $\pm$ sign in the first line becomes $+$, and the term in the last line must be omitted.

Eq. (7.21) corresponds to the HF equations (7.8) and (7.9) derived in the previous section. In fact it can be rewritten as:

$$\hat{s}(\kappa,\phi)=\frac{\bar{\mathbf{B}}+\bar{\mathbf{B}}_{eff}}{\sqrt{2}\,r_s\lambda_2(\kappa,\phi)}\,, \tag{7.23}$$

expressing the proportionality of the spin quantization direction $\hat{s}$ and the total self-consistent magnetic field. $\bar{\mathbf{B}}_{eff}=\frac{g\mu_B}{e^2k_F}\mathbf{B}_{eff}$ is obtained by rescaling Eq. (7.10) to dimensionless form.

The second condition (7.22) was not obtained in the previous section, and corresponds to the fact that many solutions of the HF equation exist, that in general don't correspond to minima of the total energy. The simplest example is provided by the usual HF approximation for the electron liquid in absence of spin-orbit: in this case every occupation of the plane wave states provides a solution of the HF equations. The condition (7.22) can be rewritten:

$$\lambda_1=\frac{\epsilon_\pm(k_F\boldsymbol{\rho}_\pm(\phi))}{Ry}\,, \tag{7.24}$$

where $\epsilon_\pm(\mathbf{k})$ are the single particle energies defined by Eq. (7.4). Therefore the condition (7.24) requires the chemical potential to be constant at the two Fermi surfaces defined by $\rho_\pm(\phi)$, and equal between the two bands.

8. Isotropic Hartree-Fock solutions

We begin in this Chapter the study of the mean field phase diagram of the electron liquid with linear Rashba spin-orbit, by establishing the different types of solutions for the HF problem in absence of magnetic field. The analysis is greatly simplified by the assumption of isotropy in the plane of motion. The concept of generalized chirality χ is in this case a useful tool to parameterize the occupation of a large class of Slater determinants. At a given occupation, the HF equations allow to determine the self consistent distribution of the spin quantization axis $\hat{s}_{\mathbf{k}}$ and, by making use of the circular symmetry, they can reduced to a unidimensional integral equation for the azimuthal angle $\beta_{\mathbf{k}}$. The knowledge of χ and $\beta_{\mathbf{k}}$ provides a compact, complete description of the solution, and allows one to calculate every other desired property of the system.

8.1 Isotropic Hartree-Fock equation

The most general isotropic choice for the angles $\beta_{\mathbf{k}}$ and $\gamma_{\mathbf{k}}$ is expressed as follows:

$$\beta_{\mathbf{k}} = \bar{\beta}(\kappa) \ , \tag{8.1}$$

$$\gamma_{\mathbf{k}} = \phi_{\mathbf{k}} + \delta\bar{\gamma}(\kappa) \ , \tag{8.2}$$

where $\kappa = k/k_F$ is the rescaled wavevector. While $\bar{\beta}(\kappa)$ is a central quantity, we show in Appendix B that the energy is minimized by:

$$\delta\bar{\gamma}(\kappa) = \frac{\pi}{2} \ . \tag{8.3}$$

.

We can now specify the HF equations (7.8) and (7.9) to the case under consideration. Eq. (7.8) is automatically satisfied, while Eq. (7.9) can be simplified to the following form, written with dimensionless quantities:

$$\tan\bar{\beta}(\kappa)=\frac{\int_{\sqrt{|1-\chi|}}^{\sqrt{1+\chi}}\mathrm{d}\kappa'\int_0^{2\pi}\frac{\kappa'\,\sin\bar{\beta}(\kappa')\cos\theta}{\sqrt{\kappa'^2+\kappa^2-2\kappa\kappa'\cos\theta}}\,\mathrm{d}\theta+4\pi\bar{\alpha}\,\kappa}{\int_{\sqrt{|1-\chi|}}^{\sqrt{1+\chi}}\mathrm{d}\kappa'\int_0^{2\pi}\frac{\kappa'\,\cos\bar{\beta}(\kappa')}{\sqrt{\kappa'^2+\kappa^2-2\kappa\kappa'\cos\theta}}\,\mathrm{d}\theta}\ . \tag{8.4}$$

A remarkable property of this integral equation is that any explicit dependence from the density parameter r_s is absent. Therefore at a fixed spin-orbit coupling $\bar{\alpha}$ and chirality χ, a solution $\beta_{\mathbf{k}}$ can be obtained at every density by simple rescaling of $\mathbf{k}$ with the Fermi wavevector.

Another interesting property is given by the following powerful symmetry:

$$\bar{\beta}_{1/\chi}(\kappa)=\bar{\beta}_{\chi}(\sqrt{\chi}\,\kappa)\ , \tag{8.5}$$

which relates solutions with reciprocal values of the generalized chirality.

8.2 Energy and polarization

We give here explicit formulas to calculate the total energy of a HF solution. The general form is:

$$\mathcal{E}_{HF}[\chi;\bar{\beta}]=\mathcal{E}_K(\chi)+\mathcal{E}_{so}[\chi;\bar{\beta}]+\mathcal{E}_x[\chi;\bar{\beta}]\ , \tag{8.6}$$

where we the appropriate dependence on $\bar{\alpha}$ and r_s for the different terms is understood. The kinetic energy term is the same of the noninteracting case:

$$\mathcal{E}_K(\chi)=\begin{cases}\frac{1+\chi^2}{r_s^2} & \text{for } 0\le\chi<1\\ \frac{2\chi}{r_s^2} & \text{for } \chi\ge 1\end{cases}\ . \tag{8.7}$$

The Rashba term can be obtained by:

$$\mathcal{E}_{so}[\chi;\bar{\beta}]=-\bar{\alpha}\,\frac{2\sqrt{2}}{r_s}\int_{\sqrt{|1-\chi|}}^{\sqrt{1+\chi}}\kappa^2\,\sin\bar{\beta}(\kappa)\,\mathrm{d}\kappa\ . \tag{8.8}$$

The exchange energy can be calculated from:

$$\mathcal{E}_x[\chi;\bar{\beta}]=\mathcal{E}_x^{(0)}(\chi)+\delta\mathcal{E}_x[\chi;\bar{\beta}]\ , \tag{8.9}$$

where $\mathcal{E}_x^{(0)}(\chi)$ is the exchange energy for a given occupation (as determined by χ) in the case in which all the spin quantization axis coincide, and it is given by the following expression:

$$\mathcal{E}_x^{(0)}(\chi) = -\frac{4\sqrt{2}}{\pi r_s}\,\frac{|1+\chi|^{3/2}+|1-\chi|^{3/2}}{3} + \frac{8\sqrt{2}}{3\pi r_s}\sqrt{\chi+1}\left[\chi\,E\left(\frac{\chi-1}{\chi+1}\right) - K\left(\frac{\chi-1}{\chi+1}\right)\right]\theta(\chi-1)\ , \tag{8.10}$$

where the elliptic functions are in the notation of Abramowitz-Stegun [51]. The correction $\delta\mathcal{E}_x[\chi;\bar{\beta}]$ reads as follows:

$$\delta\mathcal{E}_x[\chi;\bar{\beta}] = \frac{1}{2\sqrt{2}\pi r_s}\int_{\sqrt{|1-\chi|}}^{\sqrt{1+\chi}}\kappa'\,\mathrm{d}\kappa'\int_{\sqrt{|1-\chi|}}^{\sqrt{1+\chi}}\kappa\,\mathrm{d}\kappa\int_0^{2\pi}\mathrm{d}\theta \times\frac{1-\cos\bar{\beta}(\kappa')\cos\bar{\beta}(\kappa)-\sin\bar{\beta}(\kappa')\sin\bar{\beta}(\kappa)\cos\theta}{\sqrt{\kappa'^2+\kappa^2-2\kappa'\kappa\cos\theta}}\ . \tag{8.11}$$

Finally, the fractional spin polarization is given by:

$$p\,[\chi;\bar{\beta}] = \frac{\langle\hat{S}_z\rangle}{N} = \int_{\sqrt{|1-\chi|}}^{\sqrt{1+\chi}}\kappa\,\cos\bar{\beta}(\kappa)\,\mathrm{d}\kappa\ , \tag{8.12}$$

where $\hat{S}_z = \sum_i \hat{\sigma}_z^{(i)}$.

The symmetry of the solutions corresponding to reciprocal chiralities (8.5) leads to corresponding relations for the above quantities:

$$\mathcal{E}_{so}[\chi;\bar{\beta}_\chi] = \chi^{3/2}\mathcal{E}_{so}[1/\chi;\bar{\beta}_{1/\chi}]\ , \tag{8.13}$$

$$\delta\mathcal{E}_x[\chi;\bar{\beta}_\chi] = \chi^{3/2}\delta\mathcal{E}_x[1/\chi;\bar{\beta}_{1/\chi}]\ , \tag{8.14}$$

$$p\,[\chi;\bar{\beta}_\chi] = \chi\,p\,[1/\chi;\bar{\beta}_{1/\chi}]\ . \tag{8.15}$$

8.3 Paramagnetic solutions

Eq. (8.4) always admits the solution $\bar{\beta}(\kappa) = \frac{\pi}{2}$, which correspond to a Slater determinant constructed with the noninteracting single particle states (2.17). This type of solutions have no net polarization, the relative momentum space spin texture being exemplified in Figure 8.1. The different contributions to the energy can be easily

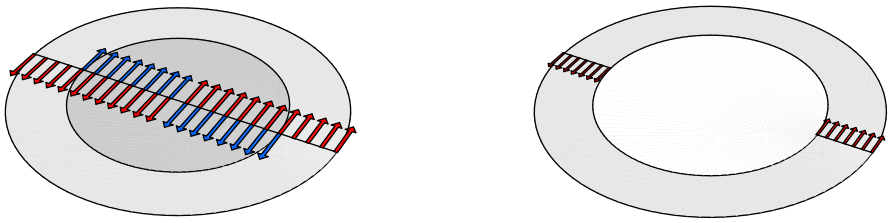

Figure 8.1. Spin texture in momentum space for the unpolarized states at $\bar{\alpha} = 0.1$. Left $\chi = 0.4$ and right $\chi = 2.5$.

calculated by making use of the formulas of the previous section, and in particular the noninteracting energy is given by Eq. (2.23).

For the exchange energy we could not obtain a closed form, and we give in Figure 8.2 the plot of the numerical result. It displays an interesting minimum at $\chi \simeq 0.9147$. At large χ the exchange energy is asymptotically vanishing, and the leading term is:

$$\mathcal{E}_x[\chi; \frac{\pi}{2}] \simeq -\frac{1 + 6\log 2 + 2\log\chi}{\pi r_s \sqrt{2\chi}} \ . \tag{8.16}$$

Once the total energy is obtained as function of χ, minimization at fixed values of $\bar{\alpha}$ and r_s gives the paramagnetic ground state in the HF approximation, which is very similar to the noninteracting ground state, the only difference being the occupation, which results in a value of the generalized chirality different from $\chi^{(0)}_{min}$, as obtained in Eq. (2.24). In Figure 8.2 we compare the HF value χ_{min} of the paramagnetic ground states to the noninteracting result $\chi^{(0)}_{min}$. The effect of the interactions is easily understood from the behavior of the function $\mathcal{E}_x[\chi; \frac{\pi}{2}]$: when it is a decreasing function of χ, it results in a value of χ_{min} larger than the noninteracting value. The opposite occurs when $\mathcal{E}_x[\chi; \frac{\pi}{2}]$ is an increasing function, while at the stationary point $\chi \simeq 0.9147$ the exchange has no effect.

The correction to the noninteracting chirality is also very small in the limit of small r_s, due to the fact that $\mathcal{E}_x[\chi; \frac{\pi}{2}]$ vanishes to quadratic order at $\chi \to 0$. The high-density limit will be examined in detail in Chapter 12.

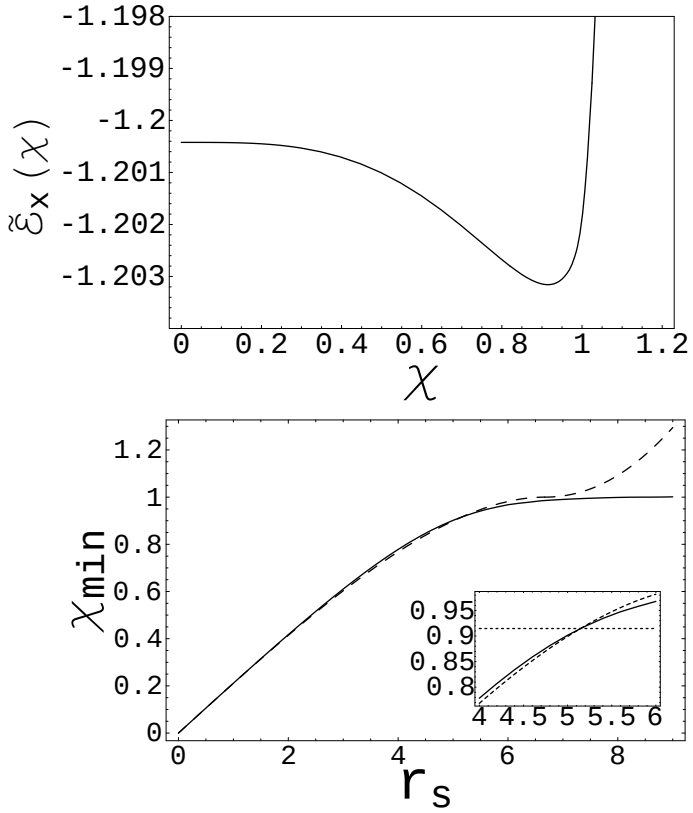

Figure 8.2. Top: plot of $\mathcal{E}_x[\chi; \frac{\pi}{2}]$ at $r_s = 1$. Bottom: plot of the chirality χ_{min} of the unpolarized ground state. The HF value (solid) can be compared to the noninteracting case (dashed).

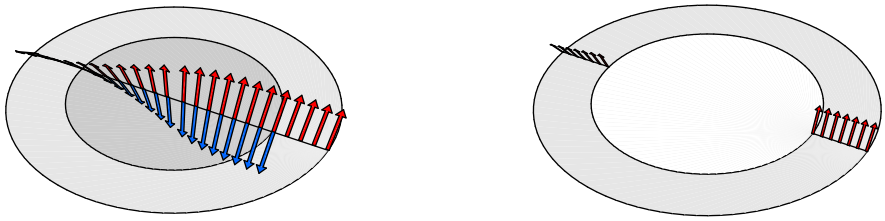

Figure 8.3. Spin texture in momentum space for the polarized states at $\bar{\alpha} = 0.1$. Left $\chi = 0.4$, right $\chi = 2.5$.

A useful exact result is the derivative of the exchange energy in $\chi = 1$, which is obtained to be $\frac{\pi-1-2K}{\pi r_s}$, where $K = \sum_{i=0}^{\infty} \frac{(-1)^i}{(2i+1)^2} \simeq 0.9160$ is the Catalan constant. This allows to find the value $\bar{\alpha}_d(r_s)$ at which $chi = 1$:

$$\bar{\alpha}_d(r_s) = \frac{1}{r_s} + \frac{\pi - 1 - 2K}{2\pi} \ , \tag{8.17}$$

where the second term is the (positive) correction to the noninteracting result.

8.4 Isotropic ferromagnetic solutions

Eq. (8.4) also admits nontrivial solutions with $\bar{\beta}(\kappa) \neq 0$ and with a net polarization along the z-axis. Examples of the momentum space spin texture arising in these states is displayed in Figure 8.3. The computation of these solutions can be practically achieved by iteration of (8.4) from an initial guess. Figure 8.4 displays several results for $\bar{\beta}(\kappa)$ at different values of χ. (8.4) needs only to be solved explicitly at, say, $\chi < 1$ by virtue of Eq. (8.5).

Once $\bar{\beta}(\kappa)$ is obtained at different values of χ, this provides the total energy and polarization as a function of χ. We show some results for the Rashba and exchange contributions to the energy in Figure 8.5, while results for the fractional polarization are given in Figure 8.6.

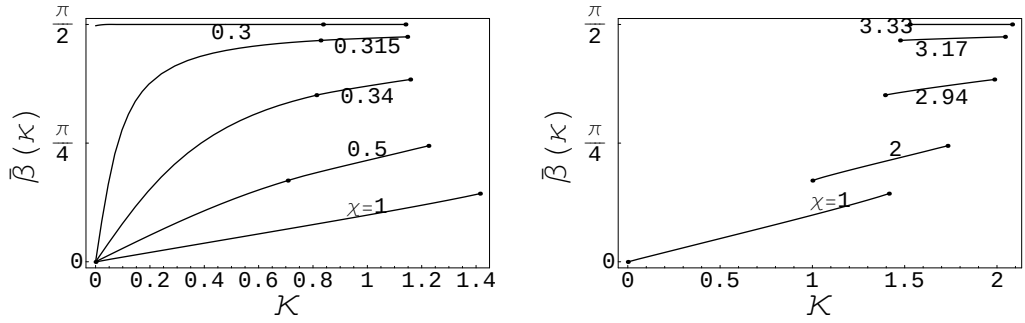

Figure 8.4. The complete $\bar{\beta}(\kappa)$ is plotted, for $\bar{\alpha} = 0.1$. Left: $\chi = 0.3$ 0.315, 0.34, 0.5, 1. Right: same plot for the reciprocal values, i.e. $\chi = 1/0.3,\ 1/0.315,\ 1/0.34,\ 1/0.5,\ 1$. The points mark the $[\sqrt{|1-\chi|}, \sqrt{1+\chi}]$ intervals.

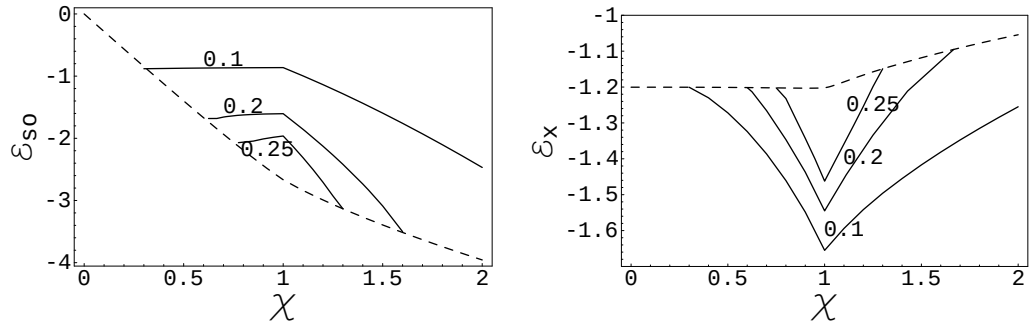

Figure 8.5. Plot of $\mathcal{E}_{so}[\chi;\bar{\beta}]$ (left) and $\mathcal{E}_{x}[\chi;\bar{\beta}]$ (right) for HF solutions at different values of $\bar{\alpha}$ and $r_s = 1$. The dashed lines refer to the unpolarized case.

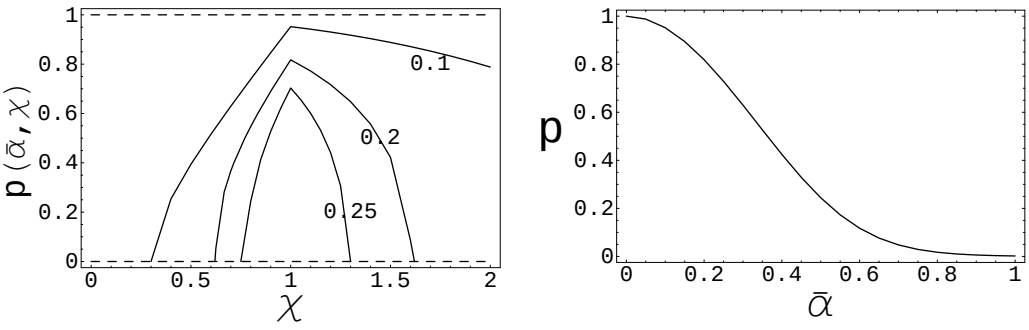

Figure 8.6. Left: fractional polarization $p\,[\chi;\bar{\beta}]$, plotted as function of χ for HF solutions at different values of $\bar{\alpha}$. Right: fractional polarization at $\chi = 1$, plotted as function of $\bar{\alpha}$.

A first remark can be made about the existence of polarized solutions determined by Eq. (8.4), which only exist in a finite interval of χ around the $\chi = 1$ value. Because of (8.5) the interval is necessarily of the form $[\chi(\bar{\alpha}), 1/\chi(\bar{\alpha})]$. This interesting result is examined in more detail in Appendix C and the final result for the allowed region is plotted in Figure 8.7.

We also notice that the all the contributions to the energy are singular at $\chi = 1$, and in particular the exchange energy $\mathcal{E}_x[\chi; \bar{\beta}]$ displays a marked cusp minimum. In fact, minimization of the total energy as function of χ at fixed values of $\bar{\alpha}$ and r_s gives that the polarized state with lowest energy has occupation $\chi_{min} = 1$. An illustration of such state with minimum energy and maximum polarization is provided in Figure 8.7. While for any value of the chirality $\chi \neq 1$ a polarized solution only exists below a critical value of $\bar{\alpha}$, the $\chi = 1$ solutions may exist for every $\bar{\alpha}$, even if we don't have a rigorous proof of this fact.

A last remark about the fractional polarization is that it is always smaller than one, even for the maximally polarized state that occurs at $\chi = 1$. In fact, since in general $\bar{\beta} \neq 0$, the fractional spin polarization does not coincide with the fraction of electrons with unpaired spin, as it is the case when spin-orbit is absent. Eventually, the polarization is vanishingly small at large values of $\bar{\alpha}$. We also notice that the fractional polarization of the $\chi = 1$ state is independent of r_s (at a fixed value of $\bar{\alpha}$) due to the fact that the solutions of (8.4) are only determined by χ and $\bar{\alpha}$.

8.5 Relative phase diagram

The relative phase diagram including the isotropic homogeneous HF solutions of the previous Sections is obtained by minimization of the total energy. This was already performed separately for the two classes of solutions, and in particular it was obtained that the ferromagnetic state has occupation determined by $\chi = 1$, which corresponds to maximum polarization. In Figure 8.8 the total energy and the corresponding value of χ_{min} are plotted against r_s, accounting for both paramagnetic and

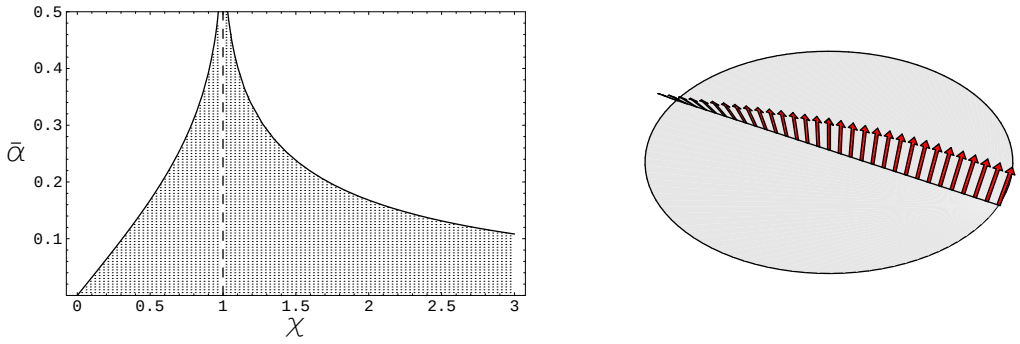

Figure 8.7. Left: region where a polarized solution is allowed. Right: spin texture in momentum space for a maximally polarized ($\chi = 1$) state at $\bar{\alpha} = 0.2$.

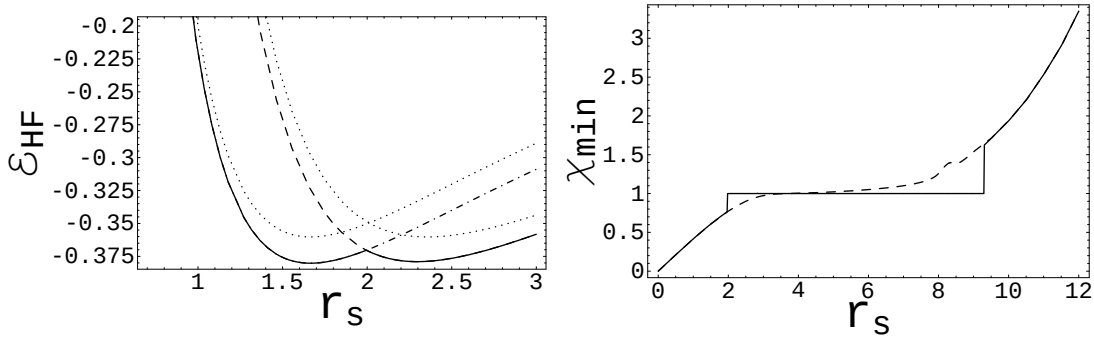

Figure 8.8. Left: plot of the total energy per particle in Ry units as function of the density parameter r_s (at $\bar{\alpha} = 0.1$). Dot-dashed curve: unpolarized ground state; dashed curve: maximally polarized ($\chi = 1$) ground state; dotted curves: corresponding results for the familiar $\bar{\alpha} = 0$ case. Right: value of the chirality χ_{min} of the homogeneous, isotropic HF state of lowest energy as function of r_s (at $\bar{\alpha} = 0.3$). The flat region with $\chi_{min} = 1$ corresponds to the polarized state while outside of this density range the system is unpolarized. The dashed line represents the value appropriate to the unpolarized state in the region where the polarized state lies lowest.

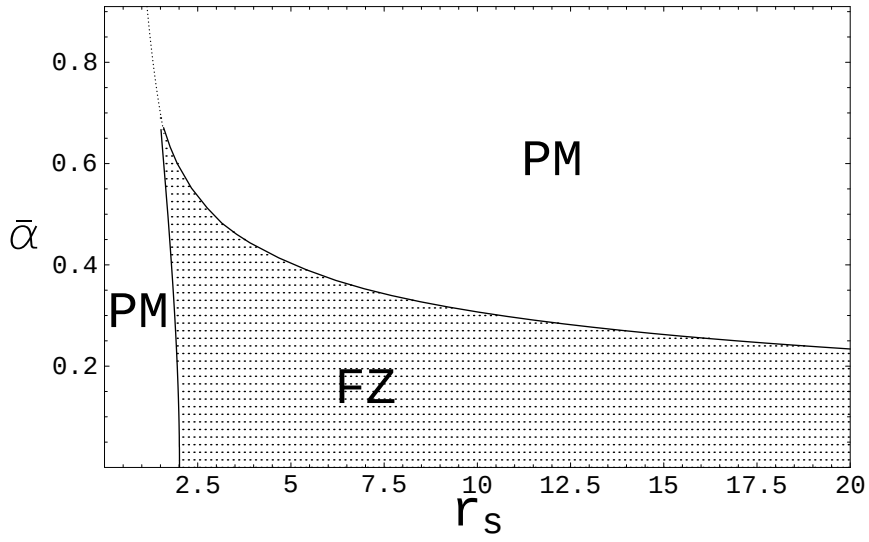

Figure 8.9. Relative phase diagram in the $(r_s, \bar{\alpha})$ plane of the isotropic HF solutions. In the shaded region the gas is polarized. The dotted curve is the $\chi = 1$ line Eq. (8.17).

ferromagnetic HF solutions. The ensuing scenario is as follows: the gas is unpolarized both at reasonably low and at high values of the density while a spin polarized state exists in a finite range of r_s. While the high density transition is the analog of the Bloch transition that occurs in absence of spin-orbit [1], the low density transition has no analog in absence of spin-orbit interaction. At large spin-orbit the polarized region is of difficult numerical evaluation but necessarily shrinks to zero, following the curve (8.17) at which the paramagnetic state has $\chi = 1$ occupation. The appearance of the ferromagnetic region can be attributed to the fact that, in presence of a finite polarization along the z-axis, the effect of the exchange energy is to remove the degeneracy of the single particle bands at $\mathbf{k} = 0$. Therefore, at the occupation $\chi = 1$, the formation of the gap contributes to the decrease of the total energy, a mechanism similar in spirit to that at work in the Perleis instability.

9. Spin susceptibility of paramagnetic states

We consider in this chapter the effect of a perturbing magnetic field on the paramagnetic solutions of the previous Chapter. Small orbital effects are neglected, and the Zeeman term contributing to the single-particle hamiltonian is given in (2.25). Rather than deriving the spin response by means of standard linear response theory we find in the present context more efficient to obtain the spin susceptibility from the relation

$$\chi_S \;=\; \frac{1}{L^2}\lim_{B\to 0}\frac{M}{B}\;, \tag{9.1}$$

where the magnetization M is determined in terms of the suitable fractional spin polarization p as follows

$$M \;=\; -\frac{\mu_B g}{2}Np\;. \tag{9.2}$$

p is defined in terms of the expectation value of the total spin operator $\hat{S}_{y(z)} = \sum_j \hat{\sigma}_{y(z),j}$:

$$p^{\parallel(\perp)} \;=\; \frac{\langle \hat{S}_{y(z)}\rangle}{N}\;. \tag{9.3}$$

The HF ground state in presence of a small magnetic field can be obtained solving (7.21) and (7.22) to linear order in the magnetic field, and the corresponding magnetization can be calculated.

Within linear response the wave vector and frequency dependent spin susceptibility of the system will be in general represented by a function $\chi_S(\bar{\alpha}, r_s, q, \omega)$ of the dimensionless spin-orbit coupling $\bar{\alpha}$ and the density parameter r_s. Given the anisotropy of the system, the spin susceptibility will also depend on the orientation of the field relative to the plane of the electron motion. For this reason we will make use of the notation $\parallel$ and $\perp$ to distinguish between the in plane magnetic field ($\mathbf{B} = B\hat{y}$) and the transverse magnetic field ($\mathbf{B} = B\hat{z}$) cases. While in the fully interacting case the calculation of the full q and ω dependence of $\chi_S^{\parallel(\perp)}(\bar{\alpha}, r_s, q, \omega)$ presents a formidable

problem, it is quite useful to at least determine its small q and ω limiting behavior. The latter is non trivial for, as it is common for response functions in general, the $q \to 0$ and $\omega \to 0$ limits are here non commuting. Accordingly, depending on the order with which these two limits are taken, one can define two distinct physical quantities, which we discuss in more detail in the next section and obtain explicitly in the remaining of the Chapter.

9.1 Isothermal and adiabatic susceptibilities

We define the isothermal spin susceptibilities:

$$\chi_S^{\parallel(\perp)}(\bar{\alpha}, r_s) \;=\; \lim_{q\to 0} \chi_S^{\parallel(\perp)}(\bar{\alpha}, r_s, q, 0) \;, \tag{9.4}$$

and the adiabatic spin susceptibilities:

$$\tilde{\chi}_S^{\parallel(\perp)}(\bar{\alpha}, r_s) \;=\; \lim_{\omega\to 0} \chi_S^{\parallel(\perp)}(\bar{\alpha}, r_s, 0, \omega) \;. \tag{9.5}$$

The quantity with more direct physical meaning is the isothermal susceptibility, which is directly related to the static magnetization of the gas when a uniform magnetic field is applied. The more obscure adiabatic susceptibility corresponds to the response to an oscillating uniform magnetic field, assuming that the time for the system to reach thermodynamic equilibrium remains much longer than the inverse of the frequency ω, as it is made to vanish. Nevertheless the $q = 0$ in plane susceptibility $\chi_S^{\parallel}(\omega)$ (and therefore its adiabatic limit $\tilde{\chi}_S^{\parallel}$) is directly related to other response functions of different kind which we discuss in the following.

The first example is the so called spin-Hall current conductivity σ_{sH}, which is defined as follows [52]:

$$\sigma_{sH} \;=\; \lim_{E\to 0} \frac{\langle \hat{J}_x^z \rangle}{E} \;, \tag{9.6}$$

where E is the magnitude of an electric field $\vec{E} = E\hat{y}$ applied along the y axis, and the operator $\hat{J}_x^z$ is defined as $\hat{J}_x^z = \frac{\hbar}{4L^2} \sum_i \{\hat{v}_{x,i},\, \hat{\sigma}_{z,i}\}$. This is related to the spin-spin response through [53]:

$$\sigma_{sH}(\omega) = -\frac{e\,\hbar^2}{m(g\mu_B)^2} \chi_S^{\parallel}(\omega) \;. \tag{9.7}$$

For non interacting electrons we have, according to (2.30), $\tilde{\chi}_S^{\parallel} = \chi_P/2$ which in turn gives the non interacting value of the spin-Hall conductance[1]:

$$\sigma_{sH}^{(0)} = -\frac{e}{8\pi} \ . \tag{9.8}$$

Another example is provided by the following spin-current response functions σ_{Sx} and σ_{Sy}, which we define as:

$$\sigma_{Sx(y)} \ = \ \lim_{B\to 0} \frac{\langle \hat{J}_{x(y)} \rangle}{B} \ , \tag{9.9}$$

where B is the magnitude of a magnetic field $\vec{B} = B\hat{y}$ applied along the y-axis, and the operator $\hat{J}_{x(y)}$ is the charge current density $\hat{J}_{x(y)} = -\frac{e}{L^2}\sum_i \ \hat{v}_{x(y),i}$. With the same method of reference [53] it is easy to obtain:

$$\sigma_{Sx}(\omega) = -\alpha \, \frac{2e}{g\mu_B} \chi_S^{\parallel}(\omega) \ . \tag{9.10}$$

In the case of pure Rashba spin-orbit, $\sigma_{Sy} = 0$. The same argument in the presence of a Dresselhaus spin-orbit $\beta(\hat{\sigma}_x\hat{p}_x - \hat{\sigma}_y\hat{p}_y)$ gives:

$$\sigma_{Sy}(\omega) = -\beta \, \frac{2e}{g\mu_B} \chi_S^{\parallel}(\omega) \ , \tag{9.11}$$

which leads to a practical way to obtain the ratio β/α from the angle between the magnetic field and the charge current [54].

We notice that the above relations are obtained in the presence of electron-electron interactions, and since for in plane magnetic field orbital effects can be neglected, they can be considered essentially exact results.

Finally, we recall the standard HF results when the spin-orbit coupling is absent. In this case, the response is isotropic and there is no need to specify the direction of the external magnetic field. The isothermal spin susceptibility is:

$$\chi_S^{\parallel(\perp)}(0, r_s) = \frac{\chi_P}{1 - \frac{\sqrt{2}r_s}{\pi}} \ , \tag{9.12}$$

while the adiabatic spin response vanishes $\tilde{\chi}_S^{\parallel(\perp)}(0, r_s) = 0$ because of the conservation of the total spin.

[1]Notice that the correct sign differs from that of reference [52].

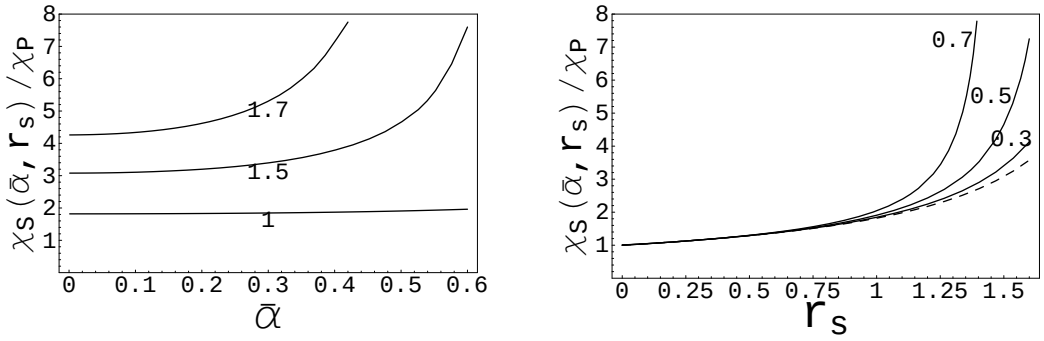

Figure 9.1. Left: plot of the isothermal transverse susceptibility, as function of the spin-orbit coupling parameter $\bar{\alpha}$, at different values of r_s. Right: plot of the isothermal transverse susceptibility, as function of the density parameter r_s, at different values of $\bar{\alpha}$. The dashed line is the $\bar{\alpha} = 0$ result of Eq. (9.12).

9.2 Isothermal transverse susceptibility

We consider the perturbation of the paramagnetic HF solution by an external magnetic field $\mathbf{B} = B\hat{z}$. We define a tilting angle $\delta\bar{\beta}(\kappa)$ of the directions $\hat{s}_{\mathbf{k}}$ from the x-y plane of motion as follows:

$$\beta_{\mathbf{k}} = \frac{\pi}{2} + \delta\bar{\beta}(k/k_F) \ . \tag{9.13}$$

For this transverse case the tilting of the spin is the only effect, and no change in the population of the bands occurs to first order in B. This latter fact can be formally proved by noticing that to first order in B, the perturbing term in (7.22) is vanishing. The equation for $\delta\bar{\beta}(\kappa)$ can be obtained by multiplying (7.21) by the unit vector $\hat{z}$ and retaining the terms to first order in B. This gives:

$$\delta\bar{\beta}(\kappa) = \frac{\int_{\kappa_-}^{\kappa_+} \kappa' \mathrm{d}\kappa' \int_0^{2\pi} \frac{\delta\bar{\beta}(\kappa')}{\sqrt{\kappa^2+\kappa'^2-2\kappa\kappa'\cos\theta}} \frac{\mathrm{d}\theta}{2\pi} - \bar{B}}{\int_{\kappa_-}^{\kappa_+} \kappa' \mathrm{d}\kappa' \int_0^{2\pi} \frac{\cos\theta}{\sqrt{\kappa^2+\kappa'^2-2\kappa\kappa'\cos\theta}} \frac{\mathrm{d}\theta}{2\pi} + 2\bar{\alpha}\kappa} \ , \tag{9.14}$$

which refers to the case of two occupied bands but can be applied directly to the case when only one band is occupied with the substitution $\kappa_\pm \to \kappa_{out(in)}$. We use the

notation $\kappa_\pm$ and $\kappa_{out(in)}$ for the rescaled radii of the unperturbed Fermi surfaces and in particular we have:

$$\kappa_\pm = \sqrt{1 \pm \chi}\ , \qquad \kappa_{out(in)} = \sqrt{\chi \pm 1}\ . \tag{9.15}$$

The fractional polarization can then be calculated from:

$$p^\perp(\bar{\alpha}, r_s) = \int_{\kappa_-}^{\kappa_+} \delta\bar{\beta}(\kappa)\, \kappa\, \mathrm{d}\kappa\ . \tag{9.16}$$

The corresponding susceptibility $\chi_S^\perp(\bar{\alpha}, r_s)$ easily follows from $p^\perp(\bar{\alpha}, r_s)$.

In general, an analytic form for $\chi_S^\perp(\bar{\alpha}, r_s)$ cannot be obtained and a numerical solution of the linear integral equation (9.14) can be calculated via standard methods [55, 56]. Some of the results are shown in Figure 9.1. We notice that the spin susceptibility is enhanced by the electron-electron interaction. The enhancement is larger for larger values of the spin-orbit coupling.

9.3 Isothermal in plane susceptibility

We consider next the perturbation of the paramagnetic HF solution from an external magnetic field in the plane of motion. For simplicity we assume $\mathbf{B} = B\hat{y}$. In this case the directions $\hat{s}_\mathbf{k}$ are tilted in the x-y plane and we define a tilting angle $\delta\bar{\gamma}(\kappa)$ according to:

$$\gamma_\mathbf{k} = \phi_\mathbf{k} + \frac{\pi}{2} - \delta\bar{\gamma}(k/k_F)\sin\phi\ . \tag{9.17}$$

We also define two parameters $a_\pm$ which determine the Fermi surfaces according to:

$$\rho_\pm(\phi) = \kappa_\pm + a_\pm \cos\phi\ . \tag{9.18}$$

The angular dependences of $\gamma_\mathbf{k}$ and $\rho_\pm(\phi)$ are exact to first order in B, as it can be surmised from the perturbing terms in (7.21) and (7.22). (7.21) can be multiplied by the radial unit vector $\hat{\kappa}$ and keeping terms to first order in B leads to the following integral equation:

$$\delta\bar{\gamma}(\kappa) = \frac{\int_{\kappa_-}^{\kappa_+} \kappa'\mathrm{d}\kappa' \int_0^{2\pi} \frac{\delta\bar{\gamma}(\kappa')\cos^2\theta}{\sqrt{\kappa^2+\kappa'^2-2\kappa\kappa'\cos\theta}} \frac{\mathrm{d}\theta}{2\pi} - \tilde{B}}{\int_{\kappa_-}^{\kappa_+} \kappa'\mathrm{d}\kappa' \int_0^{2\pi} \frac{\cos\theta}{\sqrt{\kappa^2+\kappa'^2-2\kappa\kappa'\cos\theta}} \frac{\mathrm{d}\theta}{2\pi} + 2\bar{\alpha}\kappa}\ , \tag{9.19}$$

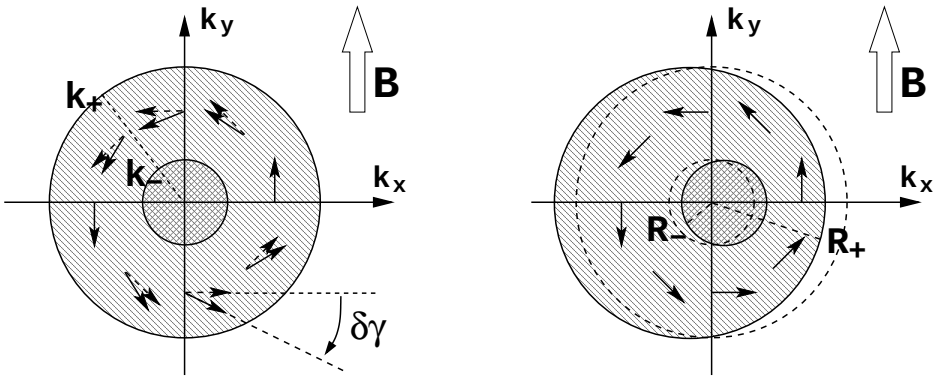

Figure 9.2. Tilting and repopulation contributions to the polarization, for an in plane magnetic field.

where

$$\tilde{B} = \bar{B} - a_+\kappa_+ \int_0^{2\pi} \frac{\sin^2\theta}{\sqrt{\kappa^2+\kappa_+^2-2\kappa\kappa_+\cos\theta}}\,\frac{\mathrm{d}\theta}{2\pi} + a_-\kappa_- \int_0^{2\pi} \frac{\sin^2\theta}{\sqrt{\kappa^2+\kappa_-^2-2\kappa\kappa_-\cos\theta}}\,\frac{\mathrm{d}\theta}{2\pi}\ . \tag{9.20}$$

The expressions (9.19) and (9.20) hold unchanged for the case of a single occupied band. In that case $\kappa_\pm \to \kappa_{out(in)}$.

Approximation of the second HF equation (7.22) to first order in B leads to the following linear system:

$$\begin{pmatrix} m_{++} m_{+-} \\ m_{-+} m_{--} \end{pmatrix} \begin{pmatrix} a_+ \\ a_- \end{pmatrix} = \begin{pmatrix} c_+ \\ c_- \end{pmatrix}\ , \tag{9.21}$$

where the matrix elements are mere numbers:

$$m_{\pm\pm} = 2\bar{\alpha} \mp \frac{2\sqrt{2}}{r_s}\,\kappa_\pm \mp \left[\frac{1}{3\pi} - \frac{2K}{\pi} + \int_0^{\kappa_\mp/\kappa_\pm} \kappa\,\mathrm{d}\kappa \int_0^{2\pi} \frac{(1-\cos\theta)(1-\kappa\cos\theta)}{(1+\kappa^2-2\kappa\cos\theta)^{3/2}}\,\frac{\mathrm{d}\theta}{2\pi}\right]\ , \tag{9.22}$$

$$m_{\pm\mp} = \pm\kappa_\mp \int_0^{2\pi} \frac{(1-\cos\theta)\,\cos\theta}{\sqrt{\kappa_+^2+\kappa_-^2-2\kappa_+\kappa_-\cos\theta}}\,\frac{\mathrm{d}\theta}{2\pi}\ , \tag{9.23}$$

while the $c_\pm$ are functionals of $\delta\bar{\gamma}(\kappa)$:

$$c_\pm = \bar{B} - \int_{\kappa_-}^{\kappa_+} \kappa\,\mathrm{d}\kappa \int_0^{2\pi} \frac{\delta\bar{\gamma}(\kappa)\sin^2\theta}{\sqrt{\kappa^2+\kappa_\pm^2-2\kappa\kappa_\pm\cos\theta}}\,\frac{\mathrm{d}\theta}{2\pi}\ . \tag{9.24}$$

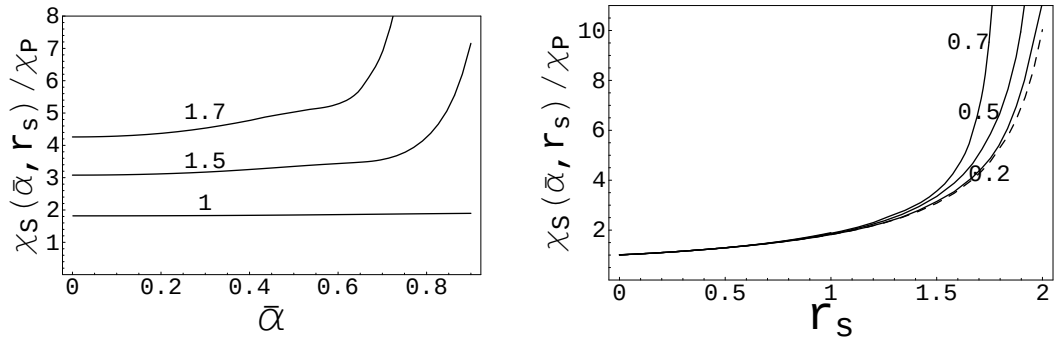

Figure 9.3. Left: plot of the inplane transverse susceptibility, as function of the spin-orbit coupling parameter $\bar{\alpha}$, at different values of r_s. Right: plot of the inplane transverse susceptibility, as function of the density parameter r_s, at different values of $\bar{\alpha}$. The dashed line is the $\bar{\alpha} = 0$ result of Eq. (9.12).

$K = \sum_{i=0}^{\infty} \frac{(-1)^i}{(2i+1)^2}$ is the Catalan constant and the equations for the case of a single band are obtained with the substitution $\kappa_\pm \to \kappa_{out(in)}$ and the following modifications: the sign of the $\frac{2\sqrt{2}}{r_s}\kappa_{out(in)}$ term in (9.22) is $-$ instead of $\pm$ and the $(1-\cos\theta)$ factors in (9.22) and (9.23) are replaced by $(-1-\cos\theta)$.

The fractional polarization can be calculated by means of the relation:

$$p^{\parallel}(\bar{\alpha}, r_s) = \frac{1}{2}\int_{\kappa_-}^{\kappa_+} \delta\bar{\gamma}(\kappa)\,\kappa\,\mathrm{d}\kappa + \frac{1}{2}(\kappa_+ a_+ - \kappa_- a_-)\ . \tag{9.25}$$

This expression contains two terms of different origin. The first contribution to the polarization arises from the tilting of the spin orientations $\hat{s}_{\mathbf{k}}$, at unperturbed occupation numbers, while the second contribution is related to the change in population only, with untilted spins. The origin of the two terms is illustrated in Figure 9.2.

Results for the spin susceptibility are displayed in Figure 9.3. The same comment about the enhancement of the spin susceptibility from the combination of electron-electron interactions and spin-orbit coupling applies here, in a similar way to the transverse case. However the effect is smaller, as it can be ascertained by comparing Figure 9.3 and Figure 9.1. Therefore we obtain the interesting consequence that, at variance with the case of the usual HF spin susceptibility (9.12), the spin response at finite Rashba spin-orbit is anisotropic.

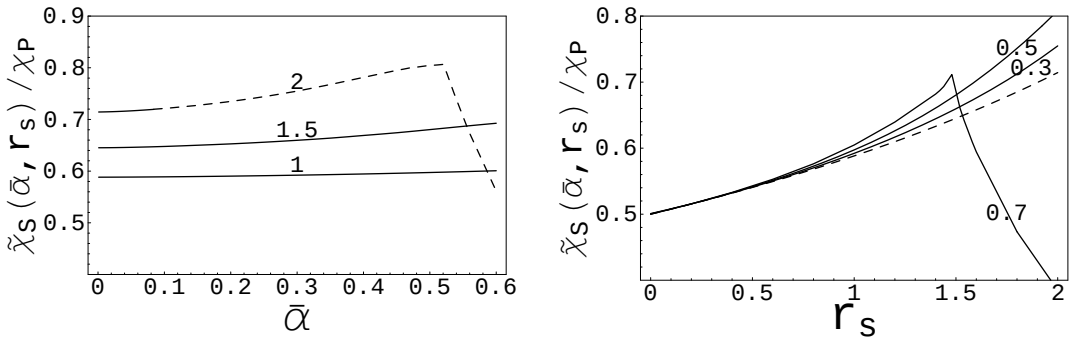

Figure 9.4. Left: plot of the adiabatic in plane susceptibility, as function of the spin-orbit coupling parameter $\bar{\alpha}$, at different values of r_s. The $r_s = 2$ curve is dashed in the region when the HF unperturbed ground state is polarized and the calculation does not apply. Right: plot of the adiabatic in plane susceptibility, as function of the density parameter r_s, at different values of $\bar{\alpha}$. For the $\bar{\alpha} = 0.7$ curve the result does not apply in a very small region around the singularity, where $\chi = 1$ and the gas is polarized. The dashed line is the $\bar{\alpha} \to 0$ result.

9.4 Adiabatic susceptibilities

We finally consider the adiabatic susceptibilities, for which we have to introduce only minor modifications to the treatment of the isothermal response that we have just discussed. Upon reflection, one can convince himself that correct results for this case are obtained by simply neglecting the repopulations effects. In fact, when $\omega = 0^+$ the gas evolves adiabatically following the external perturbation and since the external field is adiabatically switched on at $t = -\infty$ from the $\mathbf{B} = 0$ ground state, the occupation numbers $n_{\mathbf{k}\pm}$ do not change during the time evolution and coincide with those of the noninteracting $t = -\infty$ state.

For the case of a transverse field no change of the unperturbed occupations numbers occurs at first order in B, and therefore we have that the adiabatic and isothermal spin susceptibilities coincide:

$$\tilde{\chi}_S^{\perp}(\bar{\alpha}, r_s) = \chi_S^{\perp}(\bar{\alpha}, r_s) \ . \tag{9.26}$$

We notice at this point that the adiabatic susceptibility is not analytic in the limit of $\bar{\alpha} \to 0$. In fact, it can be verified that the transverse case gives the standard HF result (9.12), and therefore the limit of $\tilde{\chi}_S^{\perp}(\bar{\alpha}, r_s)$ is not vanishing:

$$\lim_{\bar{\alpha}\to 0} \tilde{\chi}_S^{\perp} = \frac{\chi_P}{1 - \frac{\sqrt{2}\, r_s}{\pi}}. \tag{9.27}$$

The reason of this not analytic behavior is understood considering that the linear response applies in the limit of zero magnetic field and in particular $B \ll \hbar\alpha k_F/\mu_B$. Therefore, the region of validity of the result (9.27) becomes vanishing small as $\bar{\alpha} \to 0$.

For an in plane magnetic field, the equations for the tilting angle and fractional polarization are obtained from those of the previous section by setting the repopulation parameters $a_{\pm} = 0$. We are left with the following single integral equation for $\delta\bar{\gamma}$:

$$\delta\bar{\gamma}(\kappa) = \frac{\int_{\kappa_-}^{\kappa_+} \kappa' \mathrm{d}\kappa' \int_0^{2\pi} \frac{\delta\bar{\gamma}(\kappa') \cos^2\theta}{\sqrt{\kappa^2+\kappa'^2-2\kappa\kappa'\cos\theta}} \frac{\mathrm{d}\theta}{2\pi} - \bar{B}}{\int_{\kappa_-}^{\kappa_+} \kappa' \mathrm{d}\kappa' \int_0^{2\pi} \frac{\cos\theta}{\sqrt{\kappa^2+\kappa'^2-2\kappa\kappa'\cos\theta}} \frac{\mathrm{d}\theta}{2\pi} + 2\bar{\alpha}\kappa} \ . \tag{9.28}$$

The corresponding fractional polarization is obtained from:

$$\tilde{p}^{\parallel}(\bar{\alpha}, r_s) = \frac{1}{2} \int_{\kappa_-}^{\kappa_+} \delta\bar{\gamma}(\kappa)\, \kappa\, \mathrm{d}\kappa \ . \tag{9.29}$$

In the limit of small $\bar{\alpha}$ we get the following finite result:

$$\lim_{\bar{\alpha}\to 0} \tilde{\chi}_S^{\parallel} = \frac{\frac{\chi_P}{2}}{1 - \frac{\sqrt{2}\, r_s}{3\pi}}, \tag{9.30}$$

which corresponds to a renormalization of the noninteracting spin-Hall conductivity, according to (9.7):

$$\sigma_{sH} = \frac{-\frac{e}{8\pi}}{1 - \frac{\sqrt{2}\, r_s}{3\pi}}. \tag{9.31}$$

Finally, numerical results at finite spin-orbit coupling are displayed in Figure 9.4.

9.5 Differential instabilities

We collect in Table 9.1 the results for the $\bar{\alpha} \to 0$ limit of the noninteracting and interacting spin susceptibilities. The latter present a diverging behavior at critical

Table 9.1

Values of the ratio χ_S/χ_P in the $\bar{\alpha} \to 0$ limit. The first two lines give the results appropriate to the noninteracting case. First column: transverse case. Second column: longitudinal case.

	$B\hat{z}$	$B\hat{y}$
χ_{S0}/χ_P	1	1
$\tilde{\chi}_{S0}/\chi_P$	1	$\frac{1}{2}$
χ_S/χ_P	$\frac{1}{1-\frac{\sqrt{2}\,r_s}{\pi}}$	$\frac{1}{1-\frac{\sqrt{2}\,r_s}{\pi}}$
$\tilde{\chi}_S/\chi_P$	$\frac{1}{1-\frac{\sqrt{2}\,r_s}{\pi}}$	$\frac{\frac{1}{2}}{1-\frac{\sqrt{2}\,r_s}{3\pi}}$

values of r_s, which correspond to differential instabilities of the system. At finite spin-orbit the lines of differential instability can be found in the following way: since in the three cases the integral equation (9.1) for $\chi_S^{\perp}$, the combination of (9.19) and (9.21) for $\chi_S^{\parallel}$ and (9.28) are linear problems that can be reduced to systems of linear equations, the instability lines are obtained from the zeroes of the determinant of such linear systems.

We collect in Figure (9.5) results relative to such instabilities. A first important result is inferred from the left panel, where the isothermal differential instabilities of the paramagnetic gas, as signaled by the divergence of $\chi_S^{\perp}$ and $\chi_S^{\parallel}$, are plotted. The region of instability for field along the z-axis is contained in the region of the isotropic ferromagnetic state that we obtained in the previous Chapter. This corresponds to the fact that the phase transition is of first order, similarly to the Bloch transition in absence of spin-orbit, i.e. the differential instability is preempted by a sudden polarization instability [1]. However, the instability region for the magnetic field in the plane extends up to the largest values of r_s, when the isotropic HF ground state is paramagnetic. This proves that an anisotropic in plane polarized state has lower energy than the paramagnetic state in some regions of the phase diagram. We will extensively study this problem in the next Chapter.

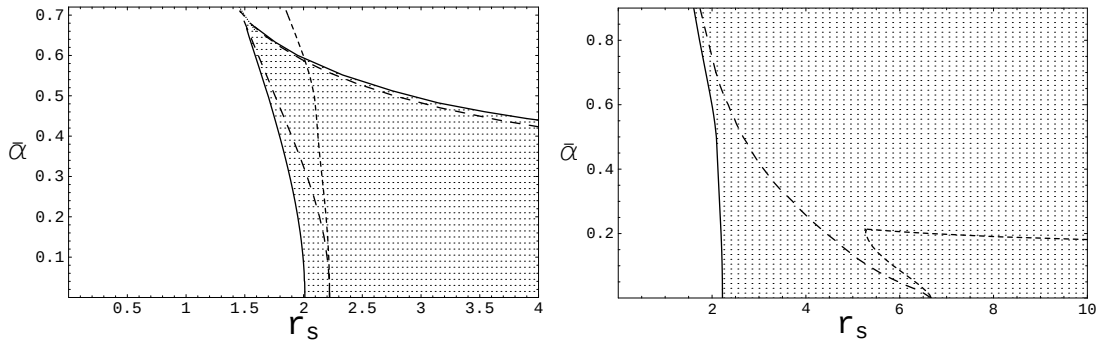

Figure 9.5. Left: isothermal instabilities of the paramagnetic HF solutions. The two long dashed lines relative to $\chi_S^{\perp}$ can be compared to the shaded region of the isotropic ferromagnetic state. The short dashed line refers to $\chi_S^{\parallel}$. Right: inplane differential instabilities. The short dashed line refers to the instability due to tilting-only (such that $\tilde{\chi}_S^{\parallel}$ is diverging) and the long dashed line to the repopulation-only case. The shaded region refers to the complete case, as determined by $\chi_S^{\parallel}$.

We also plot in the right panel of Figure (9.5) the in plane instability for $\tilde{\chi}_S^{\parallel}$. This is obtained from the in-plane response by neglecting repopulation, i.e. by setting $a_{\pm} = 0$, and results necessarily in a smaller region than the one determined by $\chi_S^{\parallel}$. A third type of repopulation-only instability is obtained by considering changes in $a_{\pm}$ only while setting $\delta\bar{\gamma} = 0$. This is also displayed in Figure (9.5). We will comment more extensively in the next Chapter, in connection to anisotropic HF solutions.

10. In plane polarized Hartree-Fock solutions

We complete in this Chapter the study of homogeneous solutions of the HF equations, by considering states polarized in the plane. Our analysis does not apply however to the semiclassical Wigner crystal phase that must exist at much lower densities.

The relevance of in-plane polarized solutions was obtained in the previous Chapter, in the study of the differential instability of the paramagnetic state in the presence of an in-plane magnetic field. We consider in the present Chapter in more detail this intriguing in-plane polarized phase, establishing the phase boundaries with the other two types of homogeneous states.

The study of this phase is complicated by the fact that the isotropy in the x-y plane is broken, and the occupation numbers $n_{\mathbf{k}\pm}$ and spin quantization axes $\hat{s}_{\mathbf{k}}$ assume complicated textures, that can be generally calculated only by numerical means. Analytical results are given in the following sections only in the limiting cases of very small or very large spin orbit coupling α.

10.1 Simple variational state

We discuss here a proof that the spatially homogeneous low density phase is a in plane polarized state. This fact was already derived by the differential instability of the paramagnetic state in the presence of an external magnetic field. However, the differential instability phase boundary is not of immediate computation, and the argument is still somewhat unsatisfactory, since only a finite portion of the $(r_s, \bar{\alpha})$ plane can be numerically examined. We find here explicitly a simple variational state that has energy lower than the paramagnetic state and we expect to be the asymptotically correct homogeneous HF ground state in the limit of very low densities.

The state is defined by:

$$n_{\mathbf{k}+} = \theta(\sqrt{2}k_F - |\mathbf{k} - \mathbf{k}_0|),\ n_{\mathbf{k}-} = 0\ ,$$
$$\hat{s}_{\mathbf{k}} = \hat{y}\ , \tag{10.1}$$

where $k_F = \sqrt{2\pi n}$ is the Fermi vector and $\theta(x)$ is the usual step function. The electrons occupy only one band, with definite spin along $\hat{y}$, the occupation being a circle of radius $\sqrt{2}k_F$ displaced from the origin. The value of $\mathbf{k}_0$ of the center of the circle which minimizes the energy is given by:

$$\mathbf{k}_0 = \frac{m\alpha}{\hbar}\,\hat{x}. \tag{10.2}$$

This can be obtained by the condition that the average velocity of the state has to be vanishing. In fact the single particle velocity operator is such that $\hat{v}_x = \hat{p}_x/m - \alpha\,\hat{\sigma}_y$, and has a contribution from the polarization along $\hat{y}$.

An example of this state is depicted in Figure 10.1. It has the maximum available exchange energy and the single particle states have wavevectors centered around the minimum of the lowest noninteracting chiral subband. Therefore, in the limit of very large r_s, when the occupation is a small droplet around $|\mathbf{k}_0|$, the kinetic and Rashba contributions are also approximately minimized. Furthermore, since the Rashba spin orbit amounts to an external magnetic field in momentum space which at $\mathbf{k}_0$ is directed along $\hat{y}$, the state is also asymptotically a solution of the HF equations.

The energy per particle can be calculated exactly and it is given by (in Ry units):

$$\mathcal{E}^{(trial)} = -\bar{\alpha}^2 + \frac{2}{r_s^2} - \frac{16}{3\pi r_s}\ . \tag{10.3}$$

The first two terms combine the kinetic and Rashba contributions. They contain a r_s^{-2} correction to the minimum single particle noninteracting energy, which is $-\frac{1}{2}m\alpha^2 = -\bar{\alpha}^2 Ry$. The last term is the exchange energy, as appropriate for a fully polarized state. (10.3) can be compared to the paramagnetic total energy:

$$\mathcal{E}^{(unpol)} \geq -\bar{\alpha}^2 - \frac{1.203}{r_s}\ , \tag{10.4}$$

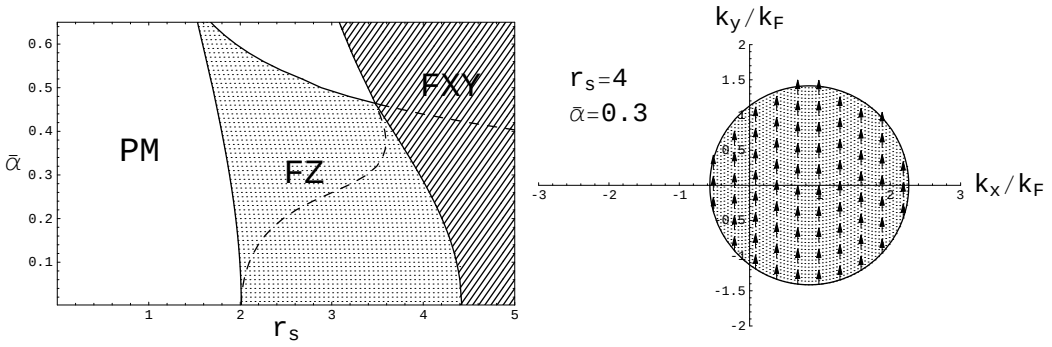

Figure 10.1. In the first figure, the relative phase diagram of the simple trial state and the exact isotropic HF solution is shown. The dashed lines are phase boundaries with the paramagnetic state. In the second figure an example of the simple trial state is shown, for particular values of r_s and $\bar{\alpha}$.

where we used $-\bar{\alpha}^2$ as a lower bound for the kinetic and Rashba contributions, and the minimum unpolarized exchange energy, which occurs when the chirality is $\chi = 0.9147$. This gives immediately $\mathcal{E}^{(unpol)} \geq \mathcal{E}^{(trial)}$ for $r_s \geq 4.044$, which proves that the low density state must be polarized.

Numerical evaluation of the region where $\mathcal{E}^{(trial)}$ is lowest in energy gives the phase diagram displayed in Figure 10.1, relative to the paramagnetic state and the in plane and out-of plane polarized states. This turns out to be qualitatively correct, while for the true HF solution the phase boundary occurs at smaller values of r_s.

10.2 Small $\bar{\alpha}$ limit

We now consider the effect of the presence of a small spin-orbit coupling on a fully polarized ground state. The calculation is analogous to that of the spin susceptibility, with the difference that we consider here the spin-orbit as a small perturbation, instead of the Zeeman term. The unperturbed state is taken to be the usual fully polarized HF solution, in absence of spin orbit:

$$n^{(0)}_{\mathbf{k}+} = \theta(\sqrt{2}k_F - k),\ n^{(0)}_{\mathbf{k}-} = 0\ ,$$

$$\hat{s}^{(0)}_{\mathbf{k}} = \hat{s}^{(0)} = \cos\theta_0\,\hat{y} + \sin\theta_0\,\hat{z}\ , \tag{10.5}$$

where the polarization forms an angle θ_0 with the x-y plane of motion.

The minimization of the functional (7.3) leads to the following conditions:

$$\lambda_1 = \frac{2\rho^2(\phi)}{r_s^2} - \frac{\sqrt{2}}{r_s}\left[2\bar{\alpha}\,\hat{\phi}\cdot\hat{s}(\rho(\phi),\phi)\,\rho(\phi) + \int_0^{2\pi}\frac{\mathrm{d}\phi'}{2\pi}\int_0^{\rho(\phi')}\frac{1+\hat{s}(\rho(\phi),\phi)\cdot\hat{s}(\kappa',\phi')}{\sqrt{\rho^2(\phi)+\kappa'^2-2\rho(\phi)\kappa'\cos(\phi-\phi')}}\,\kappa'\mathrm{d}\kappa'\right]\ , \tag{10.6}$$

and:

$$\hat{s}(\kappa,\phi) = -\frac{1}{\sqrt{2}\,r_s\lambda_2(\kappa,\phi)}\left[2\bar{\alpha}\,\kappa\,\hat{\phi} + \int_0^{2\pi}\frac{\mathrm{d}\phi'}{2\pi}\int_0^{\rho(\phi')}\mathrm{d}\kappa' \times\frac{\hat{s}(\kappa',\phi')}{\sqrt{\kappa^2+\kappa'^2-2\kappa\kappa'\cos(\phi-\phi')}}\,\kappa'\right]\ , \tag{10.7}$$

which are expressed in dimensionless form, according to the definitions of the previous Chapters. $\kappa = \rho(\phi)$ specifies the Fermi surface of the only occupied band and the two Lagrange multipliers λ_1 and $\lambda_2(\kappa,\phi)$ ensure respectively the conservation of the particle number and the normalization of the $\hat{s}(\kappa,\phi)$ unit vectors. In particular Eq. (10.6) expresses the fact that the chemical potential λ_1 at the Fermi surface has to be constant, the right hand side being the HF single particle energy evaluated at $\kappa = \rho(\phi)$. Eq. (10.7) is the requirement that the spin $\hat{s}(\kappa,\phi)$ must be parallel to a self-consistent magnetic field produced by the spin orbit coupling and exchange interaction, where $\lambda_2(\kappa,\phi)$ is proportional to the magnitude of such an effective field.

The condition satisfied by the first order correction $\delta\hat{s}(\kappa,\phi)$ to the spin directions can be obtained by multiplying Eq. (10.7) by the following unit vectors, perpendicular to the original polarization direction $\hat{s}^{(0)}$:

$$\hat{x}' = -\hat{x}\ , \tag{10.8}$$

$$\hat{y}' = \sin\theta_0\,\hat{y} - \cos\theta_0\,\hat{z}\ . \tag{10.9}$$

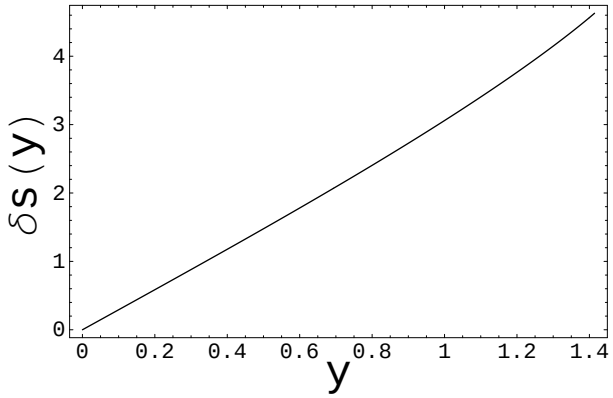

Figure 10.2. Plot of the function $\delta s(\kappa)$, describing the spin tilting of a polarized state at $\bar{\alpha} \to 0$.

The angular dependence is determined by the external perturbation, and in particular we have $2\bar{\alpha}\,\kappa\,\hat{\phi}\cdot\hat{x}' = 2\bar{\alpha}\,\kappa\sin\phi$ and $2\bar{\alpha}\,\kappa\,\hat{\phi}\cdot\hat{y}' = 2\bar{\alpha}\,\kappa\cos\phi\sin\theta_0$, which allows us to set:

$$\hat{s}(\kappa,\phi)\cdot\hat{x}' = \bar{\alpha}\,\delta s(\kappa)\sin\phi\ , \tag{10.10}$$

$$\hat{s}(\kappa,\phi)\cdot\hat{y}' = \bar{\alpha}\,\delta s(\kappa)\cos\phi\sin\theta_0\ , \tag{10.11}$$

and to obtain the following single integral equation for $\delta s(\kappa)$:

$$\delta s(\kappa) = \frac{\int_0^{\sqrt{2}}\kappa'\mathrm{d}\kappa'\int_0^{2\pi}\frac{\delta s(\kappa')\cos\theta}{\sqrt{\kappa^2+\kappa'^2-2\kappa\kappa'\cos\theta}}\frac{\mathrm{d}\theta}{2\pi} + 2\,\kappa}{\int_0^{\sqrt{2}}\kappa'\mathrm{d}\kappa'\int_0^{2\pi}\frac{1}{\sqrt{\kappa^2+\kappa'^2-2\kappa\kappa'\cos\theta}}\frac{\mathrm{d}\theta}{2\pi}}\ . \tag{10.12}$$

Since Eq. (10.12) is obtained from Eq. (10.7) to first order in $\bar{\alpha}$, it is appropriate to derive it using the unperturbed values for the Lagrange multiplier $\lambda_2^{(0)}(\kappa,\phi) = -\frac{1}{\sqrt{2}r_s}\int_0^{\sqrt{2}}\kappa'\mathrm{d}\kappa'\int_0^{2\pi}\frac{1}{\sqrt{\kappa^2+\kappa'^2-2\kappa\kappa'\cos\theta}}\frac{\mathrm{d}\theta}{2\pi}$ and the Fermi surface radius $\rho^{(0)}(\phi) = \sqrt{2}$. The function $\delta s(\kappa)$ can be evaluated numerically and it is shown in Figure 10.2.

We now consider the repopulation, described by the $\rho(\phi)$ Fermi surface. The angular dependence can be determined by the Rashba perturbation term in Eq. (10.6), for which we have $2\bar{\alpha}\,\hat{\phi}\cdot\hat{s}^{(0)} = 2\bar{\alpha}\,\cos\phi\cos\theta_0$. This allows us to set:

$$\rho(\phi) = \sqrt{2} + \bar{\alpha}\,a\cos\phi\cos\theta_0\ . \tag{10.13}$$

The coefficient a can be obtained by first order approximation of Eq. (10.6) or alternatively by the reasoning described below.

Eq. (10.13) describes an occupation which to first order in $\bar{\alpha}$ is a circle displaced from the origin by an amount $\bar{\alpha}\, a \cos\theta_0$. The center of the occupation circle can be determined by the condition that the velocity $p_x/m - \alpha\sigma_x$ to be vanishing. Since the normalization condition of the spins requires that $\delta\hat{s}(\kappa,\phi)$ is to lowest order perpendicular to the original polarization direction, the correction to the unperturbed polarization are of second order in $\bar{\alpha}$ and do not contribute to the velocity. This gives immediately:

$$a = \frac{r_s}{\sqrt{2}} \ . \tag{10.14}$$

The correction to the unperturbed energy can be calculated once $\delta s(\kappa)$ and a are known. However, since the result is of second order in $\bar{\alpha}$, the appropriate expression to be used for $\hat{s}(\kappa,\phi)$ has to be normalized to second order terms:

$$\hat{s}(\kappa,\phi) = \hat{s}^{(0)} + \delta\hat{s}(\kappa,\phi) - \bar{\alpha}^2\, \frac{\delta s(\kappa)^2}{2} (\sin^2\phi + \cos^2\phi \sin^2\theta_0)\, \hat{s}^{(0)} \ , \tag{10.15}$$

where other choices are possible for the second order term, the final results not being affected. The following kinetic, Rashba and exchange contributions can be obtained by direct calculation:

$$\delta\mathcal{E}_K = \bar{\alpha}^2 \cos^2\theta_0 \ , \tag{10.16}$$

$$\delta\mathcal{E}_{so} = -2\bar{\alpha}^2 \left(\cos^2\theta_0 + \frac{1+\sin^2\theta_0}{\sqrt{2}\, r_s} \int_0^{\sqrt{2}} \delta s(\kappa)\, \kappa^2 \mathrm{d}\kappa \right) \ , \tag{10.17}$$

$$\delta\mathcal{E}_x = -\bar{\alpha}^2 \frac{1+\sin^2\theta_0}{2\sqrt{2}\, r_s} \int_0^{\sqrt{2}} \kappa\, \mathrm{d}\kappa \int_0^{\sqrt{2}} \kappa' \mathrm{d}\kappa' \int_0^{2\pi} \frac{\delta s(\kappa)\delta s(\kappa')\cos\theta - \delta s(\kappa)^2}{\sqrt{\kappa^2+\kappa'^2-2\kappa\kappa'\cos\theta}} \frac{\mathrm{d}\theta}{2\pi} \ , \tag{10.18}$$

where the exchange energy $\mathcal{E}_x$ can be simplified by making use of the integral equation (10.12). The final result for the total energy is $\delta\mathcal{E} = \delta\mathcal{E}_K + \delta\mathcal{E}_{so} + \delta\mathcal{E}_x = \frac{1}{2}\,\delta\mathcal{E}_{so}$, where the numerical coefficient of $\delta\mathcal{E}$ is obtained by numerical integration of $\delta s(\kappa)$:

$$\delta\mathcal{E}(\theta_0) = -\bar{\alpha}^2 \left[\cos^2\theta_0 + \frac{2.211}{r_s} (1+\sin^2\theta_0) \right] \ . \tag{10.19}$$

The final result Eq. (10.19) gives immediately the phase with lowest energy at $\bar{\alpha} \simeq 0$:

$$\theta_0 = \tfrac{\pi}{2} \quad \text{for} \quad r_s^* < r_s < 2.211 \ , \tag{10.20}$$

$$\theta_0 = 0 \quad \text{for} \quad r_s > 2.211 \ , \tag{10.21}$$

where $r_s^* = \frac{3\pi}{8(2-\sqrt{2})} \simeq 2.011$ is the usual HF critical density below which the electron liquid in absence of spin orbit is paramagnetic. Therefore the out-of-plane ferromagnetic state survives in a narrow interval of intermediate densities before the low density in-plane ferromagnetic phase.

With little effort the boundary curvature between the paramagnetic and out-of-plane ferromagnetic state can be obtained. Expanding to second order in $\bar{\alpha}$ the total energy of the paramagnetic state we get $\delta\mathcal{E}^{(unpol)} = -2\bar{\alpha}^2$ and the phase boundary is obtained equating the total energies:

$$\left(\frac{1}{r_s^2} - \frac{8\sqrt{2}}{3\pi r_s}\right) - 2\bar{\alpha}^2 = \left(\frac{2}{r_s^2} - \frac{16}{3\pi r_s}\right) - \frac{4.422}{r_s}\,\bar{\alpha}^2 \ ,$$

which around $r_s \lesssim r_s^*$ gives:

$$\bar{\alpha} = \sqrt{0.6172\,(r_s^* - r_s)} \ . \tag{10.22}$$

This corresponds to a shift of the critical density to lower r_s at finite spin-orbit coupling. For the transition between the two ferromagnetic states the curvature of the phase boundary requires the expansion of the energies to higher order in $\bar{\alpha}$, and cannot be obtained from our previous result Eq. (10.19).

As a final remark, we compare the perturbative in plane polarized ground state to the simple trial state of the previous section. While the occupations are the same for both states, the spin tilting of the perturbative state as determined by $\delta s(\kappa)$ is independent of the density, which is in apparent contradiction to the intuitive expectation that the trial state is the correct solution at large r_s. However, we notice that the perturbative treatment can be considered reliable only in close proximity of the unperturbed state, a fact that allows us to immediately infer that the displacement

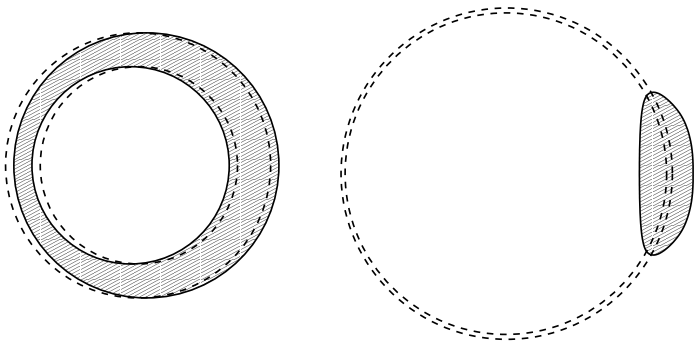

Figure 10.3. Left panel: instability of an isotropic paramagnetic state to an anisotropic polarized state via repopulation. Right panel: qualitative sketch of the final polarized state for a large $\bar{\alpha}$ value.

of the occupation center is very small, $a \ll \sqrt{2}$. Instead, the trial state is expected to be a reliable approximation in the opposite limit, when $a \gg \sqrt{2}$. From (10.14) we can surmise that at every fixed $\bar{\alpha}$, the perturbative treatment fails above a certain value of $r_s \sim 1/\bar{\alpha}$.

10.3 Large $\bar{\alpha}$ limit

We now discuss the large $\bar{\alpha}$ limit, which is such that the HF solution does not converge to a paramagnetic state, and a perturbative treatment is not possible. This could be perhaps surprising, since in this limit the noninteracting energy becomes the dominating contribution and the electron spin is required to be aligned in the azimuthal direction, as dictated by the Rashba spin-orbit coupling. The breaking down of a possible perturbative solution has to be ascribed to the fact that in this limit the momentum space occupation is a large narrow ring of states with almost degenerate energy, and the occupation can be rather wildly modified, with negligible cost of noninteracting energy.

We now identify more explicitly the instability of the paramagnetic state as a repopulation instability. Consider in the second panel of Figure 9.5 the in plane differential instabilities of the paramagnetic state, where the three curves refer to three

possible cases: (i) both repopulation and spin tilting are considered ($a_\pm \neq 0$ and $\delta\bar{\gamma}(\kappa) \neq 0$), (ii) repopulation only ($\delta\bar{\gamma}(\kappa) = 0$), (iii) spin tilting only ($a_\pm = 0$). While the region of spin tilting instability shrinks to zero at large $\bar{\alpha}$, the instability region asymptotically coincides with the repopulation instability only. Such repopulation instability exists for every density r_s, at large enough $\bar{\alpha}$. Therefore, the phase boundary of the in plane polarized state is such that $r_s \to 0$ when $\bar{\alpha} \to \infty$.

For $\bar{\alpha} \to \infty$ the occupation of the paramagnetic state is a narrow ring with large radius, where the inner and outer radii are expressed in terms of the generalized chirality as $\kappa_\pm = \sqrt{\chi \pm 1} \simeq \sqrt{\chi}$. We then consider a infinitesimal change in the Fermi surfaces, described as follows:

$$\rho_\pm(\phi) = \kappa_\pm \left(1 \pm \eta \cos\phi\right) , \tag{10.23}$$

while keeping unchanged the azimuthal direction of the spin quantization axis $\hat{s}(\kappa, \phi) = \hat{\phi}$. This induces a infinitesimal polarization along $\hat{y}$, by thickening one side of the ring with respect to the other (see Figure 10.3). In practice, one is moving electrons from one side of the ring to the diametrically opposite one, an operation that implies a flipping of the spin. The exchange energy for such a state is obtained as follows, in the limit of large χ:

$$\mathcal{E}_x \simeq -\frac{1 + 6\log 2 + (2+\eta^2)\log\chi}{\pi r_s \sqrt{2\chi}} , \tag{10.24}$$

which is a generalization of the $\eta = 0$ result (8.16). Using that $\chi \simeq \frac{(r_s\bar{\alpha})^2}{2}$ to leading order (both for the interacting and noninteracting paramagnetic state) we get:

$$\delta\mathcal{E} \simeq \left[\frac{1}{2r_s^4\bar{\alpha}^2} - \frac{2\log(\bar{\alpha}r_s)}{\pi\bar{\alpha}r_s^2}\right] \eta^2 , \tag{10.25}$$

where the first term is the leading term in the kinetic and spin orbit contribution. This is negligible in the limit of large $\bar{\alpha}$, for every density r_s, which leads to a negative energy change at finite η and proves the instability of the paramagnetic state.

Such an instability leads to a HF ground state which in the limit $\bar{\alpha} \to \infty$ is a fully polarized droplet in momentum space. The droplet has dimensionless area 2π and is centered around $\boldsymbol{\kappa}_0 = \frac{\bar{\alpha} r_s}{\sqrt{2}}\,\hat{x}$. Expansion of the energy functional (7.3) gives:

$$\mathcal{E}_{HF} \simeq -\bar{\alpha}^2 + \frac{1}{\pi r_s^2}\int_{\mathcal{D}} \kappa_x^2 \,\mathrm{d}\boldsymbol{\kappa} - \frac{\sqrt{2}}{(2\pi)^2 r_s}\int_{\mathcal{D}}\frac{\mathrm{d}\boldsymbol{\kappa}\,\mathrm{d}\boldsymbol{\kappa}'}{|\boldsymbol{\kappa}-\boldsymbol{\kappa}'|}\ , \tag{10.26}$$

which neglects terms vanishing when $r_s\bar{\alpha} \to \infty$. The spin quantization axes were assumed to be asymptotically along $\hat{\phi}$, and the integrals are performed around the occupied region $\mathcal{D}$ which we have translated from $\boldsymbol{\kappa}_0$ to the origin. The energy corresponds to particles that interact via an attractive Coulomb potential, in the presence of an external parabolic confining potential along the x direction. The occupation resulting from (10.26) is independent of $\bar{\alpha}$ and consists of some oblate region of finite fixed extent along y, the exact shape being determined by the density r_s. Therefore the (10.26) becomes an exact approximation when $\bar{\alpha} \to \infty$ at constant r_s.

We notice that the (10.26) becomes also exact in the $r_s \to \infty$ at constant $\bar{\alpha}$, if the occupation has finite extent. In this case the external confining potential becomes negligible and the exchange energy leads to a circle occupation as discussed in the first section.

10.4 Numerical analysis and results

To calculate the HF in-plane polarized ground states at generic values of r_s and $\bar{\alpha}$ it is necessary to resort to direct numerical minimization of the energy. This we perform as follows: we restrict ourselves to the case of a single occupied band, so that the occupation is determined by $n_{\mathbf{k}+} \equiv n_{\mathbf{k}}$. We also assume that the direction of the spin quantization axes $\hat{s}_{\mathbf{k}}$ lies in the plane of motion. From the initial trial occupation numbers $n_{\mathbf{k}}$ and spin orientations $\hat{s}_{\mathbf{k}}$ we calculate the effective magnetic field, which is given by:

$$\vec{B}_{eff}(\mathbf{k}) = -\alpha\,\hbar k\,\hat{\phi}_{\mathbf{k}} - \frac{1}{2L^2}\sum_{\mathbf{k}'} n_{\mathbf{k}'} v_{\mathbf{k}-\mathbf{k}'}\hat{s}_{\mathbf{k}'}\ . \tag{10.27}$$

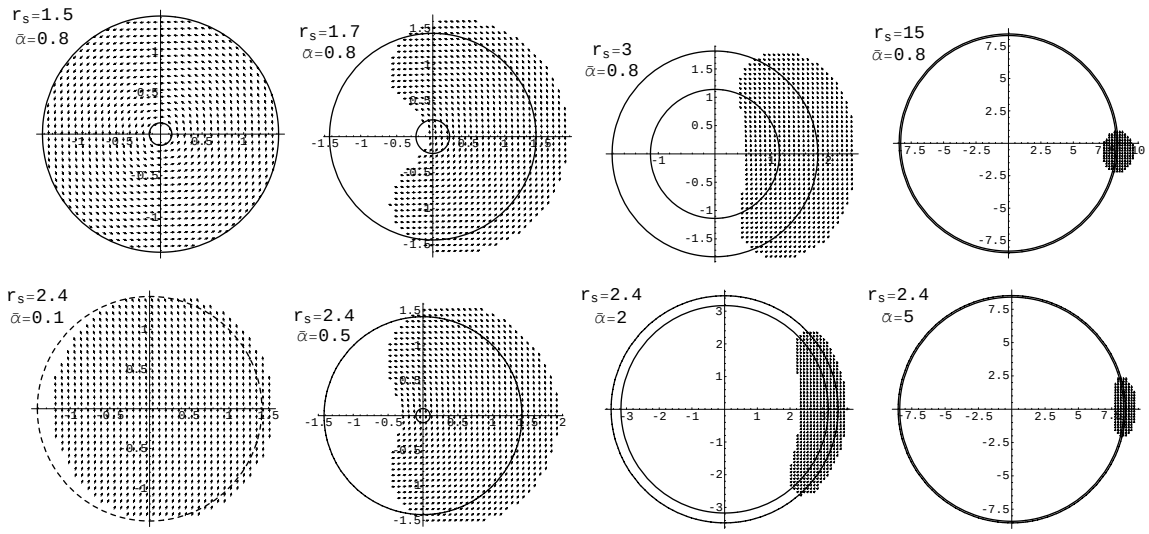

Figure 10.4. Top: examples of occupation and spin texture in the dimensionless momentum space for states at $\bar{\alpha} = 0.8$ and increasing values of r_s. The circles mark the paramagnetic state occupation. Note the different length scale of each case. Bottom: solutions at fixed $r_s = 2.4$ and increasing values of $\bar{\alpha}$. In the first case the $\chi = 1$ occupation circle in dashing for reference.

In the next iteration the electrons have spin oriented along $\hat{s}_{\mathbf{k}} = \frac{\vec{B}_{eff}(\mathbf{k})}{|\vec{B}_{eff}(\mathbf{k})|}$, as calculated from the previous configuration.

Once a set of $n_{\mathbf{k}}$ and $\hat{s}_{\mathbf{k}}$ is given, one can also calculate the single particle energies $\epsilon(\mathbf{k})$:

$$\epsilon(\mathbf{k}) = \frac{\hbar \mathbf{k}^2}{2m} - \frac{1}{2L^2} \sum_{\mathbf{k}'} v_{\mathbf{k}-\mathbf{k}'}\, n_{\mathbf{k}'} - |\vec{B}_{eff}(\mathbf{k})| \ . \tag{10.28}$$

At this point a new set of occupation numbers $n_{\mathbf{k}}$ is determined by setting $n_{\mathbf{k}} = 1$ for the lowest N values of $\epsilon(\mathbf{k})$ and zero otherwise. This therefore generates a new set of $n_{\mathbf{k}}$ and $\hat{s}_{\mathbf{k}}$. The procedure is iterated on a finite grid of wavevectors to achieve self-consistency.

In Figure 10.4 we reproduce a set of states with the same spin orbit coupling $\bar{\alpha}$ at increasing values of r_s. At high density the convergence is to the paramagnetic state while at low densities the simple trial state of Section 10.1 is recovered. We also notice that the phase transition from the paramagnetic state is first order: in fact the occupation becomes simply connected across the transition point. The polarization is also discontinuous.

In Figure 10.4 a second set of states is also presented with fixed density r_s and increasing spin orbit coupling $\bar{\alpha}$. At small $\bar{\alpha}$ the occupation is a displaced circle, as we discussed for the perturbative case. In the limit of large $\bar{\alpha}$ the oblate completely polarized droplet is obtained.

Physical quantities of these self-consistent solutions must be calculated by refinement of the grid as to approach the continuous limit. This last step presents some complication and is briefly discussed in Appendix E. There, we also show results for the total energy. The polarization of the anisotropic solutions can also be obtained, and it is plotted in Figure 10.5. At large values of r_s the solution is asymptotically converging to the trial variational state, and the fractional polarization saturates to one. The polarization of the mean field solution with lowest energy is also plotted in Figure 10.5 as a function of r_s, at the particular value $\bar{\alpha} = 0.4$. The first discontinuity corresponds to the transition from the paramagnetic state to the isotropic ferromag-

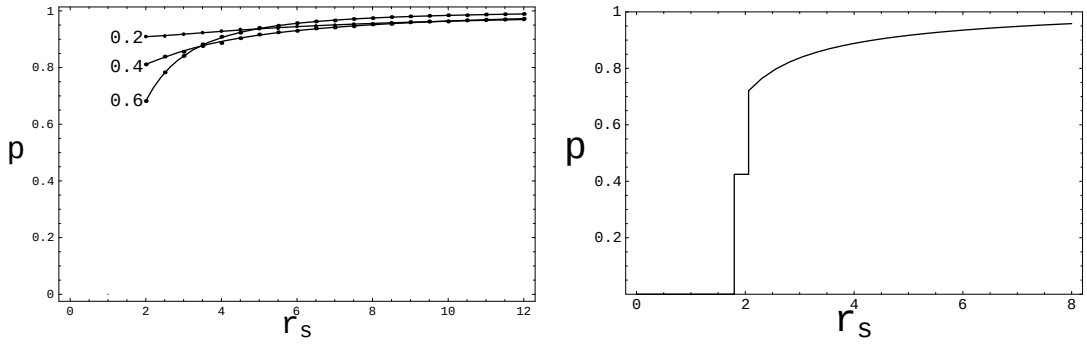

Figure 10.5. Left: fractional polarization of the in plane ferromagnetic HF solutions as a function of the density parameter r_s for different values of the spin orbit coupling $\bar{\alpha}$. Right: polarization of the HF ground state at $\bar{\alpha} = 0.4$ as function of r_s. In the region of the isotropic ferromagnetic solution, the fractional polarization is constant.

netic solution, while the second discontinuity corresponds to the transition to the in plane polarized phase.

The complete phase diagram including the paramagnetic solution and both types of ferromagnetic states is shown in Figure 10.6. At low spin-orbit coupling $\bar{\alpha} \lesssim 0.6$ the gas is polarized at a critical value of r_s up to the lowest densities. At higher density the ferromagnetic state is polarized perpendicular to the plane of motion, while a phase transition to an in plane ferromagnetic state occurs at lower density. The latter preempts the reentrant transition to the paramagnetic state.

At large values of $\bar{\alpha} \gtrsim 0.6$ the reentrant transition from the out-of-plane polarized state to the paramagnetic state survives. The actual FZ polarized region shrinks at large spin orbit and follows the curve at which the paramagnetic state has generalized chirality $\chi = 1$, which is the dotted line in Figure 10.6. The transition to the in plane polarized phase is directly from the paramagnetic state. We can compare the phase boundary with the differential instability of the paramagnetic state, which is the short dashed line in Figure 10.6. As expected, the transition is first order, and the differential instability of the paramagnetic state occurs when the system is already polarized. The boundary of the in-plane polarized phase was actually evaluated only

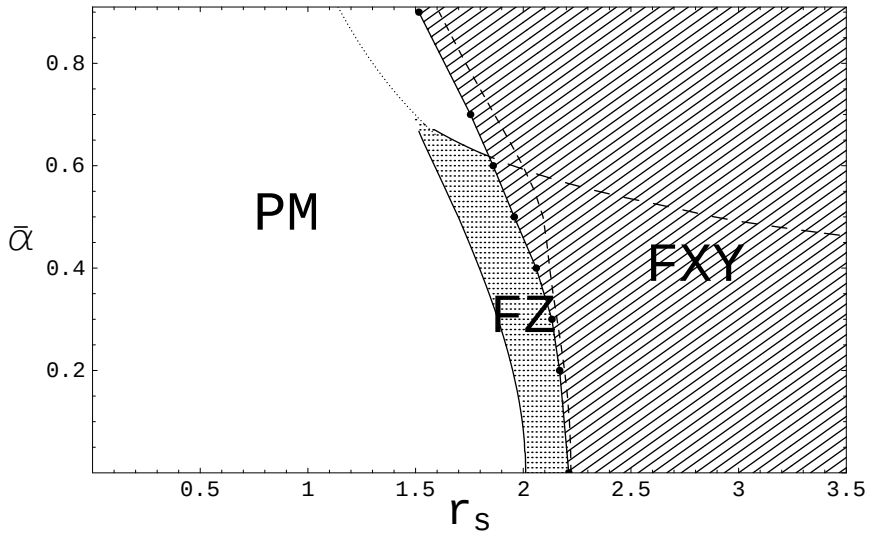

Figure 10.6. Complete HF phase diagram. The FZ region is of difficult evaluation at large $\bar{\alpha}$, but follows the dotted $\chi = 1$ curve. The marked points refer to actually computed points of the phase boundary. The short dashed line is the differential instability of the paramagnetic state for in plane external magnetic field. The last dashed line is the reentrant transition boundary between the FZ and PM phases.

at the marked points. At small $\bar{\alpha}$ it is difficult to obtain the critical density, because the two polarized phases have almost indistinguishable energy, but the exact $\bar{\alpha} \to 0$ value was obtained from perturbation theory in Section 10.2.

11. Hartree-Fock theory with generalized spin-orbit coupling

The treatment carried out in detail in the presence of linear Rashba spin-orbit can be immediately extended to other types of spin-orbit coupling. We collect in this Chapter results of the Hartree-Fock approximation for the hamiltonian $\hat{H}_n$ of Eq. (6.1), in the particular cases $n = 2$ or 3.

It is clear from the general structure of the Hartree-Fock theory that the spin-susceptibility is enhanced in all situations. We consider explicitly in this Chapter the form of the phase-diagram, which has a different form from the result obtained in the previous Chapter for linear Rashba spin-orbit coupling. Interestingly, the transition is directly to a ferromagnetic state polarized in the plane. This is not surprising, since the formation of the $n = 1$ transverse phase is due to the presence of a cusp in the single particle spectrum at $\mathbf{k} = 0$, which is a peculiar feature of the linear spin-orbit.

11.1 Hartree-Fock equations

The condition satisfied by the Hartree-Fock ground state can be obtained as in Chapter 7. In particular, it is convenient to obtain the appropriate equations by minimizing the energy with the appropriate constrains. The only difference pertains the spin-orbit energy which is given by:

$$\mathcal{E}_{so} = -\frac{2\sqrt{2^n}\,\bar{\gamma}}{r_s^n} \int_0^{2\pi} \frac{\mathrm{d}\phi}{2\pi} \int_{\rho_-(\phi)}^{\rho_+(\phi)} \hat{s}_0(\phi) \cdot \hat{s}(\kappa,\phi)\, \kappa^{n+1} \mathrm{d}\kappa \ , \tag{11.1}$$

where the notation is the same of Section 7.3. The definition of $\bar{\gamma}$ is given in Eq. (3.23) and the form of $\hat{s}_0(\phi) = -\sin(n\phi)\hat{x} + \cos(n\phi)\hat{y}$ corresponds to Eq. (3.17).

Minimization with respect to the quantization directions leads to the following equation:

$$\hat{s}(\kappa,\phi) = \frac{1}{\sqrt{2}\, r_s \lambda_2(\kappa,\phi)} \left[\bar{\mathbf{B}} - 2\bar{\gamma}\, \frac{\sqrt{2^{n-1}}}{r_s^{n-1}}\, \kappa^n\, \hat{s}_0(\phi) \right. \tag{11.2}$$

$$- \int_0^{2\pi} \frac{\mathrm{d}\phi'}{2\pi} \int_{\rho_-(\phi')}^{\rho_+(\phi')} \frac{\hat{s}(\kappa', \phi')}{\sqrt{\kappa^2 + \kappa'^2 - 2\kappa\kappa' \cos(\phi - \phi')}} \, \kappa' \mathrm{d}\kappa' \Bigg] \,,$$

while minimization with respect to the occupation numbers gives the couple of equations:

$$\begin{aligned} \lambda_1 =& \frac{2\rho_\pm^2(\phi)}{r_s^2} \pm \frac{\sqrt{2}}{r_s} \Bigg[\bar{\mathbf{B}} \cdot \hat{s}(\rho_\pm(\phi), \phi) - 2\bar{\gamma} \, \frac{\sqrt{2^{n-1}}}{r_s^{n-1}} \, \hat{s}_0(\phi) \cdot \hat{s}(\rho_\pm(\phi), \phi) \, \rho_\pm^n(\phi) \\ & - \int_0^{2\pi} \frac{\mathrm{d}\phi'}{2\pi} \int_{\rho_-(\phi')}^{\rho_+(\phi')} \frac{1 + \hat{s}(\rho_\pm(\phi), \phi) \cdot \hat{s}(\kappa', \phi')}{\sqrt{\rho_\pm^2(\phi) + \kappa'^2 - 2\rho_\pm(\phi)\kappa' \cos(\phi - \phi')}} \, \kappa' \mathrm{d}\kappa' \Bigg] \\ & - \frac{2\sqrt{2}}{r_s} \int_0^{2\pi} \frac{\mathrm{d}\phi'}{2\pi} \int_0^{\rho_\mp(\phi')} \frac{\kappa' \mathrm{d}\kappa'}{\sqrt{\rho_\pm^2(\phi) + \kappa'^2 - 2\rho_\pm(\phi)\kappa' \cos(\phi - \phi')}} \,. \end{aligned} \tag{11.3}$$

The above equations are written for the case of two occupied bands. For a single occupied band Eq. (11.2) is unchanged and Eq. (11.3) is modified as follows: the $\pm$ sign in the first line becomes $+$, and the term in the last line must be omitted.

11.2 Small coupling limit

Due to the perturbative character of the $n = 2, 3$ spin-orbit terms, an analysis at generic values of the coupling $\bar{\gamma}$ is impossible. Therefore we restrict ourselves to the case of small coupling, which still allows to obtain a complete picture of the mean-field phase-diagram. For this case Eqs. (11.2) and (11.3) simplify to:

$$\begin{aligned} \hat{s}(\kappa, \phi) =& - \frac{1}{\sqrt{2}\, r_s \lambda_2(\kappa, \phi)} \Bigg[2\bar{\gamma} \, \frac{\sqrt{2^{n-1}}}{r_s^{n-1}} \, \kappa^n \, \hat{s}_0(\phi) \\ & + \int_0^{2\pi} \frac{\mathrm{d}\phi'}{2\pi} \int_0^{\rho(\phi')} \frac{\hat{s}(\kappa', \phi')}{\sqrt{\kappa^2 + \kappa'^2 - 2\kappa\kappa' \cos(\phi - \phi')}} \, \kappa' \mathrm{d}\kappa' \Bigg] \,, \end{aligned} \tag{11.4}$$

$$\begin{aligned} \lambda_1 =& \frac{2\rho^2(\phi)}{r_s^2} - \frac{\sqrt{2}}{r_s} \Bigg[2\bar{\gamma} \, \frac{\sqrt{2^{n-1}}}{r_s^{n-1}} \, \hat{s}_0(\phi) \cdot \hat{s}(\rho(\phi), \phi) \, \rho^n(\phi) \\ & + \int_0^{2\pi} \frac{\mathrm{d}\phi'}{2\pi} \int_0^{\rho(\phi')} \frac{1 + \hat{s}(\rho(\phi), \phi) \cdot \hat{s}(\kappa', \phi')}{\sqrt{\rho^2(\phi) + \kappa'^2 - 2\rho(\phi)\kappa' \cos(\phi - \phi')}} \, \kappa' \mathrm{d}\kappa' \Bigg] \,, \end{aligned} \tag{11.5}$$

which are approximated to first order in $\bar{\gamma}$ by setting $\hat{s}(\kappa, \phi) = \hat{s}^{(0)} + \delta\hat{s}(\kappa, \phi)$ and $\rho(\phi) = \sqrt{2} + \delta\rho(\phi)$, where $\hat{s}^{(0)} = \hat{z}$ or $\hat{s}^{(0)} = \hat{y}$ for the transverse or in-plane case respectively.

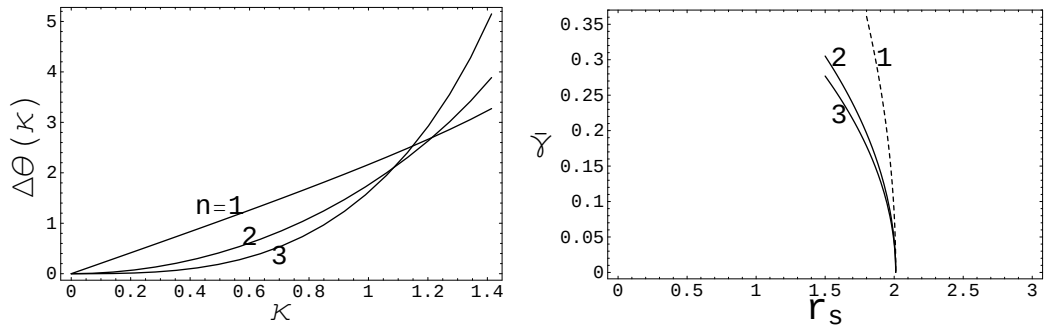

Figure 11.1. Left: Plot of the solutions of Eq. (11.8), for different values of n. Right: Bloch transition for different values of n. $n = 2, 3$ correspond to in-plane polarized states and $n = 1$ to a transverse ferromagnetic state. For this last case, the phase boundary to an in-plane polarized phase at $r_s \simeq 2.211$ is not shown.

For the transverse case we have, to first order in γ:

$$\delta\hat{s}(\kappa,\phi) = \bar{\gamma}\frac{\sqrt{2^n}}{r_s^{n-1}}\,\Delta\theta(\kappa)\,\hat{s}_0(\phi)\ , \tag{11.6}$$

$$\delta\rho(\phi) = 0\ , \tag{11.7}$$

where $\Delta\theta(\kappa)$ satisfies the integral equation:

$$\Delta\theta(\kappa) = \frac{\int_0^{\sqrt{2}}\kappa'\mathrm{d}\kappa'\int_0^{2\pi}\frac{\Delta\theta(\kappa')\cos\theta}{\sqrt{\kappa^2+\kappa'^2-2\kappa\kappa'\cos n\theta}}\frac{\mathrm{d}\theta}{2\pi}+\sqrt{2}\,\kappa^n}{\int_0^{\sqrt{2}}\kappa'\mathrm{d}\kappa'\int_0^{2\pi}\frac{1}{\sqrt{\kappa^2+\kappa'^2-2\kappa\kappa'\cos\theta}}\frac{\mathrm{d}\theta}{2\pi}}\ , \tag{11.8}$$

which is easily derived by Eq. (11.4). The corresponding solutions are plotted in Figure 11.1.

For the in-plane case we have:

$$\delta\hat{s}(\kappa,\phi) = -\bar{\gamma}\frac{\sqrt{2^n}}{r_s^{n-1}}\,\Delta\theta(\kappa)\,\sin(n\phi)\hat{x}\ , \tag{11.9}$$

$$\delta\rho(\phi) = \bar{\gamma}\,\frac{a}{r_s^{n-1}}\,\cos(n\phi)\ , \tag{11.10}$$

where $\Delta\theta(\kappa)$ satisfies the same integral equation Eq. (11.8) and a is obtained using Eq. (11.5):

$$a = \frac{2^{n-1}r_s}{\sqrt{2}-C_n r_s}\ . \tag{11.11}$$

The constant $C_n = \frac{\sqrt{2}}{\pi}\sum_{m=0}^{n}\frac{1}{1-2m}$ was already defined in Eq. (6.9).

The change in total energy can be calculated to quadratic order by making use of the previous results. For both cases is found to be equal to $\frac{1}{2}\mathcal{E}_{so}$. In particular we have:

$$\delta\mathcal{E}_{\perp} = -\bar{\gamma}^2\,\frac{2^n}{r_s^{2n-1}}\int_0^{\sqrt{2}}\Delta\theta(\kappa)\kappa^{n+1}\,\mathrm{d}\kappa\ , \tag{11.12}$$

and:

$$\delta\mathcal{E}_{\parallel} = -\bar{\gamma}^2\,\frac{2^n}{r_s^{2n-1}}\Big[\frac{2^{n-2}}{\sqrt{2}-C_n r_s}\sqrt{2}r_s + \frac{1}{2}\int_0^{\sqrt{2}}\Delta\theta(\kappa)\kappa^{n+1}\,\mathrm{d}\kappa\Big]\ . \tag{11.13}$$

The constant entering in Eqs. (11.12) and (11.12) is obtained numerically as follows:

$$\int_0^{\sqrt{2}}\Delta\theta(\kappa)\kappa^{n+1}\,\mathrm{d}\kappa \simeq \begin{cases} 1.413 & \text{for } n=2\ , \\ 1.011 & \text{for } n=3\ , \end{cases} \tag{11.14}$$

which allows to compare the values of $\delta\mathcal{E}_{\perp}$ and $\delta\mathcal{E}_{\parallel}$. For $n = 2, 3$ and $r_s > r_s^* = \frac{3\pi}{8(2-\sqrt{2})} \simeq 2.011$ we obtain $\delta\mathcal{E}_{\perp} > \delta\mathcal{E}_{\parallel}$ and therefore we conclude that the Bloch transition is directly to an in-plane polarized phase.

With a method similar to the case of Rashba spin-orbit, it is possible to obtain the curvature of the phase boundary. In fact, it is sufficient to equate (11.13) to the second-order approximation of the paramagnetic phase energy:

$$\left(\frac{1}{r_s^2} - \frac{8\sqrt{2}}{3\pi r_s}\right) - \frac{2^n\bar{\gamma}^2 r_s^{2-2n}}{1-C_n r_s} = \left(\frac{2}{r_s^2} - \frac{16}{3\pi r_s}\right) + \delta\mathcal{E}_{\parallel}\ , \tag{11.15}$$

which gives:

$$\bar{\gamma} \simeq \begin{cases} \sqrt{0.1822(r_s^* - r_s)} & \text{for } n=2\ , \\ \sqrt{0.1501(r_s^* - r_s)} & \text{for } n=3\ . \end{cases} \tag{11.16}$$

This final result is displayed in Figure 11.1. It has to be noted that the presence of a finite spin-orbit coupling favors the transition to the ferromagnetic state in all of the three cases.

11.3 Exact numerical results

The same result of the previous section can also be calculated exactly, with similar results. The in-plane polarized states are obtained on a finite grid, and one example is

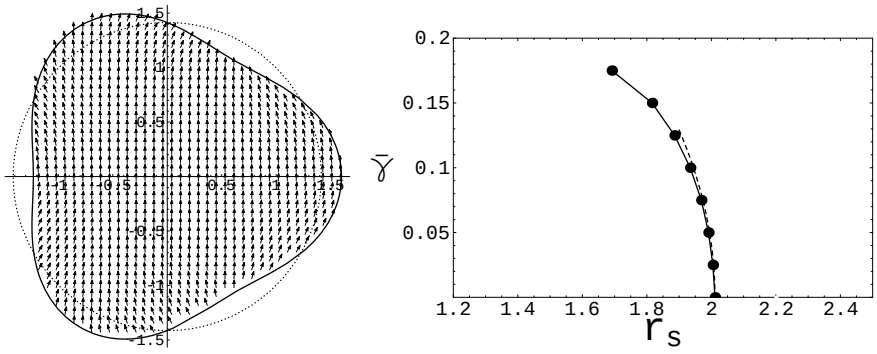

Figure 11.2. Left: example of an in-plane polarized state for $n = 3$, at $r_s = 2$ and $\bar{\gamma} = 0.175$. The solid line denotes the perturbative result for the Fermi surface, as obtained in Section 11.2, which has a good agreement with the numerical solution. Right: exact boundary of the Bloch transition for $n = 3$. The boundary is computed at the marked points and the dashed line is the approximation (11.16).

shown in Figure 11.2 for the case $n = 3$. The energies are calculated by extrapolation to the continuous limit, as described in Appendix E. The resulting boundary of the polarized region can be obtained, by equating the energy of the polarized states to that of the paramagnetic phase, which was obtained in Chapter 6. This result is plotted in the second panel of Figure 11.2.

12. High density limit in the presence of Rashba spin-orbit coupling

So far, we have examined the properties of the two-dimensional electron liquid in the framework of the Hartree-Fock approximation. This allows to completely characterize the properties of the system, but only in an approximate manner. In fact, it is found that the Hartree-Fock approximation gives qualitatively correct results for the case without spin-orbit, but its validity is very limited from the quantitative point of view. A simple exact treatment of the problem is only amenable in the asymptotic regimes, of which we examine here the high density limit.

This limit can be studied in the form of a series expansion in the small dimensionless density parameter:

$$r_s = \frac{1}{\sqrt{\pi n a_B^2}} \ , \tag{12.1}$$

where a_B is the effective Bohr radius and n is the number density. At small r_s, the first correction to the noninteracting problem is provided by the exchange energy and was obtained in Chapter 6 for a generalized spin-orbit coupling. In the particular case of linear Rashba spin-orbit it was found that the leading contribution of the exchange is zero and therefore a more careful treatment is necessary.

The other relevant dimensionless parameter is $\bar{\alpha} = \frac{\hbar\alpha}{e^2}$. Alternatively, the following coupling strength g can be used:

$$g = \sqrt{2}\bar{\alpha} r_s \ . \tag{12.2}$$

This formula is a particular case of (3.24) and expresses the ratio of the spin-orbit and kinetic energy. It is clear that g is vanishing small in the high density limit. We will obtain in the following the leading corrections to the chirality and to the exchange-correlation energy due to the Rashba spin-orbit coupling, in terms of the small parameters r_s and g.

12.1 Non interacting electrons

The noninteracting problem in the presence of Rashba spin-orbit was extensively treated in Chapter 2. We repeat here briefly some of the formulas, for ease of reference and to fix the notation used in this Chapter.

The eigenstates of the noninteracting problem given in Eq. (3.18) are plane waves with spinor functions given by:

$$|\mathbf{k}\pm\rangle = \frac{1}{\sqrt{2}} \begin{pmatrix} \pm 1 \\ i e^{i\phi_{\mathbf{k}}} \end{pmatrix} \ , \tag{12.3}$$

and all the nonintercting physical quantities are functions of g only. In particular, the eigenenergies (in Rydbergs) are equal to $\frac{2}{r_s^2}\,\epsilon_\pm(k)$ where:

$$\epsilon_\pm(k) = k^2 \mp g\,k \ . \tag{12.4}$$

In the previous formula and in the rest of the Chapter the wavevectors are expressed in terms of $k_F = \sqrt{2\pi n}$. The two Fermi surfaces are determined by the radii:

$$k_\pm = \sqrt{|1 \pm \chi|} \ , \tag{12.5}$$

where the generalized chirality χ can be larger than unity (in which case $k_\pm$ would be more appropriately labeled $k_{out/in}$). The corresponding occupation is:

$$n_\pm(k) = \theta(\sqrt{|1 \pm \chi|} - k) - \theta(\chi - 1)\theta(\sqrt{\chi - 1} - k) \ , \tag{12.6}$$

where $\theta(x)$ is the usual step function and we assume $\chi \geq 0$. In particular, we have $n_\pm(k) = \theta(k_\pm - k)$ if $0 \leq \chi \leq 1$.

The noninteracting energy is obtained as in Eq. (2.23) at a generic value of χ:

$$\mathcal{E}_0(g, r_s, \chi) = \frac{(1+\chi^2) - (\chi-1)^2\theta(\chi-1)}{r_s^2} + \frac{2g}{r_s^2}\frac{\sqrt{|1-\chi|^3} - \sqrt{|1+\chi|^3}}{3} \ , \tag{12.7}$$

while the noninteracting ground state is determined as in Eq. (2.24):

$$\chi^{(0)}_{min}(g) = g\sqrt{1 - \frac{g^2}{4}}\,\theta(\sqrt{2} - g) + \left(\frac{g^2}{4} + \frac{1}{g^2}\right)\,\theta(g - \sqrt{2}) \ . \tag{12.8}$$

Finally, the ground state energy is obtained:

$$\mathcal{E}_0(g, r_s) = \mathcal{E}_0(g, r_s, \chi^{(0)}_{min}(g)) \ . \tag{12.9}$$

12.2 Exchange-correlation energy

The exchange-correlation energy of the electron liquid without spin-orbit is well known from decades of theoretical investigations [1]. At a generic values of the density, the value of $\mathcal{E}_{xc}(r_s)$ is obtained numerically with the Monte Carlo method [1, 23] [1]. The high density limit can be studied in the form of a perturbative expansion [22]:

$$\mathcal{E}_{xc}(r_s) = -\frac{8\sqrt{2}}{3\pi r_s} - 0.385 - \frac{2\sqrt{2}}{3\pi}(10 - 3\pi)\, r_s \ln r_s + \dots \ , \tag{12.10}$$

where the first term is the exchange energy, the constant term is the result of the numerical integration of the second order correlation energy, and the last contribution can be calculated from the infinite sum of diverging ring diagrams, as first discovered for the three-dimensional case [57].

On the other hand, the computation of the exchange-correlation energy at finite spin-orbit coupling is a problem which is unexplored. We define $\delta\mathcal{E}_{xc}(g, r_s)$ from the equation:

$$\mathcal{E}(g, r_s) = \mathcal{E}_0(g, r_s) + \mathcal{E}_{xc}(r_s) + \delta\mathcal{E}_{xc}(g, r_s) \ , \tag{12.11}$$

where the noninteracting energy is given by (12.7), (12.8) and (12.9). The correction $\delta\mathcal{E}_{xc}(g, r_s)$ is generally neglected, for example in density functional studies including the spin-orbit interaction. A partial justification to this procedure is given below, where we show that $\delta\mathcal{E}_{xc}$ is actually vanishing to the quadratic order in g for the particular case of the Rashba spin-orbit. However, $\delta\mathcal{E}_{xc}$ is not zero in general and it might lead to important effects in the case of large g (e.g. at low density).

Formally, the total energy of the interacting system can be calculated via a perturbative expansion, as for example to obtain Eq. (12.10). In the presence of spin-orbit coupling, each perturbative term acquires a dependence from g and χ. The value of χ refers to the noninteracting state used in the perturbative expansion, which does not need to be the noninteracting ground state. As a consequence, we can write the total energy as:

$$\mathcal{E}(g, r_s, \chi) = \mathcal{E}_0(g, r_s, \chi) + \mathcal{E}_{xc}(r_s) + \delta\mathcal{E}_{xc}(g, r_s, \chi) \ , \tag{12.12}$$

[1] See however the next Chapter for the case of finite polarization.

where $\mathcal{E}_0(g, r_s, \chi)$ is given in (12.7).

The interacting chirality $\chi_{min}(g, r_s)$ can be obtained by minimization of (12.12), which also gives the final interacting ground state energy (12.11). One has to notice that there are two different contributions to $\delta\mathcal{E}_{xc}(g, r_s)$. The first is given directly by $\delta\mathcal{E}_{xc}(g, r_s, \chi_{min})$, while the second arises from the renormalization of χ in the noninteracting energy $\mathcal{E}_0(g, r_s, \chi)$.

In concluding this Section, we comment about some aspects of the perturbative expansion. One requirement for its validity is the fact that by adiabatic switching on/off of the electron-electron interaction only a multiplicative phase-factor is introduced. This is not automatically true for degenerate excited states and the use of a generic value of χ different from $\chi^{(0)}_{min}(g)$ is a delicate point. For the class of noninteracting states parametrized by χ we assume that this property holds true, otherwise the presence of isotropic Fermi surfaces would be destroyed.

Another interesting point is that it is not clear if an analog of the Luttinger theorem is valid in this case. In other words, if the Fermi surfaces of the actual interacting ground state correspond to the value $\chi_{min}(g, r_s)$ obtained as described above. This is obviously true in the Hartree-Fock approximation, where interacting and noninteracting (paramagnetic) states coincide, but it is not clear in general terms.

12.3 The high-density limit

Taking the $r_s \to 0$ limit at a constant value of $\bar{\alpha}$ corresponds also to a vanishing strength of the spin orbit coupling g, as it is clear from (3.24). Furthermore, since $\chi_{min}(g, r_s)$ is given in first approximation by the noninteracting value (12.8), we also have $\chi \simeq g$. Therefore, we have to obtain an expansion of (12.12) in the small parameters r_s, g and χ, which are all of $\mathcal{O}(r_s)$.

The high density limit correction is correctly obtained in the Hartree-Fock theory. The exchange energy of the unpolarized state is studied in Chapter 8:

$$\mathcal{E}(g, r_s, \chi) = \mathcal{E}_0(g, r_s, \chi) + \mathcal{E}_{xc}(r_s) + \delta\mathcal{E}_x(r_s, \chi) + \dots \ , \tag{12.13}$$

where $\delta\mathcal{E}_x(r_s,\chi) \equiv \delta\mathcal{E}_x[\chi;\frac{\pi}{2}]$, as defined in Eq. (8.11). This quantity gives the correction to the exchange energy due to the spin-orbit coupling and its plot is easily obtained from the first panel of Figure 8.2, if the constant $\frac{8\sqrt{2}}{3\pi}$ is added.

The asymptotic form of $\delta\mathcal{E}_x(\chi)$ at small χ is given by:

$$\delta\mathcal{E}_x(r_s,\chi) = \frac{\sqrt{2}}{48\pi r_s}\chi^4(\ln\chi - C) + \dots \ , \tag{12.14}$$

where $C = 3\ln 2 - \frac{23}{12} \simeq 0.162775$ and the omitted terms are $\mathcal{O}(\chi^6)$. In Eq. (12.14) the term quadratic in χ is missing, and therefore it seems *a priori* possible that the exchange contribution is only a subleading term.

However, we will show that this is not the case. We will prove in Section 12.4.1 the following general form for the formal expression of a generic diagrammatic contribution of order n to the total energy:

$$\delta D_n = r_s^{n-2}[c_{2,n}(g-\chi)^2 + \dots] \ , \tag{12.15}$$

where the omitted terms are of higher order in g and χ. In the particular case of the exchange energy we have $c_{2,1} = 0$.

The generic contribution (12.15) does not produce any correction to lowest order in the value of $\mathcal{E}(g,r_s,\chi)$ and its derivative $\frac{\partial\mathcal{E}(g,r_s,\chi)}{\partial\chi}$ since $\chi \simeq g$ in first approximation. Therefore the lowest order correction to $\chi_{min}(g,r_s)$ and $\delta\mathcal{E}_{xc}(g,r_s)$ is zero to all orders of perturbation theory, and one can consider in the high density limit the exchange energy only.

By making use of (12.13), with the definition (12.7) and (12.14) one obtains:

$$\chi_{min}(g,r_s) = \chi^{(0)}_{min}(g)\left[1 - \frac{\sqrt{2}}{24\pi}\, r_s g^2(\ln g - C + \frac{1}{4}) + \dots\right] \ , \tag{12.16}$$

which represents the analytic form of the small chirality enhancement discussed in Chapter 8. The relative correction is of order $\mathcal{O}(r_s^3)$ and, as anticipated, it is quadratic in the spin-orbit coupling.

In calculating the correction to the total energy, one has to notice that $\chi_0(g)$ is a stationary value of the noninteracting energy. Therefore, the correction to the

noninteracting energy due to the renormalized value of χ is of order $\mathcal{O}(\frac{(rs^4)^2}{rs^2}) = \mathcal{O}(r_s^6)$ and can be safely neglected. The leading term is given by $\delta\mathcal{E}_x(r_s, g)$:

$$\delta\mathcal{E}_{xc}(g, r_s) = \frac{\sqrt{2}g^4}{48\pi r_s}(\ln g - C) + \dots \ , \tag{12.17}$$

while correlation corrections are of higher order.

12.4 Formally exact properties

We prove here two formally exact properties satisfied by the total energy and the self-energy of the interacting system with Rashba spin-orbit. The proof is based on the diagrammatic expansion but is carried out at a generic order of the perturbation series. Detailed questions relative to the convergence of the single diagrams and the appropriateness of certain mathematical manipulations are treated loosely. Since the proof is valid for a generic type of two-body interaction, we will assume that the expressions are analytically well behaved. The explicit treatment of the lowest order contributions for the case of the Coulomb interaction is provided in the next Section.

The perturbative rules in the presence of spin-orbit have little modifications to the case without spin-orbit [1]. For clarity we discuss them here briefly. The Green function is defined as:

$$G_\mu(k, t) = -i\langle T\hat{b}_{\mathbf{k}\mu}(t)\hat{b}^\dagger_{\mathbf{k}\mu}(0)\rangle \ , \tag{12.18}$$

where the average is on the interacting ground state. $\hat{b}^\dagger_{\mathbf{k}\mu}|0\rangle$ is a noninteracting eigenstate in the presence of spin-orbit, as in (3.18). The Green function is diagonal for the paramagnetic phase. To prove this fact we can assume $\mathbf{k}$ along x and consider the transformation $\hat{R}_y$, corresponding to the $y \to -y$ reflection. We have that $\langle \hat{R}_y^{-1}\hat{b}_{\mathbf{k}\nu}\hat{b}^\dagger_{\mathbf{k}\mu}\hat{R}_y\rangle = \mu\nu\,\langle \hat{b}_{\mathbf{k}\nu}\hat{b}^\dagger_{\mathbf{k}\mu}\rangle$, due to the form of the single-particle states. The paramagnetic ground state can be assumed to have a definite parity with respect to $\hat{R}_y$ and therefore we obtain a vanishing result when $\mu\nu = -1$. The same property does not hold if such symmetry is broken, as for example for a polarized ground-state.

The noninteracting Green function is:

$$G_{0\mu}(k,\omega) = \frac{1-n_\mu(k)}{\omega-\epsilon_\mu(k)+i\eta} + \frac{n_\mu(k)}{\omega-\epsilon_\mu(k)-i\eta} \ , \tag{12.19}$$

where $n_\mu(k)$ is defined in (12.6) and contains the dependence on χ, while $\epsilon_\mu(k)$ is defined in (12.4) and contains the dependence on g. We expressed frequencies in units of $\frac{\epsilon_F}{\hbar} = \frac{\hbar k_F^2}{2m}$ and energy in Rydbergs, which gives $\hbar = \frac{\epsilon_F}{Ry} = \frac{2}{r_s^2}$.

The perturbation theory for the Green function diagrams has the usual rules, which in the units of our choice contemplate a factor $\frac{2\sqrt{2}r_s}{q}$ for an interaction line with momentum q and an overall factor $i^n(-1)^L$ (i.e. $\hbar$ is omitted in the prefactor, while L is as usual the number of loops and n the order of the diagram). The most important modification is that each vertex (as in Figure 12.1) is associated with the scalar product $\langle \mathbf{k}\mu|\mathbf{k}'\mu'\rangle$, beside the delta functions ensuring frequency/momentum conservation. The form of the spinors is given in (12.3).

The self energy is defined from $G_\mu(k,\omega) = 1/\left(\omega - \epsilon_\mu(k) - \Sigma_\mu(k,\omega)/\hbar\right)$ and therefore a similar set of rules apply, except a multiplicative $\hbar = \frac{2}{r_s^2}$ overall factor which converts it to an energy.

12.4.1 An exact property of the energy expansion

The total energy is obtained from the following integration over the coupling constant formula [1]:

$$\begin{aligned} &\mathcal{E}(g,r_s,\chi) = \mathcal{E}_0(g,r_s,\chi) + \\ &+\frac{1}{2}\sum_\mu \int_0^1 \frac{\mathrm{d}\lambda}{\lambda} \int \frac{\mathrm{d}\mathbf{k}}{(2\pi)^2} \int \frac{\mathrm{d}\omega}{2\pi i} G_\mu^\lambda(k,\omega)\Sigma_\mu^\lambda(k,\omega) \ , \end{aligned} \tag{12.20}$$

where an additional factor λ is included for each interaction line. As it is clear by the form of the integrand, this is the sum of closed diagrams containing one or more fermionic loops. A diagram of order n has an overall factor $\lambda^n r_s^{n-2}$, in agreement with (12.15). We now consider in detail the form of one of these contributions, and we

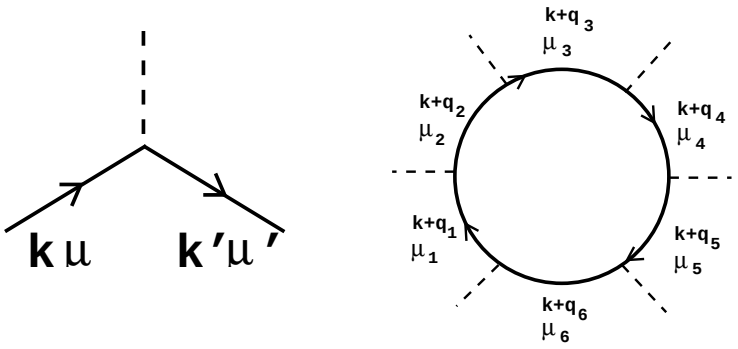

Figure 12.1. Left: interaction vertex, associated with a $\langle \mathbf{k}\mu|\mathbf{k}'\mu'\rangle$ factor. Right: fermionic loop, appearing in energy diagrams.

suppose for simplicity that one loop is present only. The proof can be easily extended to the general case of many loops. If the loop contains N solid lines we can write:

$$D = \int [\ldots] \sum_{\{\mu_i\}} \int \frac{\mathrm{d}\mathbf{k}}{(2\pi)^2} \prod_{i=1}^{N} G_{0\mu_i}(p_i, \omega_i) \langle \mathbf{p}_i \mu_i | \mathbf{p}_{i+1} \mu_{i+1} \rangle \ , \tag{12.21}$$

where $\{\mu_i\} \equiv \{\mu_1, \mu_2, \ldots \mu_N\}$ and $N+1 \equiv 1$. The internal momenta and frequencies are $\mathbf{p}_i = \mathbf{k} + \mathbf{q}_i$ and $\omega_i = \omega + \Omega_i$, as in Figure 12.1, where $\mathbf{k}$ and ω are the momentum and frequency flowing in the loop. Finally, $[\ldots]$ is the remaining expression of the diagram which is independent on $\mathbf{k}$ and ω.

One can now take derivatives with respect to χ and g of the above expression. The derivatives only act on the noninteracting Green functions, given by (12.19), and in particular $\frac{\partial}{\partial \chi}$ acts on the occupation functions and $\frac{\partial}{\partial g}$ on the energy denominators. After setting $\chi = g = 0$ the spin summation can be performed explicitly and gives zero in the case of the first derivatives. The second derivatives of D have more complicated expressions that in general are nonvanishing.

We now introduce the following 'resolved' Green function at vanishing spin-orbit, so that the unperturbed Green function is $G_0(k, \omega) = \tilde{G}_0(k, k, \omega)$:

$$\tilde{G}_0(k_\chi, k_g, \omega) = \frac{1 - n_0(k_\chi)}{\omega - k_g^2 + i\eta} + \frac{n_0(k_\chi)}{\omega - k_g^2 - i\eta} \ , \tag{12.22}$$

where $n_0(k) = \theta(1-k)$. We then consider the following expression corresponding to the same diagram (12.21):

$$D_{ab} = \int [\ldots] \int \frac{\mathrm{d}\mathbf{k}_\chi \mathrm{d}\mathbf{k}_g}{(2\pi)^2}\, 2\,\delta^2(\mathbf{k}_\chi - \mathbf{k}_g) \left[\frac{\vec{\nabla}_{\mathbf{k}_a} \cdot \vec{\nabla}_{\mathbf{k}_b}}{4}\right] \prod_{i=1}^{N} \tilde{G}_0(p_i^\chi, p_i^g, \omega_i) \ , \quad (12.23)$$

where each of the indexes a, b can be χ or g while $\mathbf{p}_i^\chi = \mathbf{k}_\chi + \mathbf{q}_i$ and $\mathbf{p}_i^g = \mathbf{k}_g + \mathbf{q}_i$. It is clear that, omitting the differential operator in the square parenthesis, the above expression corresponds to the value of D at $\chi = g = 0$. On the other side, the operator $\vec{\nabla}_{\mathbf{k}_\chi}$ acts on the occupation functions of the $\tilde{G}_0$ while $\vec{\nabla}_{\mathbf{k}_g}$ on the energy denominators, in a way similar to the derivatives in χ and g of (12.21). In fact, one can show by an explicit comparison:

$$\left.\frac{\partial^2 D}{\partial a \partial b}\right|_0 = D_{ab} \ . \quad (12.24)$$

The explicit calculation is straightforward and the details are provided in Appendix F.1.

Finally, the quantities D_{ab} are immediately seen from (12.23) to be related among them, by simple integrations by parts. Therefore we obtain:

$$\left.\frac{\partial^2 D}{\partial \chi^2}\right|_0 = \left.\frac{\partial^2 D}{\partial g^2}\right|_0 = -\left.\frac{\partial^2 D}{\partial \chi \partial g}\right|_0 \ , \quad (12.25)$$

which corresponds to the general form given in (12.15).

12.4.2 An exact property of the self-energy

The self-energy $\Sigma_\mu(k,\omega)$ satisfies a similar exact relation to linear order in g, which reads as follows:

$$\left.\frac{\partial \Sigma_\mu(k,\omega)}{\partial g}\right|_0 = -\frac{\mu}{2}\frac{\partial \Sigma_0(k,\omega)}{\partial k} \ , \quad (12.26)$$

where $\Sigma_0(k,\omega)$ is the unperturbed ($g = \chi = 0$) self energy. In the derivation we can suppose $\chi \simeq g$, as appropriate to linear order in g for the interacting ground state.

The proof is readily obtained by considering the explicit form of a diagram contributing to the self-energy, in the same notation of (12.21):

$$D_\Sigma = \int [\ldots] \sum_{\{\mu_i\}} \prod_{i=1}^{N} G_{0\mu_i}(p_i, \omega_i) \prod_{j=0}^{N} \langle \mathbf{p}_j \mu_j | \mathbf{p}_{j+1} \mu_{j+1} \rangle \ , \quad (12.27)$$

where only Green functions connected which the external momentum $\mathbf{k}$ are explicitly written. Therefore $\mathbf{p}_i = \mathbf{k} + \mathbf{q}_i$ while $\mathbf{p}_0 = \mathbf{p}_{N+1} = \mathbf{k}$ and $\mu_0 = \mu_{N+1} = \mu$.

The derivative $\frac{\partial}{\partial g}$ involves all the Green functions appearing in the diagram. However, one has not to worry about the ones that are not written in (12.27), since these are involved in fermionic loops. In this case, using $\frac{\partial G_{0\mu}}{\partial g} \propto \mu$ and the spin sum ($N+1 \equiv 1$ and $\mu_j \in \{\mu_i\}$):

$$\sum_{\{\mu_i\}} \mu_j \prod_{i=1}^{N} \langle \mathbf{p}_i \mu_i | \mathbf{p}_{i+1} \mu_{i+1} \rangle = 0 \ , \tag{12.28}$$

one has that the contributions from these terms are vanishing.

On the other side the expression for the same unperturbed diagram is simply:

$$D_{\Sigma_0} = \int [\ldots] \prod_{i=1}^{N} G_0(p_i, \omega_i) \ , \tag{12.29}$$

and the derivative with respect to k acts in a similar way on the Green functions as $\frac{\partial}{\partial g}$ in (12.27). Therefore the equality (12.26) is verified diagram by diagram. We refer to Appendix F.2 for more details.

A perhaps better form of (12.26), valid to linear order in g, is as follows:

$$\Sigma_\mu(k, \omega) = \Sigma_0(k - \frac{\mu g}{2}, \omega) + \ldots \ . \tag{12.30}$$

This expression of the self-energy (12.30) confirms that the Fermi surfaces of the electron liquid are obtained when $k_\pm \mp \frac{g}{2} \simeq 1$ which is equivalent to $k_\pm = \sqrt{1 \pm \chi}$ at first order in g. Furthermore, it is obtained that all the quasiparticle properties (effective mass, lifetime, ...) are equal to the case without spin-orbit, at the appropriate density r_s, to linear order in g. We notice that this fact was proved already in Ref. [17] for the RPA approximation and the corrections quadratic in g are explicitly obtained. The results of Ref. [17] are exact in the high density limit. However, we notice that the property (12.30) is more general, since it is exact at generic values of r_s, if the requirement $\bar{\alpha} \ll \frac{1}{r_s}$ is satisfied.

12.5 Explicit evaluation of correlation terms

The derivations given in the previous Section are general but of formal character. In particular, we did not worry about many detailed questions of convergence of the formal expressions and appropriateness of the mathematical manipulations, as for example the exchange of order of derivatives and integrations. For the self-energy our conclusions are confirmed by the treatment of Ref. [17]. We consider now explicitly the details of the first two terms of the perturbative expansion, i.e. the second-order correlation energy and the ring-diagrams sum, which appear in the classical expansion (12.10) at $\alpha = 0$.

12.5.1 Second order correlation energy

The second-order correlation energy $\mathcal{E}_2(g, \chi)$ is obtained by standard perturbation theory, where in the intermediate state two electron-hole pairs are present such that occupied states with wavevectors $\mathbf{k}$, $\mathbf{k}'$ and spin indexes μ, μ' have scattered to new unoccupied states:

$$(\mathbf{k}, \mu) \to (\mathbf{p}, \sigma) \quad \text{and} \quad (\mathbf{k}', \mu') \to (\mathbf{p}', \sigma') \ , \tag{12.31}$$

where $\mathbf{p} = \mathbf{k} + \mathbf{q}$ and $\mathbf{p}' = \mathbf{k}' - \mathbf{q}$.

As it is well known, two different terms contribute to $\mathcal{E}_2(g, \chi)$, corresponding to the two different ways to scatter back to the original state:

$$(\mathbf{p}, \sigma) \to (\mathbf{k}, \mu) \quad \text{and} \quad (\mathbf{p}', \sigma') \to (\mathbf{k}', \mu') \ , \tag{12.32}$$

$$(\mathbf{p}, \sigma) \to (\mathbf{k}', \mu') \quad \text{and} \quad (\mathbf{p}', \sigma') \to (\mathbf{k}, \mu) \ , \tag{12.33}$$

referring respectively to direct and exchange processes.

Therefore we can write:

$$\mathcal{E}_2(g, \chi) = \mathcal{E}_2^D(g, \chi) + \mathcal{E}_2^X(g, \chi) \ . \tag{12.34}$$

where the direct and exchange contributions are given by:

$$\mathcal{E}_2^D(g,\chi) = -\frac{1}{4\pi^3}\sum_{\mu,\mu',\sigma,\sigma'}\int \mathrm{d}\mathbf{q}\int \mathrm{d}\mathbf{k}\int \mathrm{d}\mathbf{k}'\,\frac{|\langle \mathbf{p}\,\sigma|\mathbf{k}\mu\rangle|^2\,|\langle \mathbf{p}'\,\sigma'|\mathbf{k}'\mu'\rangle|^2}{q^2} \times\frac{n_\mu(k)n_{\mu'}(k')(1-n_\sigma(p))(1-n_{\sigma'}(p'))}{\epsilon_\sigma(p)-\epsilon_\mu(k)+\epsilon_{\sigma'}(p')-\epsilon_{\mu'}(k')}\ , \quad (12.35)$$

$$\mathcal{E}_2^X(g,\chi) = \frac{1}{4\pi^3}\sum_{\mu,\mu',\sigma,\sigma'}\int \mathrm{d}\mathbf{q}\int \mathrm{d}\mathbf{k}\int \mathrm{d}\mathbf{k}'\,\frac{\langle \mathbf{p}\,\sigma|\mathbf{k}\mu\rangle\,\langle \mathbf{k}\mu|\mathbf{p}'\sigma'\rangle\,\langle \mathbf{p}'\sigma'|\mathbf{k}'\mu'\rangle\,\langle \mathbf{k}'\mu'|\mathbf{p}\,\sigma\rangle}{q\,|\mathbf{k}-\mathbf{k}'+\mathbf{q}|} \times\frac{n_\mu(k)n_{\mu'}(k')(1-n_\sigma(p))(1-n_{\sigma'}(p'))}{\epsilon_\sigma(p)-\epsilon_\mu(k)+\epsilon_{\sigma'}(p')-\epsilon_{\mu'}(k')}\ . \quad (12.36)$$

By direct evaluation of the derivatives of these expressions one obtains the quadratic expansion in χ and g as follows:

$$\mathcal{E}_2^D(g,\chi) \simeq -0.614 - \frac{(g-\chi)^2}{4} + \dots\ , \quad (12.37)$$

$$\mathcal{E}_2^X(g,\chi) \simeq \quad 0.229 + \dots\ , \quad (12.38)$$

where for the case of the exchange term the second-order spin-orbit correction is exactly vanishing. The explicit calculation can be done in a straightforward but tedious way, and details are collected in the Appendices F.3 and F.4.

The above formulas display the expected form of the spin-orbit correction at small coupling g. In principle, they could also be useful in obtaining higher orders corrections in (12.17), which are completely negligible to the order of approximation considered here.

To further confirm the correctness of the previous discussion, we evaluate numerically the second-order contributions. The evaluation of these multi-dimensional integral is complicated in the general case by the presence of singularities in the integration domain. The singularities arise, for generic values of g and χ, from the energy denominators. In fact, the excitation energy is guaranteed to be positive when $\chi = \chi^{(0)}_{min}(g)$, while in the general case the energy denominator can be zero or negative. We only obtain here the simple case $\chi = \chi^{(0)}_{min}(g)$.

The direct and exchange second-order terms are plotted separately as functions of g in Figure 12.2. The sum of the two is plotted in a bigger range of values in

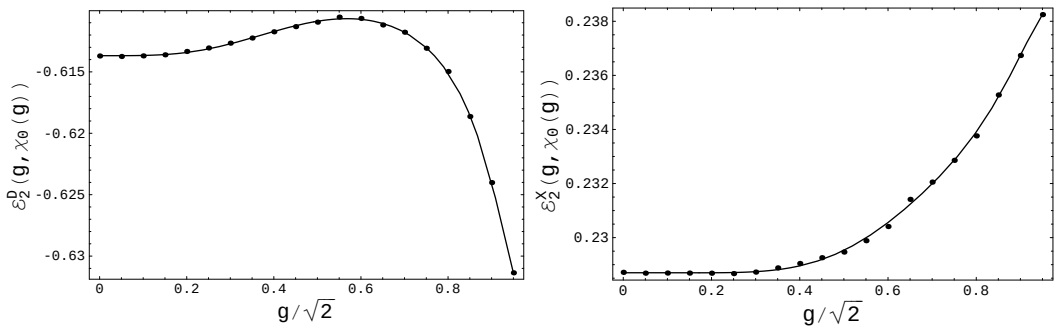

Figure 12.2. Plot of the second-order correlation energy for the noninteracting ground state, as function of g. The generalized chirality is $\chi = \chi^{(0)}_{min}(g)$ and the range of both plots is such that $g < \sqrt{2}$, which gives $\chi < 1$. The left panel shows the direct term $\mathcal{E}^D_2(g, \chi^{(0)}_{min}(g))$ and the right panel the exchange term $\mathcal{E}^X_2(g, \chi^{(0)}_{min}(g))$. The points represent numerical results from Monte-Carlo integrations, and the lines are polynomial fits of the results.

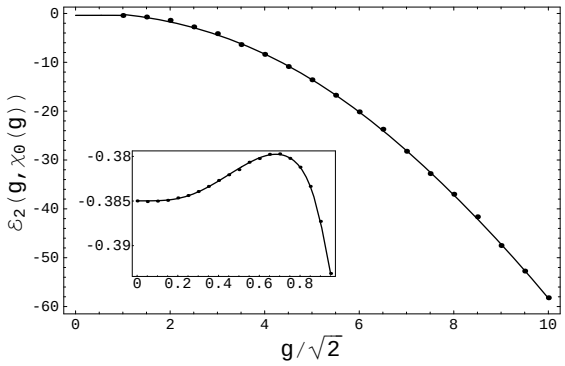

Figure 12.3. Plot of the total second-order correlation energy $\mathcal{E}_2(g, \chi^{(0)}_{min}(g))$ for the noninteracting ground state, as a function of g. The inset shows the region of small g, when $\chi < 1$, and is obtained as the sum of the curves displayed in the previous Figure 12.2. The points represent numerical results from Monte-Carlo integrations, and the lines are polynomial fits of the results.

Figure 12.3. We notice in Figure 12.2 that in the limit $g \to 0$ both functions $\mathcal{E}_2^D$ and $\mathcal{E}_2^X$ display a flat behavior in agreement with the fact that the g^2 contribution is vanishing. The direct term is larger and dominates in the sum of the two, displayed in Figure 12.3. The characteristic behavior, similar to the case of the exchange energy (see Figure 8.2) is probably due to a $g^4 \ln g$ leading term.

It is also noticeable that at large values of g the correlation energy becomes very large, which corresponds to the highly correlated non-perturbative regime of large spin-orbit, already manifested in the Hartree-Fock treatment.

12.5.2 Ring diagrams contribution

The higher order terms in the perturbative treatment of the two-dimensional electron liquid are in general diverging for the case of the bare Coulomb interaction. However, a method to obtain the next leading correction to the correlation energy was devised for the three-dimensional case [57], and consists in summing to infinite order the most diverging diagrams so that the final result is finite. This was applied in the two-dimensional case in Ref. [22] and is extended with minor modifications including the Rashba spin-orbit.

The general expression of the generic ring diagram is ($n > 1$):

$$\mathcal{E}_R^{(n)}(g, r_s, \chi) = -\frac{(-1)^n}{\pi n r_s^2} \int_{-\infty}^{+\infty} \mathrm{d}u \int_0^{\infty} q^2 \mathrm{d}q \left(\frac{Q_q(u) r_s}{2\sqrt{2}\pi q} \right)^n , \tag{12.39}$$

where $Q_q(u)$ is given by the following expression:

$$\sum_{\mu,\sigma} \int \mathrm{d}\mathbf{k}\; n_\mu(k)(1 - n_\sigma(p)) \frac{(\epsilon_\sigma(p) - \epsilon_\mu(k)) |\langle \mathbf{p}\,\sigma | \mathbf{k}\mu \rangle|^2}{(\epsilon_\sigma(p) - \epsilon_\mu(k))^2/4 + u^2 q^2} . \tag{12.40}$$

$\mathcal{E}_R^{(n)}(g, r_s, \chi)$ has a (formal) dependence of r_s^{n-2}. These quantities are diverging, except the $n = 2$ term which is a compact expression for Eq. (12.35). The infinite sum of the diverging ring diagrams gives:

$$\mathcal{E}_R(g, r_s, \chi) = \frac{1}{\pi r_s^2} \int_{-\infty}^{+\infty} \mathrm{d}u \int_0^{\infty} q^2 \mathrm{d}q \left[\ln\left(1 + \frac{Q_q(u) r_s}{2\sqrt{2}\pi q}\right) - \frac{Q_q(u) r_s}{2\sqrt{2}\pi q} + \frac{1}{2}\left(\frac{Q_q(u) r_s}{2\sqrt{2}\pi q}\right)^2 \right] , \tag{12.41}$$

which is a finite quantity.

By patterning the calculation done in the absence of spin-orbit coupling, one can apparently obtain the exact coefficient of the leading contribution in the $r_s \to 0$, which has a $r_s \ln r_s$ dependence. This is determined by the small-q integration region, and therefore what is usually done is to substitute $Q_{q\to 0}(u)$ in (12.41). The value is obtained by neglecting in (12.40) terms involving scattering to the opposite branch, because of the $|\langle \sigma \mathbf{p}|\mu\, \mathbf{k}\rangle|^2$ factor which is ~ 1 for the intra-band and $\sim q^2$ for the inter-band contributions:

$$Q_q(u) \simeq \sum_\mu \int \frac{\mathrm{d}\mathbf{k}}{q}\, \frac{2\, n_\mu(k)(1-n_\mu(p))\,(k-\frac{\mu g}{2})\cos\phi_{\mathbf{k}}}{(k-\frac{\mu g}{2})^2\cos^2\phi_{\mathbf{k}}+u^2}$$
$$= \frac{2\pi k_+}{\tilde{k}_+} R(\frac{u}{\tilde{k}_+}) + \frac{2\pi k_-}{\tilde{k}_-} R(\frac{u}{\tilde{k}_-})\ , \qquad (12.42)$$

where $R(u) = 1 - \frac{1}{\sqrt{1+1/u^2}}$ and we have assumed $\chi < 1$ (as appropriate in the $r_s \to 0$ limit) so that $k_\pm = \sqrt{1 \pm \chi}$. Finally we defined $\tilde{k}_\pm = k_\pm \mp g/2$. Using this result in (12.41) and performing the integration in $\mathrm{d}q$ one extracts the coefficient of the $r_s \ln r_s$ contribution:

$$\mathcal{E}_R(g, r_s, \chi) \simeq -\frac{r_s \ln r_s}{3\sqrt{2}(2\pi)^4} \int_{-\infty}^{+\infty} [Q_0(u)]^3\, \mathrm{d}u\ , \qquad (12.43)$$

which gives the standard result $-\frac{2\sqrt{2}}{3\pi}(10-3\pi) r_s \ln r_s$ with $Q_0(u) = 4\pi R(u)$. Using $Q_0(u)$ as in Eq. (12.42), the result can still be obtained analytically in terms of the function

$$F(x,y) = \int_{-\infty}^{+\infty} [R(u/x)]^2 R(u/y)\, \mathrm{d}u\ , \qquad (12.44)$$

which has the explicit expression:

$$F(x,y) = 4(x+y) - \pi x - 4xE(1-\frac{y^2}{x^2}) + \frac{2x^2 \arccos\frac{y}{x}}{\sqrt{x^2-y^2}}\ . \qquad (12.45)$$

Here $E(x)$ is the complete elliptic integral of the second type [51], and one should use the identity $\frac{\arccos\frac{y}{x}}{\sqrt{x^2-y^2}} = \frac{\mathrm{arccosh}\frac{y}{x}}{\sqrt{y^2-x^2}}$ for $y > x$.

The final result reads:

$$\mathcal{E}_R(g, r_s, \chi) \simeq -\frac{r_s \ln r_s}{6\sqrt{2}\pi} \left[(10-3\pi) \left(\frac{k_+^3}{\tilde{k}_+^2} + \frac{k_-^3}{\tilde{k}_-^2} \right) \right. \qquad (12.46)$$

$$+\frac{3k_+k_-^2}{\tilde{k}_+\tilde{k}_-^2}F(\tilde{k}_+,\tilde{k}_-)+\frac{3k_-k_+^2}{\tilde{k}_-\tilde{k}_+^2}F(\tilde{k}_-,\tilde{k}_+)\Bigg] \ ,$$

which does not have the expected form. In fact, for small values of g and χ we have:

$$\delta\mathcal{E}_R(g,r_s,\chi)\simeq-\frac{r_s\ln r_s}{6\sqrt{2}\pi}\Big[(\frac{208}{5}-\frac{51\pi}{4})\,g^2+\frac{27}{10}(-16+5\pi)\,g\,\chi+(-\frac{42}{5}+\frac{9\pi}{4})\,\chi^2\Big] \ , \tag{12.47}$$

which is not $\propto(\chi-g)^2$.

This apparent contradiction to our general result can be understood in the following terms. The $q\to 0$ limit of $Q_q(u)$ obtained in (12.42) violates the general condition to have a correction $\propto(\chi-g)^2$, and therefore leads to a corresponding violation in the final result. However, one notices that this value is a good approximation to $Q_q(u)$ only for $q\ll g$. Therefore, the above calculation is valid if g is kept constant when r_s becomes small, which corresponds to a diverging spin-orbit coupling $\bar{\alpha}$.

In the more canonical limit of $\bar{\alpha}$ kept constant, the contribution to the integration of the region $q\ll g$ (which shrinks to zero with $g=\sqrt{2}\bar{\alpha}r_s$) is negligible compared to the $r_s\log r_s$ leading term. Outside this interval of q the correction to the function $Q_q(u)$ satisfies the $\propto(\chi-g)^2$ condition, and therefore also the final result for the coefficient of the $r_s\log r_s$ term has the expected form.

Although the final result is reassuring, the previous discussion shows the delicate questions that could arise from possible nonanalytic behavior of the spin-orbit expansion of the energy. In particular, in our formal derivation in Section 12.4.1 we performed the derivatives in χ and g at a generic density r_s, which strictly speaking corresponds to the limit $g\to 0$ *before* $r_s\to 0$. One can hope that, as it happens for the ring-diagram sum, the same expansion (12.15) holds when $r_s\to 0$ at constant $\bar{\alpha}$, which implies in this case $g\to 0$ at the same time. Instead, in the other limit of $g\to 0$ *after* $r_s\to 0$ we showed that the same form of the expansion is not valid in general.

We finally notice that this problem of the order of the limits do not arise for the second-order correlation energy, which has no dependence on r_s. Therefore, these correlation contributions that we explicitly examined in detail do not introduce any

modifications to the Hartree-Fock result and Eqs. (12.16) and (12.17) are valid expressions for the high density limit.

13. High density limit for polarized electrons

We consider in this last Chapter the high-density expansion of the correlation energy for the two-dimensional electron liquid in the absence of spin-orbit. This problem was studied in the classic Ref. [22]. The final expression for the paramagnetic case (in Rydbergs) reads:

$$\mathcal{E}_c(r_s, p=0) = -0.385 - \frac{2\sqrt{2}}{3\pi}(10-3\pi)\, r_s \ln r_s + \dots \ , \tag{13.1}$$

for the case of a paramagnetic system. We will consider the effects of a finite polarization as parameterized by $p = \frac{2S_z}{\hbar n}$, where S_z is the uniform spin polarization density. For generic values of the polarization, the coefficients of the expansion (13.1) become functions of p and the $p = 1$ result can be obtained by making use of a simple transformation [22].

The constant term in (13.1) is obtained from second-order perturbation theory and is the sum of two distinct contributions. The first is the second-order exchange energy, which is independent of p and can be calculated analytically [58]. The second one stems from the second-order direct energy term, commonly referred to as the first ring diagram. The latter has been recently evaluated numerically for generic values of p in Ref. [59]. These contributions are accurately represented by the interpolation formula of Ref. [23].

As discussed in the previous Chapter, the next perturbative term is obtained as an infinite sum of ring diagrams, which results in the sub-leading $r_s \ln r_s$ term. This elegant method was originally developed for the corresponding unpolarized three dimensional case [57], a problem in which the ring diagrams sum up to give the leading $\ln r_s$ contribution to the correlation energy[1]. For the three dimensional case the exact polarization dependence was also determined [60] .

[1]At variance with the two dimensional case, in three dimension all the individual ring diagrams correspond to divergent contributions.

13.1 Ring diagrams contribution

We obtain here the generic dependence of the $r_s \ln r_s$ term on p. This is simply obtained from the calculation described in the previous Chapter. In the absence of spin-orbit coupling, the same procedure of Section 12.5.2 is repeated with the following modifications: the spinor functions of the individual eigenstates are quantized along a common direction, and therefore $|\mathbf{k}\pm\rangle$ are substituted by $|\uparrow\rangle$,$|\downarrow\rangle$ where we identify $\pm$ with $\uparrow,\downarrow$. Furthermore, we set $g = 0$ and substitute $\chi \to p$.

As a result, we have that the explicit expression for $Q_q(u)$ is given by:

$$Q_q(u) = \sum_{\sigma=\uparrow,\downarrow} \int \frac{\mathrm{d}\mathbf{k}}{q} \frac{q + 2k_x}{(\frac{q}{2} + k_x)^2 + u^2} n_\sigma(k)(1 - n_\sigma(k')) \ , \tag{13.2}$$

where $k' = \sqrt{(k_x + q)^2 + k_y^2}$. The polarization dependence of $Q_q(u)$ is implicitly determined by the occupation functions $n_\sigma(k) = \theta(k_\sigma - k)$, where the rescaled Fermi wavevectors are:

$$k_{\uparrow(\downarrow)} \ = \ \sqrt{1 \pm p} \ , \tag{13.3}$$

This form of $Q_q(u)$ has to be used to obtain the ring-diagrams contribution to the correlation energy $\mathcal{E}_R(p)$, which is expressed in the same form of Eq. (12.41).

The $q = 0$ value is immediately obtained as in (12.42) and reads:

$$Q_0(u) = 2\pi[\, R(u/k_\uparrow) + R(u/k_\downarrow)\,] \ , \tag{13.4}$$

where $R(u) = 1 - \frac{1}{\sqrt{1+1/u^2}}$. This result is used to extract the high-density limit of $\mathcal{E}_R(p)$. At high densities Eq. (12.43) can be used for $\mathcal{E}_R(p)$:

$$\mathcal{E}_R(p) \simeq -\frac{r_s \ln r_s}{3\sqrt{2}(2\pi)^4} \int_{-\infty}^{+\infty} [Q_0(u)]^3 \, \mathrm{d}u \ , \tag{13.5}$$

which gives the standard result (13.1) by making use of $Q_0(u) = 4\pi R(u)$, i.e.

$$\mathcal{E}_R(0) \ \simeq \ -\frac{2\sqrt{2}}{3\pi}(10 - 3\pi)\, r_s \ln r_s \ . \tag{13.6}$$

and can be exactly integrated at finite values of p in the same way we obtained Eq. (12.46).

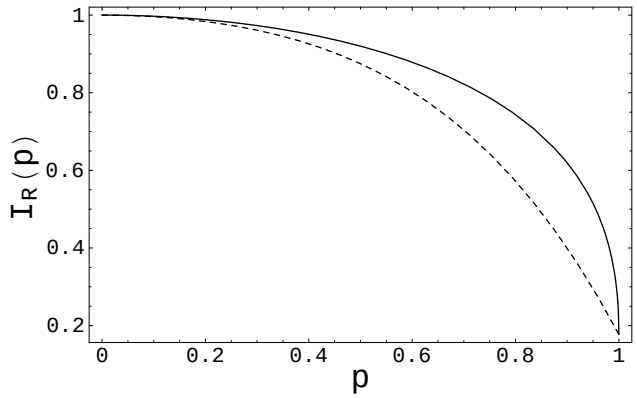

Figure 13.1. Plot of the scaling factor $I_R(p)$ (defined in Eq. (13.7)) as a function of the fractional polarization p. Solid line: exact expression (13.8). Dashed line: Eq. (13.9) as obtained from the interpolation formula proposed in Ref. [23].

The final result can be expressed in terms of a scaling function defined by:

$$I_R(p) \;=\; \lim_{r_s\to 0} \frac{\mathcal{E}_R(p)}{\mathcal{E}_R(0)} \;. \tag{13.7}$$

The explicit expression of $I_R(p)$ is given by:

$$I_R(p) = \frac{1}{8}\left(k_\uparrow + k_\downarrow + 3\,\frac{F(k_\uparrow,k_\downarrow)+F(k_\downarrow,k_\uparrow)}{10-3\pi}\right) \;, \tag{13.8}$$

where $F(x,y)$ is defined in (12.45). This formula readily gives the correct value at $p=0$ using $F(1,1)=10-3\pi$. At $p=1$, using $F(\sqrt{2},0)=F(0,\sqrt{2})=0$, we obtain the known result [22] $I_R(1)=\frac{\sqrt{2}}{8}$.

As it turns out the exact result $I_R(p)$ is not well reflected in the most recent interpolation formulas of Monte-Carlo calculations provided in the literature. In particular, from the correlation energy formula of Ref. [23], denoted here as $\mathcal{E}_c^{MC}(r_s,p)$, the following limit is obtained:

$$\begin{aligned} I_R^{MC}(p) &= \lim_{r_s\to 0} \frac{\mathcal{E}_c^{MC}(r_s,p)-\mathcal{E}_c^{MC}(0,p)}{\mathcal{E}_R(0)} \\ &\simeq\; 1-0.3932\,p^2-0.4297\,p^4 \;, \end{aligned} \tag{13.9}$$

which is compared in Figure 13.1 to the exact result of Eq. (13.8). The difference is remarkable, even if the specific aim of Ref. [23] is to address the polarization

dependence of the whole correlation energy. Agreement of $I_R^{MC}(p)$ with the exact result is only achieved for $p = 0$ and $p = 1$, values known from the extant literature. A noticeable failure is the behavior near $p = 1$, where the polynomial (13.9) gives a finite slope while the leading term in the exact expression is:

$$I_R(p) \simeq \frac{\sqrt{2}}{8} + \frac{14 - 3\pi}{4(10 - 3\pi)} \sqrt{1 - p} \; . \tag{13.10}$$

Around $p = 0$, while being correctly quadratic in p, Eq. (13.9) displays an incorrect coefficient. The exact coefficient is given by:

$$I_R(p) \simeq 1 - \frac{168 - 45\pi}{160(10 - 3\pi)} \, p^2 \simeq 1 - 0.2893 \, p^2 \; . \tag{13.11}$$

The disagreement between $I_R(p)$ and the Monte Carlo based interpolation $I_R^{MC}(p)$ is hardly surprising for the latter was obtained by sampling the energy at a number of polarization values for each of the values $r_s = 1, 2, 5, 10$, which are clearly outside of the $r_s \ll 1$ perturbative regime[2]. In practice, $I_R(p)$ refers to the sub-leading term in the density expansion, so that it gives only small corrections to the total energy. Nevertheless, incorporating this exact formula would certainly result in an improved empirical expression for the polarization dependence of the correlation energy.

13.2 High-density limit expansion

For ease of reference, we collect here the explicit form of all the leading terms contributing to the perturbative expansion of the total energy of the two dimensional electron liquid at finite polarization. The general formula (in Ry units) reads:

$$\mathcal{E}(r_s, p) = \mathcal{E}_K(r_s, p) + \mathcal{E}_x(r_s, p) + \mathcal{E}_c(r_s, p) \; . \tag{13.12}$$

In this expression $\mathcal{E}_K(r_s, p)$ represents the noninteracting kinetic energy and is given by:

$$\mathcal{E}_K(r_s, p) = \frac{1 + p^2}{r_s^2} \; , \tag{13.13}$$

[2]It should be kept in mind that in practice the perturbative theoretic expression of the energy of the electron liquid based on the ring diagrams does provide a quantitatively accurate description only at very small values of r_s (see also Ref. [1]).

while $\mathcal{E}_x(r_s, p)$ represents the exchange energy:

$$\mathcal{E}_x(r_s, p) = -\frac{8\sqrt{2}}{3\pi} \frac{(1+p)^{3/2} + (1-p)^{3/2}}{2r_s} \ . \tag{13.14}$$

The expansion for the correlation energy takes the form:

$$\mathcal{E}_c(r_s, p) = \mathcal{E}_2(p) - \frac{2\sqrt{2}}{3\pi}(10 - 3\pi)\, I_R(p)\, r_s \ln r_s + \dots \ , \tag{13.15}$$

where the omitted corrections are of order $\mathcal{O}(r_s)$. In this expression $I_R(p)$ is defined by Eqs. (13.8), (12.45) and (13.3). The density independent term is in turn given by:

$$\mathcal{E}_2(p) = \mathcal{E}_2^{(b)} + \mathcal{E}_2^{(r)}(p) \ , \tag{13.16}$$

where [58]:

$$\mathcal{E}_2^{(b)} = 0.2287 \ , \tag{13.17}$$

and [59]:

$$\mathcal{E}_2^{(r)}(p) = -0.6137\, I_2(p) \ , \tag{13.18}$$

where the scaling function $I_2(p)$ is given by:

$$I_2(p) = 1 - \frac{(1+p)\ln(1+p) + (1-p)\ln(1-p)}{4\ln 2} - \frac{\delta f(p)}{2} \ , \tag{13.19}$$

with[3]:

$$\delta f(p) \simeq 0.0636\, p^2 - 0.1024\, p^4 + 0.0389\, p^6 \ . \tag{13.20}$$

[3]It should be noted that as in the original paper, Eq. (13.20) does not account for a small dip near $p = 1$ seemingly uncovered in the numerical work of Ref. [59].

14. Conclusions

We have considered in this Thesis many phenomena relative to the effects of the spin-orbit interaction in two-dimensional electronic systems, which we treated by including a model of generalized spin-orbit coupling that is relevant for many practical situations. This includes the well known linear Rashba spin-orbit for electrons and cubic spin-orbit for holes, produced by an asymmetric confinement potential. We have also shown that for heavy-holes an in-plane magnetic field results in a particular form of quadratic spin-orbit coupling, which we believe is very relevant for the interpretation of recent magnetotransport measurements [20].

The presence of spin-orbit coupling allows to control in some degree the polarization of the system, as exemplified in the presence of lateral potentials constraining the two-dimensional system to a quasi one-dimensional wire. The case of linear Rashba spin-orbit was already extensively examined in the literature for the case of a bulk, in which a finite in-plane polarization is produced if a current is driven through the sample [32–36]. This is linear in the spin-orbit coupling, while no transverse polarization is present and the controversial spin-Hall current was also shown to be vanishing[1] [6]. We obtained that in the opposite regime of a strongly laterally confined system the opposite holds true: the in-plane component of the polarization is strongly suppressed, appearing only as a third-order perturbative effect. The inhomogeneous nonequilibrium polarization is approximately perpendicular to the plane of motion, and has opposite signs in the vicinity of the two boundaries. The crossover between the two opposite regimes was examined. We stress that similar numerical results obtained in the literature [41, 61] on the spin-Hall effect are simply understood in terms of the geometrical structure of the wavefunctions, while the concept of a spin-Hall current has little relevance.

[1]The correct vanishing result contradicts the early report of Ref. [52].

The more interesting example of quasi one-dimensional holes is motivated by recent experimental activity [4]. We have shown that the cubic nature of spin-orbit coupling reflects itself in a peculiar form of the one-dimensional spectrum, in which the two lowest subbands cross at a finite value of the wavevector. This behavior is related to the reflection symmetry in the lateral direction of confinement, and therefore is destroyed in the presence of a lateral asymmetry or a magnetic field along the wire. In a smooth point-contact the adiabatic transmission of the holes is a subtle question at the degeneracy points, which makes it possible to control the polarization of the current at the onset of the conducting regime, by tuning the value of the longitudinal magnetic field. The low-field polarization is in agreement with the surprising experimental result of Ref. [4], and offers a clear qualitative demonstration of the particular nature of the spin-orbit coupling for holes. A switch of the polarization is predicted at relatively high values of the magnetic field.

In the remaining part of this Thesis we have extensively discussed the effects of the electron-electron interactions in the presence of spin-orbit coupling. This represents a formidable problem of great relevance, which is essentially unexplored in the literature. In fact, the classical interacting electron liquid is the subject of decades of theoretical studies [1] and still is unsatisfactory in many respects for the simple case of parabolic dispersion. On the other side, many systems require to account at the same time of band structure effects in the noninteracing hamiltonian, of which the spin-orbit coupling terms are examples.

The simplest theory of the interacting liquid is the Hartree-Fock approximation, which is very limited from the quantitative point of view, but it is known to give a correct qualitative picture in the absence of spin-orbit coupling. In fact, the Hartree-Fock theory exactly includes the effect of the exchange, which is the leading correction to the noninteracting properties in the high density limit. A simple analysis on the basis of the exchange energy leads to interesting results for the high density phase in the presence of spin-orbit. We introduced the concept of generalized polarization, which refers more properly to the occupation of the single-particle states and is distinct from

the spin-polarization of the system. We have shown that the generalized polarization resulting from a finite spin-orbit is in most cases surprisingly quenched by the exchange energy. This conclusion is in qualitative agreement with recent experimental measures [20].

The proper spin susceptibility is enhanced by many-body effects, as in the usual case without spin-orbit coupling. The transition to a ferromagnetic state is also slightly favored by the presence of a finite spin-orbit coupling. Nevertheless, a strong anisotropy is introduced in the system close to the ferromagnetic Bloch transition, between the in-plane and transverse directions. This anisotropy is reflected both in the spin-susceptibility and in the polarization of the ferromagnetic phase. For the case of small linear Rashba spin-orbit the transverse phase is favored at the value of the Bloch transition, and an additional in-plane polarized phase occurs at lower densities. The in-plane phase is always favored for quadratic and cubic spin-orbit.

Beside providing an exactly solvable and intuitively transparent approach in which to include a general form of spin-orbit coupling and the leading contribution of many-body effects, the Hartree-Fock solutions are the foundation of more elaborate treatments. At generic densities, the ground state properties are obtained numerically by improved versions of the Hartree-Fock wave functions, as in particular the Jastrow wave function in variational calculation, or by evolution in imaginary time in the Diffusion Monte-Carlo method [1]. It seems natural that the highly nontrivial nature of the Hartree-Fock polarized wave functions needs to be included from the start in this type of calculations.

Alternately, the correlation can be included with accuracy in the asymptotic limits, of which we treated in detail the high density regime with linear Rashba spin-orbit. Unfortunately, very small effects are obtained in this case, and the system is proved to be indistinguishable from the usual electron liquid, to lowest order in the spin-orbit coupling. As a byproduct of the detailed analysis of the correlation terms, we obtained a new analytical result for the polarization dependence of the ring diagram contribution, in the traditional case of vanishing spin-orbit. Our result is not accu-

rately reflected in the interpolation formulas [23] commonly used in density-functional calculations.

The other two interesting limits are those of very low densities and very large spin-orbit coupling that we did not examine in detail. In the first case the system will form a Wigner crystal, although the properties of the system will be strongly affected by the spin-orbit coupling. We also proved that the limit of very large linear Rashba spin-orbit coupling is highly correlated, even at the largest densities. This is due to the vanishing bandwidth of the single-particle spectrum. The Hartree-Fock wavefunction we obtained is a homogeneous in-plane polarized state, but large correlation corrections might very possibly lead to a non homogeneous phase [21]. The knowledge of the true behavior of the system in these limits might lead insight to the general structure of the phase-diagram at finite values of the density and spin-orbit coupling.

APPENDICES

A. Lateral confinement with cubic spin-orbit

We discuss here more in detail the problem of the lateral confinement for the two-dimensional hamiltonian (5.2). For simplicity we consider hard wall barriers:

$$V_U(W,y) = \begin{cases} 0 & \text{for } |y| \le W/2 \ , \\ U & \text{for } |y| > W/2 \ , \end{cases} \tag{A.1}$$

and we will take eventually $U \to \infty$, in which case an appropriate basis in the interval $[-W/2, W/2]$ is $\varphi_n(y) = \sqrt{\frac{2}{W}} \sin \frac{n\pi(y+W/2)}{W}$, where n is a positive integer.

We first note that using for example the procedure discussed in Chapter 4, it is possible to find eigenstates of (5.2) which also satisfy the zero boundary condition in $y = \pm W/2$. These are obtained by linear combination of the four plane waves which are eigenstates of (5.2) with the same energy ϵ and longitudinal wavevector k_x.

However, these eigenstates are not correct and, in particular, are found to be non-orthogonal. The reason is that solutions found in this way completely disregard the behavior of the wavefunctions inside the barriers. In particular, calculating the matrix elements of the $\hat{p}_y^3$ operator in the usual way (i.e. assuming that $\varphi_n(y)$ is exactly zero in the barriers), one obtains:

$$\langle \varphi_n(y) | \hat{p}_y^3 \, \varphi_m(y) \rangle = i \left(\frac{\hbar}{W} \right)^3 \frac{2nm^3\pi^2}{n^2 - m^2} ((-1)^{n+m} - 1) \ , \tag{A.2}$$

which are not matrix elements of an hermitian operator. In fact, the eigenstates determined by making use of (A.2) are not orthogonal.

A more careful definition of the basis wavefunctions is:

$$\psi_n(y) = \begin{cases} \varphi_n(y) & \text{for } |y| \le W/2 \ , \\ \frac{n\pi}{u} \sqrt{\frac{2}{W^3}} \, e^{u\,(y+W/2)} & \text{for } y < -W/2 \ , \\ (-1)^{n+1} \frac{n\pi}{u} \sqrt{\frac{2}{W^3}} \, e^{-u\,(y-W/2)} & \text{for } y > W/2 \ , \end{cases} \tag{A.3}$$

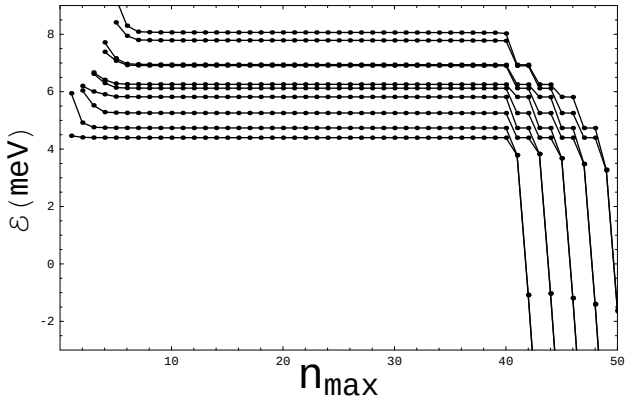

Figure A.1. Lowest 10 eigenstates of $\hat{H}_{0,3} + V_\infty(W, \hat{y})$ (given by (5.2) and (A.1)), as a function of the size $2n_{max}$ (including spin) of the truncated basis. This is chosen to be $e^{ik_x x}\psi_n(y)|\pm\rangle$ where $\psi_n(y)$ is discussed in (A.3) and $n \leq n_{max}$. The parameters used are $m = 0.3m_0$, $\gamma\hbar^3 = 100$ meV nm^3, $W = 100$ nm and $k_x = 0.2$ nm^{-1}. The condition (A.5) gives $n_{max} \ll 40$, at which value the eigenenergies start to diverge.

where $u = \sqrt{\frac{2mU}{\hbar^2}}$ is assumed to be (infinitely) large. Using this definition one obtains:

$$\begin{aligned} &\langle\psi_n(y)|\hat{p}_y^3\,\psi_m(y)\rangle \\ &= i\left(\frac{\hbar}{W}\right)^3 \frac{nm(n^2+m^2)\pi^2}{n^2-m^2}((-1)^{n+m}-1)\ . \end{aligned} \tag{A.4}$$

This is the correct hermitian form of the matrix elements but leads to a spectrum which is unbounded, as it shown in Figure A.1. Therefore, it has to be regularized, for example by introducing a momentum cutoff. In the specific case one can restrict the basis $\psi_n(y)$ to values of n that for a particular value of k_x satisfy:

$$\sqrt{\frac{n^2\pi^2}{W^2} + k_x^2} \ll \frac{1}{2m\gamma\hbar}\ , \tag{A.5}$$

where the large wavevector on the right side is such that the spin-orbit energy $\gamma\hbar^3k^3$ equals the kinetic energy. Otherwise, the spectrum is rather independent of the specific value of the cutoff, as exemplified in Figure A.1. Analogous problems are well known to occur in envelope-function multiband calculations based on perturbative hamiltonians [3, 62] (e.g. the Kane model).

B. Proof of Eq. (8.3)

Consider in (7.3) the only contribution of the exchange energy that depends on $\gamma_{\mathbf{k}}$. It has the following form:

$$-\frac{1}{4L^2}\sum_{\mathbf{k},\mathbf{k}',\mu,\mu'} v_{\mathbf{k}-\mathbf{k}'}\,\mu\mu'\,n_{\mathbf{k}\,\mu}n_{\mathbf{k}'\mu'}\cos\left(\gamma_{\mathbf{k}}-\gamma_{\mathbf{k}'}\right)\sin\beta_{\mathbf{k}}\sin\beta_{\mathbf{k}'}\ . \tag{B.1}$$

This can be rewritten in dimensionless form and by using the circular symmetry:

$$-\int_{\sqrt{|1-\chi|}}^{\sqrt{1+\chi}} y\,\mathrm{d}y\int_{\sqrt{|1-\chi|}}^{\sqrt{1+\chi}} y'\,\mathrm{d}y'\int_0^{2\pi}\frac{\sin\bar{\beta}(y')\sin\bar{\beta}(y)\cos\theta}{\sqrt{y'^2+y^2-2y'y\cos\theta}}\cos(\delta\bar{\gamma}(y)-\delta\bar{\gamma}(y'))\,\mathrm{d}\theta\ . \tag{B.2}$$

The integration in $\mathrm{d}\theta$ can be performed exactly and leads to a positive function of y and y'. We also have $\sin\bar{\beta}\geq 0$ (since $\bar{\beta}\in[0,\pi]$) and we conclude that $\delta\bar{\gamma}(y)=\delta\bar{\gamma}(y')$ for the exchange energy to be minimized. The angle $\delta\bar{\gamma}(y)$ is therefore a constant. Requiring that the Rashba contribution is minimum, we arrive at the desired conclusion:

$$\delta\bar{\gamma}(y)=\frac{\pi}{2}\ . \tag{B.3}$$

C. Existence of isotropic polarized HF solutions

We consider here polarized solutions of Eq. (8.4). For definiteness we assume $\cos\bar{\beta}(\kappa) > 0$. In fact, it is easy to understand that $\cos\bar{\beta}(\kappa)$ does not change sign, to minimize the energy. Eq. (8.4) can be rewritten:

$$\int_{\sqrt{|1-\chi|}}^{\sqrt{|1+\chi|}} \kappa'\,\mathrm{d}\kappa' \int_0^{2\pi} \frac{\sin\bar{\beta}(\kappa)\cos\bar{\beta}(\kappa') - \sin\bar{\beta}(\kappa')\cos\bar{\beta}(\kappa)\cos\theta}{\sqrt{\kappa'^2+\kappa^2-2\kappa\kappa'\cos\theta}}\,\mathrm{d}\theta = 4\pi\bar{\alpha}\,\kappa\cos\bar{\beta}(\kappa) \tag{C.1}$$

After applying $\int \kappa \mathrm{d}\kappa$ to both sides and changing variables of integration $\kappa \leftrightarrow \kappa'$ in the $\sin\bar{\beta}(\kappa)\cos\bar{\beta}(\kappa')$ term we obtain an equation of the form:

$$\int_{\sqrt{|1-\chi|}}^{\sqrt{|1+\chi|}} F_\chi(\kappa)\cos\bar{\beta}(\kappa)\,\mathrm{d}\kappa = 4\pi\bar{\alpha}\int_{\sqrt{|1-\chi|}}^{\sqrt{|1+\chi|}} \kappa^2\cos\bar{\beta}(\kappa)\,\mathrm{d}\kappa \tag{C.2}$$

where $F_\chi(\kappa) = \kappa\int_{\sqrt{|1-\chi|}}^{\sqrt{|1+\chi|}} \kappa'\,\mathrm{d}\kappa' \int_0^{2\pi} \frac{\sin\bar{\beta}(\kappa')(1-\cos\theta)}{\sqrt{\kappa'^2+\kappa^2-2\kappa\kappa'\cos\theta}}\,\mathrm{d}\theta$ is finite function of κ (smaller than the value obtained setting $\sin\bar{\beta}=1$).

Eq. (C.2) can be only satisfied below a certain critical $\bar{\alpha}_c$ (at fixed χ) because for large $\bar{\alpha}_c$ the left integrand is much smaller than the right one in the whole integration region. However, this argument for $\bar{\alpha}_c$ fails if $\chi = 1$ because the right integrand vanishes quadratically in $\kappa = 0$.

To explicitly compute the boundary of the allowed region plotted in Figure 8.7 it is convenient to write the solution in close proximity of the boundary in the form $\bar{\beta}(\kappa) = \frac{\pi}{2} - \delta\bar{\beta}(\kappa)$, where $\delta\bar{\beta}(\kappa)$ is a very small angle. First order expansion of (8.4) leads to the following integral equation:

$$\int_{\sqrt{|1-\chi|}}^{\sqrt{1+\chi}} \kappa'\,\mathrm{d}\kappa' \int_0^{2\pi} \frac{\delta\bar{\beta}(\kappa') - \delta\bar{\beta}(\kappa)\cos\theta}{\sqrt{\kappa^2+\kappa'^2-2\kappa\kappa'\cos\theta}}\,\mathrm{d}\theta = 4\pi\bar{\alpha}\,\kappa\,\delta\bar{\beta}(\kappa)\ , \tag{C.3}$$

which is linear and of the Fredholm type [55,56], the kernel having a weak singularity at $\kappa = \kappa'$. In particular, the (C.3) can be reduced to a linear system and the values of $\bar{\alpha}$ and χ for which the determinant is vanishing correspond to the boundary of the allowed region.

D. Particle current at finite magnetic field

We discuss in this Appendix the rather technical point of the particle current present in the paramagnetic ground state, when perturbed by a magnetic field. We restrict ourselves to the case of linear response examined in Chapter 9. Because of the spin-orbit interaction, the particle velocities $\hat{v}_x$ and $\hat{v}_y$ have a contribution from the spin polarization. For example:

$$\hat{v}_x = \frac{\partial \hat{H}_0}{\partial \hat{p}_x} = \frac{\hat{p}_x}{m} - \alpha \hat{\sigma}_y \ . \tag{D.1}$$

In the isothermal case the particle current in the ground state has to be vanishing. In fact, if this is not the case, a state with lower energy is obtained after a galileian transformation. This property can be immediately verified to hold in the transverse case, where the occupation numbers retain the circular symmetry, and the polarization is out of the plane. Therefore we have $\langle \sum_i \frac{\hat{p}_{x,i}}{m} \rangle = \langle \sum_i \alpha \hat{\sigma}_{y,i} \rangle = 0$, and the average velocity is also vanishing.

The in plane case is more complicated. Here, in view of the fact that the average position of the occupied region in momentum space is displaced off the origin we have $\langle \sum_i \frac{\hat{p}_{x,i}}{m} \rangle \neq 0$. However the ground state has a net in plane polarization, and since $\langle \sum_i \frac{\hat{p}_{x,i}}{m} \rangle = \langle \sum_i \alpha \hat{\sigma}_{y,i} \rangle$ the two contributions to the velocity cancel each other. In particular, the following relation (D.2) corresponding to vanishing particle current can be derived starting from the HF equations (9.19) and (9.21):

$$\bar{\alpha} \int_{\kappa_-}^{\kappa_+} \delta\bar{\gamma}(\kappa)\, \kappa \, \mathrm{d}\kappa - \frac{\sqrt{2}}{r_s}(\kappa_+^2 a_+^2 + \kappa_-^2 a_-^2) + \bar{\alpha}\,(\kappa_+ a_+ - \kappa_- a_-) = 0 \ . \tag{D.2}$$

We rewrite (9.19) as follows:

$$2\bar{\alpha}\,\kappa\,\delta\bar{\gamma}(\kappa) = \int_{\kappa_-}^{\kappa_+} \kappa' \mathrm{d}\kappa' \int_0^{2\pi} \frac{\delta\bar{\gamma}(\kappa')\cos^2\theta - \delta\bar{\gamma}(\kappa)\cos\theta}{\sqrt{\kappa^2 + \kappa'^2 - 2\kappa\kappa'\cos\theta}} \, \frac{\mathrm{d}\theta}{2\pi} - \tilde{B} \ . \tag{D.3}$$

After integration $\int_{\kappa_-}^{\kappa_+} \mathrm{d}\kappa$ of both sides and a change of variables we get:

$$2\bar{\alpha} \int_{\kappa_-}^{\kappa_+} \kappa\, \delta\bar{\gamma}(\kappa)\mathrm{d}\kappa \; = \tag{D.4}$$

$$-\int_{\kappa_-}^{\kappa_+} \tilde{B}\, \mathrm{d}\kappa - \int_{\kappa_-}^{\kappa_+} \mathrm{d}\kappa' \int_{\kappa_-}^{\kappa_+} \mathrm{d}\kappa \int_0^{2\pi} \delta\bar{\gamma}(\kappa') \cos\theta \frac{\partial}{\partial\kappa} \sqrt{\kappa^2 + \kappa'^2 - 2\kappa\kappa' \cos\theta}\, \frac{\mathrm{d}\theta}{2\pi} \; .$$

At this point, the right hand side can be transformed as follows:

$$-\int_{\kappa_-}^{\kappa_+} \tilde{B}\, \mathrm{d}\kappa + \int_{\kappa_-}^{\kappa_+} \mathrm{d}\kappa' \int_{\kappa_-}^{\kappa_+} \mathrm{d}\kappa \int_0^{2\pi} \frac{\partial}{\partial\kappa} \frac{\kappa\kappa'\, \delta\bar{\gamma}(\kappa') \sin^2\theta}{\sqrt{\kappa^2 + \kappa'^2 - 2\kappa\kappa' \cos\theta}}\, \frac{\mathrm{d}\theta}{2\pi} \tag{D.5}$$

$$= \kappa_- c_- - \kappa_+ c_+ + a_+\kappa_+ \int_{\kappa_-}^{\kappa_+} \mathrm{d}\kappa \int_0^{2\pi} \frac{\sin^2\theta}{\sqrt{\kappa^2 + \kappa_+^2 - 2\kappa\kappa_+ \cos\theta}}\, \frac{\mathrm{d}\theta}{2\pi} \tag{D.6}$$

$$-a_-\kappa_- \int_{\kappa_-}^{\kappa_+} \mathrm{d}\kappa \int_0^{2\pi} \frac{\sin^2\theta}{\sqrt{\kappa^2 + \kappa_-^2 - 2\kappa\kappa_- \cos\theta}}\, \frac{\mathrm{d}\theta}{2\pi} \; ,$$

where in (D.5) we have integrated by parts with respect to $\mathrm{d}\theta$ and in (D.6) we used the previous definitions (9.20) and (9.24) of $\tilde{B}$ and $c_\pm$. We can now substitute (9.21) and after straightforward manipulations we get to:

$$\bar{\alpha} \int_{\kappa_-}^{\kappa_+} \delta\bar{\gamma}(\kappa)\, \kappa\, \mathrm{d}\kappa - \frac{\sqrt{2}}{r_s}(\kappa_+^2 a_+^2 + \kappa_-^2 a_-^2) + \bar{\alpha}\, (\kappa_+ a_+ - \kappa_- a_-) = \sum_{\mu=\pm} \frac{a_\mu}{2} \kappa_\mu I(\kappa_\mu, \kappa_{-\mu}) \; ,$$

where:

$$I(\kappa_+, \kappa_-) = \frac{1}{3\pi} - \frac{2K}{\pi} + \int_0^{\kappa_-/\kappa_+} \kappa\, \mathrm{d}\kappa \int_0^{2\pi} \frac{(1-\cos\theta)(1-\kappa\cos\theta)}{(1+\kappa^2 - 2\kappa\cos\theta)^{3/2}}\, \frac{\mathrm{d}\theta}{2\pi} \tag{D.7}$$

$$-\kappa_- \int_0^{2\pi} \frac{(1-\cos\theta)\cos\theta}{\sqrt{\kappa_-^2 + \kappa_+^2 - 2\kappa_-\kappa_+ \cos\theta}} \frac{\mathrm{d}\theta}{2\pi} + \int_{\kappa_-}^{\kappa_+} \mathrm{d}\kappa \int_0^{2\pi} \frac{\sin^2\theta}{\sqrt{\kappa^2 + \kappa_+^2 - 2\kappa\kappa_+ \cos\theta}}\, \frac{\mathrm{d}\theta}{2\pi} \; .$$

Finally, it can be shown that this apparently complicated expression for $I(\kappa_-, \kappa_+)$ is exactly zero, for arbitrary values of κ_+ and κ_-. This proves relation (D.2) corresponding to a vanishing current.

We now consider the in plane adiabatic case. Here there is no repopulation and the polarization is different from zero. A finite current is present in the ground state. However, since the magnetic field is oscillating, although with almost vanishing frequency $\omega = 0^+$, the average current is still zero. Since the repopulation contribution is zero, it is immediate to obtain from (D.1) that the charge current density is:

$$\langle \hat{J}_x \rangle = \alpha \frac{e\langle \hat{S}_y \rangle}{L^2} = -\alpha \frac{2e}{g\mu_B} \tilde{\chi}_S^{\parallel} B \; ,$$

which is in complete agreement with (9.10).

E. Continuous limit for numerical in-plane polarized solutions

The in-plane polarized solutions of Chapter 10 are obtained by discretization on a finite grid. If the side of the grid is divided in N intervals, the exchange energy involves N^4 terms which makes the self consistent iterations cumbersome when increasing grid size. However, we find that the numerical error scales as $\sim 1/N$ and extrapolation of the energies gives very acceptable results at moderate grid size. We give in Figure E.1 an example of the procedure. When the state converges to a paramagnetic solution, the energies can be obtained with a simple quadrature, and the reliability of the method can be tested. An example of the phase transition between the out-of-plane and the in plane polarized state is displayed in the second panel of Figure E.1.

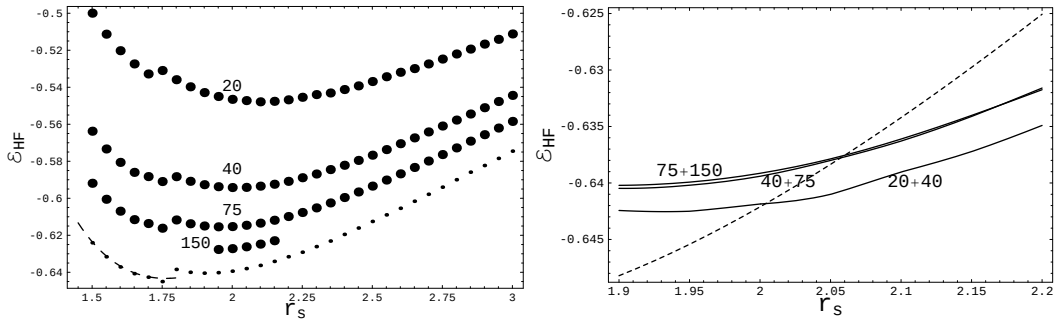

Figure E.1. Left: results for the total energy of the in plane polarized state at $\bar{\alpha} = 0.4$. The large dots refer to results obtained with different grid lattice constants $4/N$ (N indicated in the Figure) while the small dots are the extrapolated results. At small r_s the convergence is to a paramagnetic solution (dashed line). Right: transition point between the two types of polarized states. The solid lines are the energy of the in-plane polarized state, as obtained by extrapolation from pairs of grid results of the previous panel. The dashed line is the out-of-plane polarized state energy.

F. Details of derivations for Chapter 12

We present here for the convenience of the reader a more detailed derivation of some of the results discussed in Chapter 12.

The following useful formulas are easily obtained for the derivatives of the occupation functions (at $\chi = 0$):

$$\left.\frac{\partial n_\mu(k)}{\partial \chi}\right|_0 = \frac{\mu}{2}\,\delta(1-k)\ , \tag{F.1}$$

$$\left.\frac{\partial^2 n_\mu(k)}{\partial \chi^2}\right|_0 = \frac{\delta'(1-k)-\delta(1-k)}{4}\ , \tag{F.2}$$

for the derivatives of the Green functions (at $g = \chi = 0$):

$$\left.\frac{\partial G_{0\mu}(p,\omega)}{\partial \chi}\right|_0 = \mu\, i\delta(\omega-p^2)\,\delta(1-p)\ , \tag{F.3}$$

$$\left.\frac{\partial G_{0\mu}(p,\omega)}{\partial g}\right|_0 = -\mu\,[G_0(p,\omega)]^2\,p\ , \tag{F.4}$$

$$\left.\frac{\partial^2 G_{0\mu}(p,\omega)}{\partial \chi^2}\right|_0 = i\delta(\omega-p^2)\,\frac{\delta'(1-p)-\delta(1-p)}{2}\ , \tag{F.5}$$

$$\left.\frac{\partial^2 G_{0\mu}(p,\omega)}{\partial g\partial \chi}\right|_0 = p\,\delta'(\omega-p^2)\,i\delta(1-p)\ , \tag{F.6}$$

$$\left.\frac{\partial^2 G_{0\mu}(p,\omega)}{\partial g^2}\right|_0 = 2[G_0(p,\omega)]^3\,p^2\ , \tag{F.7}$$

for the derivatives of the 'resolved' Green functions (at $\mathbf{p}^g = \mathbf{p}^\chi = \mathbf{p}$), where we use $\mathbf{p}^a = \mathbf{k}_a + \mathbf{q}$ (a can be equal to χ or g):

$$\left.\frac{\vec{\nabla}_{\mathbf{k}_a}}{2}\,\tilde{G}_0(p^\chi,p^g,\omega)\right|_0 = -\left.\frac{\partial G_{0\mu}(p,\omega)}{\partial a}\right|_0\,\frac{\mu\mathbf{p}}{p}\ , \tag{F.8}$$

$$\left.\frac{\vec{\nabla}^2_{\mathbf{k}_\chi}}{4}\,\tilde{G}_0(p^\chi,p^g,\omega)\right|_0 = \left.\frac{\partial^2 G_{0\mu}(p,\omega)}{\partial \chi^2}\right|_0\ , \tag{F.9}$$

$$\left.\frac{\vec{\nabla}_{\mathbf{k}_\chi}\cdot\vec{\nabla}_{\mathbf{k}_g}}{4}\,\tilde{G}_0(p^\chi,p^g,\omega)\right|_0 = \left.\frac{\partial^2 G_{0\mu}(p,\omega)}{\partial \chi\,\partial g}\right|_0\ , \tag{F.10}$$

$$\left.\frac{\vec{\nabla}^2_{\mathbf{k}_g}}{4}\,\tilde{G}_0(p^\chi,p^g,\omega)\right|_0 = \left.\frac{\partial^2 G_{0\mu}(p,\omega)}{\partial g^2}\right|_0 + [G_0(p,\omega)]^2\ , \tag{F.11}$$

and for the spin sums (where $N+1 \equiv 1$ and $\mu_j, \mu_k \in \{\mu_i\}$):

$$\sum_{\{\mu_i\}} \prod_{i=1}^{N} \langle \mathbf{p}_i \mu_i | \mathbf{p}_{i+1} \mu_{i+1} \rangle \quad = 2 \ , \tag{F.12}$$

$$\sum_{\{\mu_i\}} \mu_j \mu_k \prod_{i=1}^{N} \langle \mathbf{p}_i \mu_i | \mathbf{p}_{i+1} \mu_{i+1} \rangle = 2 \frac{\mathbf{p}_j \cdot \mathbf{p}_k}{p_j p_k} \ . \tag{F.13}$$

If an odd number of indexes μ_j is present the sum vanishes (see Eq. (12.28)).

F.1 Derivatives of the energy diagrams

We consider first the case of $\left.\frac{\partial^2 D}{\partial \chi^2}\right|_0$. The comparison to $D_{\chi\chi}$ is easily done, by inspection of the explicit expressions (12.21) and (12.23). In fact, we have terms containing double derivatives of the Green functions, which are equivalent because of (F.5) and (F.9). An appropriate factor of 2 in $\left.\frac{\partial^2 D}{\partial \chi^2}\right|_0$ is obtained from the spin sum (F.12). The terms involving products of the first derivatives of two Green functions are also seen to be equivalent, using (F.3) and (F.8). The factors $\frac{\mathbf{p}_j \cdot \mathbf{p}_k}{p_j p_k}$ obtained in this type of terms appear in $\left.\frac{\partial^2 D}{\partial \chi^2}\right|_0$ because of the spin sum (F.13) and in (12.23) because of the form of (F.8).

The equivalence of $\left.\frac{\partial^2 D}{\partial \chi \partial g}\right|_0$ and $D_{\chi g}$ is also immediately seen, in the same way we discussed above. The only complication appears for $\left.\frac{\partial^2 D}{\partial g^2}\right|_0$ because of an additional term D_{gg} of the following form (see Eq. (F.11)):

$$\begin{aligned} \Delta D_{gg} &= \int [\ldots] \int \frac{\mathrm{d}\mathbf{k}}{(2\pi)^2} \, 2 \sum_{j=1}^{N} [G_0(p_j, \omega_j)]^2 \prod_{i \neq j} G_0(p_i, \omega_i) \\ &= - \int [\ldots] \frac{\partial}{\partial \omega} \int \frac{\mathrm{d}\mathbf{k}}{(2\pi)^2} \, 2 \prod_{i=1}^{N} G_0(p_i, \omega + \Omega_i) \ , \end{aligned} \tag{F.14}$$

which is seen to be vanishing upon integration in the loop frequency $\mathrm{d}\omega$.

F.2 Exact property of the self-energy

For this case, we can consider the expression of $\left.\frac{\partial D_\Sigma}{\partial g}\right|_0$, which contains N terms involving the first derivatives of the Green functions explicitly appearing in Eq. (12.27). The spin sum for each term can be performed with the aid of:

$$\sum_{\{\mu_i\}} \mu_j \prod_{i=0}^{N} \langle \mathbf{p}_i \mu_j | \mathbf{p}_{i+1} \mu_{i+1} \rangle = \mu \frac{\mathbf{k}\cdot\mathbf{p}_j}{k\, p_j} \ , \tag{F.15}$$

where $\mathbf{p}_i = \mathbf{k} + \mathbf{q}_i$ while $\mathbf{p}_0 = \mathbf{p}_{N+1} = \mathbf{k}$ and $\mu_0 = \mu_{N+1} = \mu$. The index μ does not participate in the sum while μ_j does ($\mu \notin \{\mu_i\}$ and $\mu_j \in \{\mu_i\}$).

The comparison to $\frac{\partial D_{\Sigma_0}}{\partial k}$ (see Eq. (12.29)) can be immediately done using:

$$\frac{\partial G_0(p_i,\omega_i)}{\partial k} = -2\mu_i \, \frac{\partial G_{0\mu_i}(p_i,\omega_i)}{\partial g} \, \frac{\mathbf{k}\cdot\mathbf{p}_i}{k\, p_i} \ , \tag{F.16}$$

which is obtained from (F.8) (in the assumption that $\chi = g$).

F.3 Derivatives of the second order direct term

We consider here the second derivatives of $\mathcal{E}_2^D(g,\chi)$, as given by Eq. (12.35). We start from $\left.\frac{\partial^2 \mathcal{E}_2^D}{\partial g^2}\right|_0$, which only involves the energy denominator of (12.35). The spin summation is easily evaluated by making use of:

$$\sum_{\mu,\mu',\sigma,\sigma'} |\langle \mathbf{p}\,\sigma | \mathbf{k}\mu\rangle|^2 \, |\langle \mathbf{p}'\,\sigma' | \mathbf{k}'\mu'\rangle|^2 (\sigma p - \mu k + \sigma' p' - \mu' k')^2 = 8q^2 \ . \tag{F.17}$$

which follows from (F.12) and (F.13).

We than evaluate the angular integration in $\mathrm{d}\mathbf{q}$ and integrations in $\mathrm{d}k_y$, $\mathrm{d}k'_y$ to obtain the following expression:

$$\left.\frac{\partial^2 \mathcal{E}_2^D}{\partial g^2}\right|_0 = -\frac{1}{\pi^2} \int_0^\infty \frac{\mathrm{d}q}{q^2} \int_{-1}^{1} \mathrm{d}k_x \mathrm{d}k'_x \, \frac{L(q,k_x) L(q,-k'_x)}{(q + k_x - k'_x)^3} \ , \tag{F.18}$$

We have introduced the geometrical factor $L(q,k_x) = \int n_0(k)(1-n_0(p))\,\mathrm{d}k_y$, which is defined when $-1 \le k_x \le 1$:

$$L(q,k_x) = \begin{cases} 0 & \text{if } q < 2 \text{ and } k_x \le -\frac{q}{2} \ , \\ 2\sqrt{1-{k_x}^2} & \text{if } k_x \ge -q+1 \ , \\ 2\sqrt{1-{k_x}^2} - 2\sqrt{1-(q+k_x)^2} & \text{otherwise} \ , \end{cases} \tag{F.19}$$

The integral in (F.18) can be finally evaluated. The numerical calculation leads a result which is indistinguishable from $-\frac{1}{2}$. We believe that this result is exact, although we could not prove it analytically:

$$\left.\frac{\partial^2 \mathcal{E}_2^D}{\partial g^2}\right|_0 = -\frac{1}{2} \ . \tag{F.20}$$

The remaining derivatives are obtained immediately from the general relation Eq. (12.25). We calculate them here explicitly for completeness.

$\left.\frac{\partial^2 \mathcal{E}_2^D}{\partial g \partial \chi}\right|_0$, involves the first derivatives of the occupation functions given in (F.1). Performing the spin summations with the aid of (F.12,F.13) and after some further simplification, we arrive to the following expression:

$$\begin{aligned}\left.\frac{\partial^2 \mathcal{E}_2^D}{\partial \chi \partial g}\right|_0 = & -\frac{1}{4\pi^3}\int \frac{\mathrm{d}\mathbf{q}}{q^2}\int \mathrm{d}\mathbf{k}\int \mathrm{d}\mathbf{k}'\,\frac{n_0(k')(1-n_0(p'))}{(q^2+\mathbf{q}\cdot(\mathbf{k}-\mathbf{k}'))^2} \\ & \times\left[(\mathbf{k}\cdot\mathbf{q})\,(1-n_0(p))\,\delta(1-k)-(\mathbf{p}\cdot\mathbf{q})\,n_0(k)\,\delta(1-p)\right] \ .\end{aligned} \tag{F.21}$$

Finally, after a change of variable $\mathbf{k}\to-\mathbf{k}-\mathbf{q}=-\mathbf{p}$ in the second term of the integrand, angular integration in $\mathrm{d}\mathbf{q}$ and integrations in $\mathrm{d}k_y$ and $\mathrm{d}k_y'$ we get:

$$\left.\frac{\partial^2 \mathcal{E}_2^D}{\partial \chi \partial g}\right|_0 = -\frac{1}{\pi^2}\int_0^\infty \frac{\mathrm{d}q}{q^2}\int_{-1}^1 \mathrm{d}k_x\mathrm{d}k_x'\,\frac{k_x\,L(q,-k_x')}{\sqrt{1-k_x^2}}\left[\frac{1-n_0(p)}{(q+k_x-k_x')^2}+\frac{n_0(p)}{(k_x+k_x')^2}\right] \ , \tag{F.22}$$

where $p=\sqrt{1+q^2+2qk_x}$. This integral can be actually transformed to the opposite of (F.18), by means of an integration by parts of the two terms of the integrand, and and a suitable change of variable in the second one. Therefore we conclude:

$$\left.\frac{\partial^2 \mathcal{E}_2^D}{\partial \chi \partial g}\right|_0 = \frac{1}{2} \ . \tag{F.23}$$

The last term is $\left.\frac{\partial^2 \mathcal{E}_2^D}{\partial \chi^2}\right|_0$ which only involves derivatives of the occupation functions as given in (F.1) and (F.2). Terms containing double derivatives of the occupation functions can be transformed according to:

$$\int f(\mathbf{k})\frac{\partial^2 n_\mu(k)}{\partial \chi^2}\,\mathrm{d}\mathbf{k} = \frac{1}{4}\int \frac{\partial f(\mathbf{k})}{\partial k}\delta(1-k)\,\mathrm{d}\mathbf{k} \ . \tag{F.24}$$

.

After performing the spin summations explicitly, a change of primed and unprimed variables to collect similar terms, and the usual angular integration in d$\mathbf{q}$ we arrive to:

$$\left.\frac{\partial^2\mathcal{E}_2^D}{\partial\chi^2}\right|_0 = -\frac{1}{2\pi^2}\int_0^\infty \frac{\mathrm{d}q}{q^2}\int \mathrm{d}\mathbf{k}'\, n_0(k')(1-n_0(p'))\int \mathrm{d}\mathbf{k}\,\left[\left(\frac{\partial}{\partial k}\,\frac{1-n_0(p)}{q+k_x-k'_x}\right)\delta(1-k)\right.$$
$$\left. -\left(\frac{\partial}{\partial p}\,\frac{n_0(k)}{q+k_x-k'_x}\right)\delta(1-p)\,-\frac{2\cos(\phi_{\mathbf{k}}-\phi_{\mathbf{p}})}{q+k_x-k'_x}\,\delta(1-k)\delta(1-p)\right]\,, \qquad \text{(F.25)}$$

where in the d$\mathbf{k}$, d$\mathbf{k}'$ integrations, the x axis is chosen to be along $\mathbf{q}$ so that, in particular, $p=\sqrt{k^2+q^2+2qk_x}$. It is also convenient to change variable $\mathbf{k}\to-\mathbf{k}-\mathbf{q}$ in the second term in the square brackets.

The contributions from the first two terms in the square brackets involving the derivative $\frac{\partial n_0(p)}{\partial k}=-\delta(1-p)\frac{\partial p}{\partial k}$ cancel exactly the third term. In fact we have that the coefficient multiplying the product $\delta(1-k)\delta(1-p)$:

$$\frac{\partial p/\partial k}{q+k_x-k'_x}-\frac{\partial p/\partial k}{k_x+k'_x}-\frac{2\cos(\phi_{\mathbf{k}}-\phi_{\mathbf{p}})}{q+k_x-k'_x}\,, \qquad \text{(F.26)}$$

and we can simplify this by using $k_x=\cos\phi_{\mathbf{k}}=-\frac{q}{2}$. Furthermore, $\partial p/\partial k=(k+q\cos\phi_{\mathbf{k}})/p=1-\frac{q^2}{2}$ and $\cos(\phi_{\mathbf{k}}-\phi_{\mathbf{p}})=1-\frac{q^2}{2}$ as well. Therefore, (F.26) is seen to vanish identically. The remaining part of (F.25), after integrations in dk_y, dk'_y, is given exactly by the opposite of expression (F.22). Therefore we conclude:

$$\left.\frac{\partial^2\mathcal{E}_2^D}{\partial g^2}\right|_0 = -\left.\frac{\partial^2\mathcal{E}_2^D}{\partial\chi\partial g}\right|_0 = \left.\frac{\partial^2\mathcal{E}_2^D}{\partial\chi^2}\right|_0 = -\frac{1}{2}\,. \qquad \text{(F.27)}$$

F.4 Derivatives of the second order exchange term

The fact that $\left.\frac{\partial^2\mathcal{E}_2^X}{\partial g^2}\right|_0=0$ is easily obtained using:

$$\sum_{\mu,\mu',\sigma,\sigma'}\langle\mathbf{p}\,\sigma|\mathbf{k}\mu\rangle\,\langle\mathbf{k}\mu|\mathbf{p}'\sigma'\rangle\langle\mathbf{p}'\sigma'|\mathbf{k}'\mu'\rangle\,\langle\mathbf{k}'\mu'|\mathbf{p}\,\sigma\rangle(\sigma p-\mu k+\sigma' p'-\mu' k')^2=0\,, \qquad \text{(F.28)}$$

which follows from (F.12) and (F.13). Because of the general property (12.25), also the other derivatives have to vanish. The mixed derivative $\left.\frac{\partial^2\mathcal{E}_2^X}{\partial g\partial\chi}\right|_0=0$ is easily found to be vanishing upon summation on the spin indexes.

The second derivative $\left.\frac{\partial^2 \mathcal{E}_2^X}{\partial g^2}\right|_0$ is calculated in a similar way of the direct contribution $\left.\frac{\partial^2 \mathcal{E}_2^D}{\partial g^2}\right|_0$. In particular we obtain the following sum of two integrals:

$$\left.\frac{\partial^2 \mathcal{E}_2^X}{\partial \chi^2}\right|_0 = \frac{1}{4\pi^2}\int_0^\infty \frac{\mathrm{d}q}{q}\int \mathrm{d}\mathbf{k}'\, n_0(k')(1-n_0(p')) \tag{F.29}$$
$$\times \int \mathrm{d}\mathbf{k}\, \left[(1-n_0(p))\frac{\partial}{\partial k}\,\frac{1}{|\mathbf{k}-\mathbf{k}'+\mathbf{q}|(q+k_x-k'_x)} + n_0(p)\frac{\partial}{\partial k}\,\frac{1}{|\mathbf{k}+\mathbf{k}'|(k_x+k'_x)}\right]\delta(1-k)$$
$$+\frac{1}{4\pi^2}\int_0^\infty \frac{\mathrm{d}q}{q}\int \mathrm{d}\mathbf{k}'\int \mathrm{d}\mathbf{k}\,\frac{1}{|\mathbf{k}-\mathbf{k}'+\mathbf{q}|(k_x-k'_x+q)}\left[\frac{\mathbf{k}\cdot\mathbf{k}'}{k\,k'}(1-n_0(p))(1-n_0(p')\delta(1-k)\delta(1-k')\right.$$
$$\left.+\frac{\mathbf{p}\cdot\mathbf{p}'}{p\,p'}n_0(k)n_0(k')\delta(1-p)\delta(1-p') - 2\frac{\mathbf{k}\cdot\mathbf{p}'}{k\,p'}n_0(k')(1-n_0(p))\delta(1-k)\delta(1-p')\right] .$$

where in the second one, written over the last two lines, we collected additional terms that are absent in the corresponding calculation of the previous subsection. In fact, these term do not vanish after spin summation, as it happens for the corresponding ores of the direct contribution.

To see that the total result is exactly zero, one can rewrite the derivatives in the second lines using:

$$\frac{\partial f(\mathbf{k}-\mathbf{k}')}{\partial k} = -\frac{\partial f(\mathbf{k}-\mathbf{k}')}{\partial k'_x}\cos\phi_{\mathbf{k}} - \frac{\partial f(\mathbf{k}-\mathbf{k}')}{\partial k'_y}\sin\phi_{\mathbf{k}} \ , \tag{F.30}$$

and perform an integration by parts in $\mathrm{d}\mathbf{k}'$. The derivatives of $n_0(k')(1-n_0(p'))$ produce additional δ functions, and the first integrand is reduced to a form similar to the second one. Then, it is not difficult to prove that the two integrals differ only in the sign, and cancel each other.

Therefore we have:

$$\left.\frac{\partial^2 \mathcal{E}_2^X}{\partial g^2}\right|_0 = \left.\frac{\partial^2 \mathcal{E}_2^X}{\partial \chi \partial g}\right|_0 = \left.\frac{\partial^2 \mathcal{E}_2^X}{\partial \chi^2}\right|_0 = 0 \ . \tag{F.31}$$

LIST OF REFERENCES

LIST OF REFERENCES

[1] G. F. Giuliani and G. Vignale. *Quantum Theory of the Electron Liquid*. Cambridge University Press, Cambridge, 2005.

[2] M. P. Lilly, W. Pan, R.-R. Du, and J. A. Simmons, editors. *Proceedings of the 16th International Conference on Electronic Properties of Two-Dimensional Systems (EP2DS-15)*. Elsevier, Amsterdam, 2006.

[3] R. Winkler. *Spin-Orbit Coupling Effects in Two-Dimensional Electron and Hole Systems*. Springer, Berlin, 2003.

[4] L. P. Rokhinson, V. Larkina, Y. B. Lyanda-Geller, L. N. Pfeiffer, and K. W. West. Spin separation in cyclotron motion. *Phys. Rev. Lett.*, 93:146601, 2004.

[5] H. Chen, J. J.J. Heremans, J. A. Peters, A. O. Govorov, N. Goel, S. J. Chung, and M. B. Santos. Spin-polarized reflection in a two-dimensional electron system. *Appl. Phys. Lett.*, 86:032113, 2005.

[6] H.-A. Engel, E. I. Rashba, and B. I. Halperin. Theory of spin hall effects. *cond-mat/0603306*, 2006.

[7] S. Datta and B. Das. Electronic analog of the electro-optic modulator. *Appl. Phys. Lett.*, 56:665, 1989.

[8] G. A. Prinz. Magnetoelectronics. *Science*, 282:1660, 1998.

[9] S. A. Wolf, D. D. Awschalom, R. A. Buhrman, J. M. Daughton, S. von Molnar, M. L. Roukes, A. Y. Chtchelkanova, and D. M. Treger. Spintronics: A spin-based electronics vision for the future. *Science*, 294:1488, 2001.

[10] I. Žutić, J. Fabian, and S. Das Sarma. Spintronics: Fundamentals and applications. *Rev. Mod. Phys.*, 76:323, 2004.

[11] J. Nitta, T. Akazaki, H. Takayanagi, and T. Enoki. Gate control of spin-orbit interaction in an inverted $In_{0.53}Ga_{0.47}As/In_{0.52}Al_{0.48}As$ heterostructure. *Phys. Rev. Lett.*, 78:1335, 1997.

[12] Th. Schäpers, G. Engels, J. Lange, Th. Klocke, M. Hollfelder, and H. Luth. Effect of the heterointerface on the spin splitting in modulation doped $In_xGa_{1-x}As/InP$ quantum wells for $B \to 0$. *J. Appl. Phys.*, 83:4324, 1998.

[13] G. Dresselhaus. Spin-orbit coupling effects in zinc blende structures. *Phys. Rev.*, 100:580, 1955.

[14] Y. A. Bychkov and E. I. Rashba. Properties of a 2D electron gas with lifted spectral degeneracy. *JETP Lett.*, 39:78, 1984.

[15] Y. A. Bychkov and E. I. Rashba. Oscillatory effects and the magnetic susceptibility of carriers in inversion layers. *J. Phys. C*, 17:6039, 1984.

[16] G.-H. Chen and M. E. Raikh. Exchange-induced enhancement of spin-orbit coupling in two-dimensional electronic systems. *Phys. Rev. B*, 60:4826, 1999.

[17] D. S. Saraga and D. Loss. Fermi liquid parameters in two dimensions with spin-orbit interaction. *Phys. Rev. B*, 72:195319, 2005.

[18] Y.-W. Tan, J. Zhu, H. L. Stormer, L. N. Pfeiffer, K. W. Baldwin, and K. W. West. Measurements of the density-dependent many-body electron mass in two dimensional GaAs/AlGaAs heterostructures. *Phys. Rev. Lett.*, 94:016405, 2005.

[19] R. Asgari, B. Davoudi, M. Polini, G. F. Giuliani, M. P. Tosi, and G. Vignale. Quasiparticle self-energy and many-body effective mass enhancement in a two-dimensional electron liquid. *Phys. Rev. B*, 71:045323, 2005.

[20] R. Winkler, E. Tutuc, S. J. Papadakis, S. Melinte, M. Shayegan, D. Wasserman, and S. A. Lyon. Anomalous spin polarization of GaAs two-dimensional hole systems. *Phys. Rev. B*, 72:195321, 2005.

[21] Spatially inhomogeneous solutions have been investigated in G. Simion and G. F. Giuliani, unpublished.

[22] A. K. Rajagopal and J. C. Kimball. Correlations in a two-dimensional electron system. *Phys. Rev. B*, 15:2819, 1977.

[23] C. Attaccalite, S. Moroni, P. Gori-Giorgi, and G. B. Bachelet. Correlation energy and spin polarization in the 2D electron gas. *Phys. Rev. Lett.*, 88:256601, 2002.

[24] J. M. Luttinger and W. Kohn. Motion of electrons and holes in perturbed periodic fields. *Phys. Rev.*, 97:869, 1955.

[25] J. Luo, H. Munekata, F. F. Fang, and P. J. Stiles. Observation of the zero-field spin splitting of the ground electron subband in GaSb-InAs-GaSb quantum wells. *Phys. Rev. B*, 38:10142, 1988.

[26] B. Das, D. C. Miller, S. Datta, R. Reifenberger, W. P. Hong, P. K. Bhattacharya, J. Singh, and M. Jaffe. Evidence for spin splitting in $In_xGa_{1-x}As/In_{0.52}Al_{0.48}As$ heterostructures as $B \to 0$. *Phys. Rev. B*, 39:1411, 1989.

[27] J. Luo, H. Munekata, F. F. Fang, and P. J. Stiles. Effects of inversion asymmetry on electron energy band structures in GaSb/InAs/GaSb quantum wells. *Phys. Rev. B*, 41:7685, 1990.

[28] B. Das, S. Datta, and R. Reifenberger. Zero-field spin splitting in a two-dimensional electron gas. *Phys. Rev. B*, 41:8278, 1990.

[29] J. M. Luttinger. Quantum theory of cyclotron resonance in semiconductors: General theory. *Phys. Rev.*, 102:1030, 1956.

[30] O. Madelung, editor. *Semiconductors*, volume 17a of Landolt-Börnstein, New Series III. Springer, Berlin, 1982.

[31] B. Habib, E. Tutuc, S. Melinte, M. Shayegan, D. Wasserman, S. A. Lyon, and R. Winkler. Negative differential Rashba effect in two-dimensional hole systems. *Appl. Phys. Lett.*, 85:3151, 2005.

[32] A. G. Aronov and Yu. B. Lyanda-Geller. Nuclear electric resonance and orientation of carrier spins by an electric field. *JETP Lett.*, 50:431, 1989.

[33] A. G. Aronov, Yu. B. Lyanda-Geller, and G. E. Pikus. Spin polarization of electrons by an electric current. *Sov. Phys. JETP*, 73:537, 1991.

[34] V. M. Edelstein. Spin polarization of conduction electrons induced by electric current in two-dimensional asymmetric electron system. *Solid State Commun.*, 73:233, 1990.

[35] Y. K. Kato, R. C. Myers, A. C. Gossard, and D. D. Awschalom. Current-induced spin polarization in strained semiconductors. *Phys. Rev. Lett.*, 93:176601, 2004.

[36] A. Yu. Silov, P. A. Blajnov, J. H. Wolter, R. Hey, K. H. Ploog, and N. S. Averkiev. Current-induced spin polarization at a single heterojunction. *Appl. Phys. Lett.*, 85:5929, 2004.

[37] Y. K. Kato, R. C. Myers, A. C. Gossard, and D. D. Awschalom. Observation of the spin hall effect in semiconductors. *Science*, 306:1910, 2004.

[38] J. Wunderlich, B. Kaestner, J. Sinova, and T. Jungwirth. Experimental observation of the spin-hall effect in a two-dimensional spin-orbit coupled semiconductor system. *Phys. Rev. Lett.*, 94:047204, 2005.

[39] V. Sih, R. C. Myers, Y. K. Kato, W. H. Lau, A. C. Gossard, and D. D. Awschalom. Spatial imaging of the spin hall effect and current-induced polarization in two-dimensional electron gas. *Nature Phys.*, 1:31, 2005.

[40] V. Sih, W. H. Lau, R. C. Myers, V. R. Horowitz, A. C. Gossard, and D. D. Awschalom. Generating spin currents in semiconductors with the spin hall effect. *Phys. Rev. Lett.*, 97:096605, 2006.

[41] Branislav K. Nikolic, Satofumi Souma, Liviu P. Zarbo, and Jairo Sinova. Nonequilibrium spin hall accumulation in ballistic semiconductor nanostructures. *Phys. Rev. Lett.*, 95:046601, 2005.

[42] L. P. Rokhinson, L. N. Pfeiffer, and K.W. West. Spontaneous spin polarization in quantum point contacts. *Phys. Rev. Lett.*, 96:156602, 2006.

[43] K. Nomura, J. Sinova, N. A. Sinitsyn, and A. H. MacDonald. Dependence of the intrinsic apin-hall effect on spin-orbit interaction character. *Phys. Rev. B*, 72:165316, 2005.

[44] K. Nomura, J. Wunderlich, J. Sinova, B. Kaestner, A. H. MacDonald, and T. Jungwirth. Edge-spin accumulation in semiconductor two-dimensional hole gases. *Phys. Rev. B*, 72:245330, 2005.

[45] L. I. Glazman, G. B. Lesovik, D. E. Khmel'nitskii, and R. I. Shekhter. Reflectionless quantum transport and fundamental ballistic-resitance steps in microscopic constrictions. *JETP Lett.*, 48:238, 1988.

[46] S. Datta. *Electronic Transport in Mesoscopic Systems*. Cambridge University Press, Cambridge, 1996.

[47] R. Danneau, O. Klochan, W. R. Clarke, L. H. Ho, A. P. Micolich, M. Y. Simmons, A. R. Hamilton, M. Pepper, D. A. Ritchie, and U. Zulicke. Zeeman splitting in ballistic hole quantum wires. *Phys. Rev. Lett.*, 97:026403, 2006.

[48] A. Reynoso, G. Usaj, and C. A. Balseiro. Detection of spin polarized currents in quantum point contacts via transverse electron focusing. *Phys. Rev. B*, 75:085321, 2007.

[49] L. Rokhinson, private communication.

[50] G. F. Giuliani and S. Chesi. On the two dimensional electron liquid in the presence of spin-orbit coupling. In *Highlights in the Quantum Theory of Condensed Matter,* ed. F. Beltram, p. 269, Pisa, 2005. Edizioni della Normale.

[51] M. Abramowitz and I. A. Stegun. *Handbook of Mathematical Functions*. Dover Publications, New York, 1965.

[52] J. Sinova, D. Culcer, Q. Niu, N. A. Sinitsyn, T. Jungwirth, and A. H. MacDonald. Universal intrinsic spin hall effect. *Phys. Rev. Lett.*, 92:126603, 2004.

[53] O. V. Dimitrova. Spin-hall conductivity in a two-dimensional Rashba electron gas. *Phys. Rev. B*, 71:245327, 2005.

[54] S. D. Ganichev, V. V. Bel'kov, L. E. Golub, E. L. Ivchenko, Petra Schneider, S. Giglberger, J. Eroms, J. De Boeck, G. Borghs, W. Wegscheider, D. Weiss, and W. Prettl. Experimental separation of Rashba and Dresselhaus spin splittings in semiconductor quantum wells. *Phys. Rev. Lett.*, 92:256601, 2004.

[55] S. G. Mikhlin. *Integral Equations*. Pergamon University Press, New York, 1957.

[56] W. H. Press, B. P. Flannery, S. A. Teukolsky, and W. T. Vetterling. *Numerical Recipes in C*. Cambridge University Press, Cambridge, 1988.

[57] M. Gell-Mann and K. A. Brueckner. Correlation energy of an electron gas at high density. *Phys. Rev.*, 106:364, 1957.

[58] A. Isihara and L. Ioriatti. Exact evaluation of the second-order exchange energy of a two-dimensional electron fluid. *Phys. Rev. B*, 22:214, 1980.

[59] M. Seidl. Spin-resolved second-order correlation energy of the two-dimensional uniform electron gas. *Phys. Rev. B*, 70:073101, 2004.

[60] Y. Wang and J. P. Perdew. Spin scaling of the electron-gas correlation energy in the high-density limit. *Phys. Rev. B*, 43:8911, 1991.

[61] A. Reynoso, G. Usaj, and C. A. Balseiro. Spin hall effect in clean two-dimensional electron gases with Rashba spin-orbit coupling. *Phys. Rev. B*, (11):115342, 2006.

[62] R. Winkler and U. Rössler. General approach to the envelope-function approximation based on a quadrature method. *Phys. Rev. B*, 48:8918, 1993.

VITA

VITA

Stefano Chesi was born in 1978 in Gorizia, in north-eastern Italy and lived in Monfalcone, a town in the Gorizia province, until 1997.

In the Summer of 1997 he was admitted to the prestigious Scuola Normale Superiore of Pisa, with a full scholarship for undergraduate studies. He completed the degree at the University of Pisa (M.Sc.) in the Summer of 2002. In the same year he received the Diploma from Scuola Normale Superiore.

In the Fall of 2002 he enrolled in the Department of Physics at Purdue University. He completed his requirements for the Ph.D. program in May 2007.